Ministry of Higher Education and Scientific Research
University of Baghdad
Institute of Laser for Postgraduate Studies

High sensitivity SNCS (Singlemode-Nocore-Singlemode) optical fiber pH sensor

A Thesis Submitted to the Institute of Laser for Postgraduate Studies, University of Baghdad in Partial Fulfillment of the Requirements for the Degree of Master of Science in Laser / Physics

By
Thimar A. Abd zaid

B.Sc. Physics – 2017

Supervisor
Asst. Prof. Dr. Hanan J. Taher

2021 AD **1442 AH**

بِسْمِ اللهِ الرَّحْمنِ الرَّحِيمِ

﴿وَلَمَّا بَلَغَ أَشُدَّهُ وَاسْتَوَى

آتَيْنَاهُ حُكْمًا وَعِلْمًا وَكَذَلِكَ

نَجْزِي الْمُحْسِنِينَ﴾

صدق الله العلي العظيم

سورة القصص الآية (14)

Certification

I certify that this thesis was prepared under my supervision at the Institute of Laser for Postgraduate Studies, University of Baghdad, as a partial fulfillment of requirements for the degree of "Master of Science in Laser/ Physics".

Signature:

Name: **Dr. Hanan J. Taher**

Title: **Asst. professor**

Address: Institute of Laser for Postgraduate studies,

University of Baghdad.

Date: / / 2021

(Supervisor)

In view of the available recommendation, I forward this thesis for debate by Examining Committee.

Signature:

Name: **Asst. prof. Dr. Hanan Jaafar Taher**

Title: Head of the Scientific Committee.

Address: Institute of Laser for Postgraduate studies, University of Baghdad.

Date: / / 2021

ألاهداء....

الى الذي علمني ان ما من صعود فيـــه تعب الا وراءه سهل أخضـــــر

الى من كتبني بدمه وقلبــــه ......أبـــــي

الى من رخصت الغالي لترضينـــــي

الى التي أجدها في كل لمحة ضياء ومحبة وقدحة عطر وبلة مطر أنبتت زرعـــا.......أمـــــي

الى كل من اجدني مديّناً لها عندما أقلب دفاتر عقلي وروحي .... جدتي

الى سندي في الصعاب..... اخوتي واخواتي

الى رفيق روحي الذي ساندني بكل خطاي الذي لم يزغ عن جانبي .. زوجي

الى الشموع التي أضاءت لي طريق العلم......أساتذتي

إلى من زرعوا التفاؤل في دربي وقدموا لي المساعدات والتسهيلات والأفكار والمعلومات، فلهم مني كل الشكر ..... صديقاتي

الى الاشخاص الذين ساعدوني وساندوني وكان لهم الفضل الكبير في رفع معنوياتي .

إلى من لم أعرفهم .... ولن يعرفوني

ACKNOWLEDGEMENTS

I would like to thank my supervisor assist. Prof. **Dr. Hanan J.Taher** for her guidance, kind advice, continuous follow, encouragement and help through the period of research and during writing of this thesis.

I would like to thank **Prof. Dr. Hussein A. Jawad**, the Dean of Institute of Laser for Postgraduate Studies. Special thanks to Instr. **Dr. Mahmoud S. Mahmoud**, the Deputy of Dean of Institute of Laser for Postgraduate Studies, I would like to thank Assist. **Prof. Dr. Mohamed K. Dhahir,** Head of the engineering and industrial application dept. for his support and also special sincere gratitude to all the staff and students of the institute of laser for postgraduate studies .I would like to thank assist. Prof for helping me.

My deep and sincere thanks to **Eng. Saif Akeel Mohammed** for his valuable advice and motivation.

I would like to introduce a great thank to **Dr. Ansam Majid Salman**, for to fraternal support and her continuous help and encouragement through this work.

Kind thanks are going to all the staff of the Institute for their effort during this research work.

I would like to express my thanks to "**my friends**", for their never ending moral support.

Finally, I would like to express my greatest thanks to "**my family**", for their sincere support and reliance

ABSTRACT

A simple, compact, low cost and eco-friendly pH sensor based on the multimode interference fiber sensor using simple all-fiber No-core fiber Mach-Zehnder interferometer as a sensing probe for pH level monitoring applications was designed.

On the way to fabricate an efficient sensing structure, the sensing head has been encapsulated with different coating materials including: polyvinyl alcohol/polyacrylic acid (PVA/PAA) hydrogel, pure silica nanoparticles embedded in polyvinyl alcohol/polyacrylic acid (SiO_2@PVA/PAA) hydrogel, and dye of methyl red mixed with PVA (methyl red@PVA), respectively.

On the other side, eleven different fiber sensing probe based on single mode-No-Core-single mode (SNCS) structure have been experimentally demonstrated. The sensor performance with varying No-Core fiber (NCF) length (1, 2, 3, and 4 cm) and different tuned diameters (100, 90, 80, and 70 μm) has been examined to attain the proper dimension of augmented evanescent waves. The optimum performance of the proposed sensor in sensing the variation in pH was at the length of 2 cm and NCF diameter of 70 μm. Later for more sensing enhancement, three different NCF section with 70 μm have been coated with PVA/PAA hydrogel, SiO_2@PVA/PAA hydrogel, and methyl red@PVA, respectively.

The obtained results exhibit that approximately a threefold augment of sensitivity has been realized at the planned optimum diameter (70 μm) of the NCF that coated with polymeric composite fabricated by PVA/PAA hydrogel and pure SiO_2@PVA/PAA hydrogel, respectively. Regardless, it can be observed that the coating of PVA/PAA is an applicant sensing coating substance for acidic; while, SiO_2@PVA/PAA is greater proper for the sensing of the base state. The experimental results demonstrate a high average sensitivity of 3.42 nm/pH unit for the 11 w.t. % PVA/PAA coated

sensor in the pH range from 1 to 7, and 3.2 nm/pH unit in the pH range from 8 to 14.

Furthermore, methyl red@PVA coating shows further enhancement above the aforementioned coating, which can sense both the acidic and base together. Also, the pH fiber sensor based on methyl red@PVA coating which this coating shows a high sensitivity of 4.3 nm/pH unit for the pH range from 1 to 7, and 4.1 nm/pH unit in the pH range from 8 to 14.

Finally, these coating materials show an enhancement in the sensitivity above the NCF structure before the uncoated sensor due to more enhancement of the evanescent field affected by the coating layer. To the best of the authors' knowledge, the structure was capable of detecting wide range of pH level with good sensitivity using SNCS structure coated with SiO_2- NPs thin layer and methyl red.

TABLE OF CONTENTS

Title		**Page**
Abstract		III
List of Contents		V
List of Tables		VII
List of Figures		IX
List of symbols and Abbreviations		XIV
Chapter one: Introduction and Basic Concept		
1.1	Introduction and Motivation	1
1.2	Optical Fibers	4
1.3	Types of Optical Fibers	4
1.3.1	Single mode Fiber	4
1.3.2	Multi-mode Fiber	4
1.4	Waveguide of Light in the Optical Fiber	6
1.5	Types of Optical Fiber Interferometers	8
1.5.1	Sagnac Interferometer	8
1.5.2	Fabry-Perot Interferometer	9
1.5.3	Moiré Fiber Interferometer	10
1.5.4	Mach-Zehender Interferometer	10
1.5.5	Michelson Interferometer	14
1.6	Optical Fiber Sensor (OFS)	15

1.7	pH Sensing	16
1.8	Operating Principle of the pH Sensor	17
1.9	Multi-mode Interference (MMI) Optical Fiber Sensors	18
1.10	Coating Material	19
1.11	Literature Review	20
1.12	Aim of the Work	23
Chapter Two:- Experimental Setup and Procedures		
2.1	Introduction	24
2.2	System Layout	24
2.2.1	Broadband Source	25
2.2.2	Single- Mode Fiber (Corning SMF-28)	25
2.2.3	No-Core Fiber (NCF) (Thorlabs)	26
2.2.4	Optical Spectrum Analyzer (OSA)	27
2.2.5	U-shaped or U-groove	28
2.3	Experimental Procedures	28
2.3.1	The SNCS Fiber Structure	29
2.3.2	NCF & SMF Cleaving	29
2.3.3	SMF and NCF Splicing	30
2.3.4	NCF Etching	31
2.3.5	Preparation of Hydrochloric acid (HCl) and Hydroxide Sodium (NaoH) Solution	33
2.4	Optical Fiber pH Sensors based on Multimode Interference Using SNCS Setup	34
2.5	Preparation of PVA/PAA and Silica/PVA/PAA Composite	35

2.6	Preparation of Methyl red@PVA Composite	37
2.7	The Influence of the NCF Coating on the Sensitivity	38
Chapter Three:- Results and Discussion		
3.1	Introduction	39
3.2	The Transmission Spectrum and the Stability of SNCS Structure	39
3.3	The Influence of NCF Length on the pH Sensor Sensitivity	40
3.4	The Influence of NCF Diameter on the pH Sensor.	46
3.5	The Influence of Coating on OFpHS Sensitivity	53
3.5.1	The Influence of both PAA/PVA and SiO_2/PVA/PAA Coating on OFpHS Sensitivity	53
3.5.2	The Influence of Methyl red@PVA Coating on OFpHS Sensitivity	59
3.6	Conclusions	63
3.7	Future Works	64
References		
References		65

LIST OF TABALS

Table	Title	Page
1-1	Summary of the Published Works in OFpHS	20
2-1	Optical specifications of No-Core Fiber	26
2-2	OSA Characteristics used to perform this work	27
2-3	Preparation of pH values	34
3-1	The sensitivity and the polynomial fitting coefficient for different lengths of bare NCF at fixed diameter (125 μm) for both acid and base which the pH changed from 1-14.	41
3-2	The sensitivity and the polynomial fitting coefficient for different diameters of bare NCF at fixed length (2 cm) for both acid and base which the pH changed from 1-14.	51
3-3	the performance of the proposed sensor before and after coating the NCF	62
3-4	Comparison of Sensitivity for different optical fiber pH sensors	63

LIST OF FIGURES

Figure	Title	Page
1.1	Optical fiber structure	4
1.2	(a) Schematic of single mode fiber, (b) Schematic of Multimode fiber	5
1.3	(a) Schematic of Step-index MM fiber, (b) Schematic of Graded-index Multimode fiber	5
1.4	(a) Schematic of single mode fiber, (b) Schematic of Coreless fiber	6
1.5	Light confinement in optical fiber. (a) The refraction (b) The refraction case explaining the critical angle φc, and (c) The TIR where φ greater than φc	7
1.6	The transmission of light through an optical fiber	8
1.7	Schematic of Sagnac fiber interferometer	9
1.8	Schematic of Fabry-Perot fiber interferometer	10
1.9	Schematic of Moiré fiber interferometer	10
1.10	Schematic of MZI fiber interferometer with outer couplers	11
1.11	Schematic of different kinds of MZI (a) a pair of LPGs, (b) core mismatch, (c) PCF air-holes collapse region, (d) Multi-Mode fiber, (e) SMF small core, and (f) fiber tapered.	13

1.12	Schematic of Michelson fiber interferometer	15
1.13	Develop of pH sensors	17
2.1	The experimental setup for measuring the pH based on SNCS fiber structure	24
2.2	Photo-image of Broadband source (B.B.S)	25
2.3	Top view for the SMF under microscope with magnification power (4x)	26
2.4	Photo-image of optical spectrum analyzer (OSA).	27
2.5	Schematic of U-Shape	28
2.6	The schematic block diagram of experimental work	28
2.7	Schematic of the SNCS structure	29
2.8	Microscope images of NCF end after cleaving	30
2.9	Fusion splicer between NCF and SMF	31
2.10	Calbration curve of diameter as a function of time.	32
2.11	Microscopic image of NCF diameter etching (a)100 µm (b)90 µm (c)80 µm (d)70 µm with (4X)	33
2.12	The preparation coating process (a) PVA/PAA coating (b) silica/PVA/PAA coating.	36
2.13	SEM images of SiO_2-NPs at 100 nm scales.	37

2.14	The preparation methyl red@ PVA coating process.	38
3.1	Output Spectrum of B.B.S of SMF and SNCS	40
3.2	Schematic of experimental setup of SNCS	40
3.3	Transmission spectra response of the OFpHS as a function of pH for (a) 1cm, (b) 2cm, (c) 3cm, and (d) 4cm NCF length for acid	42
3.4	Transmission spectra response of the OFpHS as a function of pH for (a) 1cm, (b) 2cm, (c) 3cm, and (d) 4cm NCF length for base	43
3.5	Linear fitting plots of the shifted dips against pH change in the function of wavelengths shift for (a) 1cm, (b) 2cm, (c) 3cm, and (d) 4cm length of NCF for acid	44
3.6	Linear fitting plots of the shifted dips against pH change in the function of wavelengths shift for (a) 1cm, (b) 2cm, (c) 3cm, and (d) 4cm length of NCF for base	45
3.7	The response sensors to variations in pH from (1-14) with different NCF lengths for (a) acid and (b) base.	46
3.8	Transmission spectra response of the OFpHS as a function of pH for (a) 100 µm, (b) 90 µm, (c) 80 µm, and (d) 70 µm NCF diameter for acid	47

3.9	Transmission spectra response of the OFpHS as a function of pH for (a) 100 µm, (b) 90 µm, (c) 80 µm, and (d) 70 µm NCF diameter for base	48
3.10	Linear fitting plots of the shifted dips against pH change in the function of wavelengths shift for (a) 100 µm, (b) 90 µm, (c) 80 µm, and (d) 70 µm NCF diameter for acid	49
3.11	Linear fitting plots of the shifted dips against pH change in the function of wavelengths shift for (a) 100 µm, (b) 90 µm, (c) 80 µm, and (d) 70 µm NCF diameter for base	50
3.12	Wavelength with an error bar, of the proposed sensor for (a) acid and (b) base.	52
3.13	The response sensors to variations in pH from (1-14) with different NCF diameters for (a) acid and (b) base	52
3.14	The optical microscope images (a) PVA/PAA and (b) SiO_2/PVA/PAA coating.	54
3.15	The FSEM images of NCF coated with (a) PAA/PVA and (b) SiO_2/PVA/PAA	54
3.16	Transmission spectra of 70 µm NCF coated with PVA/PAA for sensing different pH values for (a) acid and (b) base.	55
3.17	Transmission spectra of 70 µm NCF coated with SiO_2/PVA/PAA for sensing different pH values for (a) acid and (b) base.	56

3.18	(a) Linear fitting plots of the shifted dips (b) wavelength with an error bar, of the proposed sensor based on PVA/PAA for acidic pH range.	57
3.19	(a) Linear fitting plots of the shifted dips (b) wavelength with an error bar, of the proposed sensor based on SiO_2/PVA/PAA for acidic pH range.	58
3.20	Wavelength reproducibility of the proposed sensor for (a) acid and (b) base	59
3.21	Image under the optical microscope of the methyl red@PVA	59
3.22	Transmission spectra of 70 µm NCF coat with Methyl red@PVA for sensing different pH values for (a) acid and (b) base.	60
3.23	Linear fitting plots of the shifted dips against pH change in the function of wavelengths shift for (a) acid, and (b) base of the proposed sensor based on methyl red@PVA coating.	61

LIST OF ABBREVIATION

Abbreviations	Description
pH	Power of Hydrogen
SMF	Single mode fiber
NCF	No-core fiber
SMS	single-mode-multimode-single-mode
MMF	Multi-mode fiber
PCF	Photonic Crystal Fiber
PVA	Polyvinyl alcohol
PAA	Poly acrylic acid
SiO_2	Silicon Dioxide
RI	Refractive Index
TIR	Total Internal Reflection
NA	Numerical Aperture
OFSs	Optical fiber sensors
MMI	Multimode interference
PC	polarization controller
PMF	Polarization Maintain Fiber
FBG	fiber Bragg grating
MZIs	Mach-Zehnder interferometer sensor
OC	Optical coupler
LPGs	long period gratings
RI	Refractive index
SNCS	single mode-no-core-single mode fiber

OSA	Optical spectrum analyzer
BBS	Broadband source
HF	Hydrofluoric acid
SEM	Scanning electron microscopy
OPD	Optical Path Different

LIST OF SYMBOLS

SYMBOLS	DESCRIPTION	UNITS
n_{c}	Refractive index of the core	-
n_{cl}	Refractive index of the cladding	-
n_1	Refractive index of the glass	-
n_2	Refractive index of the air	-
θ_c	Critical angle	Degree/radian
D_{NCF}	The diameter of NCF	µm
L_{NCF}	Length of the NCF	mm
L_{π}	Beat length	-
M	Self-imaging number	-
n_{NCF}	the effective refractive index of NCF	-
λ_0	interference wavelength	nm
λ	Wavelength	nm

Chapter One

Introduction and Basic Concept

1.1 Introduction

pH sensor is an important optical biochemical sensor due to the importance of pH control or monitoring in many areas such as biological processes, chemical reactions, pharmaceutical, biochemistry, food quality control, etc.[1-3]. In the last few years, several research efforts have studied the differences in the optical properties of pH indicators.

Sensors can use such methods to detect the pH of liquids that cause changes in the color of indicators due to variations in absorption. However, in the last few years, pH fiber sensors have become a more exciting topic of research due to their many benefits like being lightweight, small in size, highly sensitive, possessing a fast response, good repeatability and stability over that of common sensors. Numerous configurations of optical fiber pH sensors have been constructed, utilizing thin-core fiber [4], photonic crystal fiber [5], Fabry–Perot Interferometer [6], and no-core fiber (NCF) [7].

Optical fibers are the main fabrication components for optical waveguide fiber, optical filters, optical sensor, interferometers, couplers and circulators [8-12]. In optical fiber sensor, the interference represented the main principle to measure sensitivity. There are many types of optical fiber interferometers such as Sagnac interferometer, modal interferometer, Michelson interferometer, Moiré interferometer, Fabry-Perot interferometer, and Mach-Zehnder interferometer (MZI) [13-16] .

Different structure for these interferometers can be implanted. Among them, all-fiber MZI sensor has many attractive features such as broad wavelength operation range, low insertion loss, compact and robustness. All-fiber MZI can be implemented in different ways and different types of fibers, e.g., coreless fiber, photonic crystal fiber (PCF), nano-fiber, polarization maintain fiber (PM), Bragg fiber, and multimode fiber (MMF) [17-22].

MZI based on NCF is extensively investigated by many authors but still the most promising sensing schemes due to its unique advantages of very ease of fabrication, low development cost and very high sensitivity [14].

Multimode (MMF) approaches based on NCF splicing between two single-mode fiber (SMF) sections has gained considerable attention in sensing applications. Despite MMF-based-NCF sensors showing excellent repeatability, ease of use, capable to sweep huge atmosphere surroundings and compactness, they show restricted sensitivity.

So, encapsulating the active sensing part with resonance-assisting material has for some time been considered a realistic solution and might be even contribute to improved sensing when these sections are combined with certain sensor configuration [24-26]. Utilizing different innovative materials, pH fiber sensors depend on an evanescent field interaction with the surrounding resonance coating supported by thin film-encapsulating optical waveguides allows for superb sensitivity [11-12].

Several substances have been considered as sensitive pH materials [29-32]. Lately, the utilization of hydrogel polymers as sensitive substances to improve the sensing ability of pH optical fiber sensors has been reported extensively. Sensitive dyes also play a significant role in improving the sensitivity of devices, which are used to prepare the pH detecting film due to the simplicity and cost-effectiveness of this approach. The hydrogel method was used to incorporate pH-sensitive dyes on the fiber surface [24].

Polymers such as polyvinyl-alcohol (PVA) and poly acrylic acid (PAA) are often exploited due to their brilliant optical characteristics to fabricate fiber dependent pH sensors [27,38]. This hydrogel polymer coating material swells physically when exposed to environmental change, which this refractive index will be altered noticeably by the surrounding ambient variation and possesses variable dynamic span and pH sensitivity [30–33].

While the nanomaterial attracts significant interest in the optoelectronics proposed studies, which it is inexpensive to produce, easy to prepare.

On the other side, investigation of organic substances indicated their considerable sensitivity to environmental states such as pH sensing, humidity, and so on [34–36]. Hence, the study of these substances is high encouraging with regard to the progress of different sensor types due to their small hysteresis [36,37], chemical stability and compatibility with various devices. Some organic compounds show but these compounds dissolve in water [47-48].

The present work illustrates the construction of a pH fiber sensor using a structure-based SMF-MMF-SMF. A tuned dimension section of NCF was spliced between two sections of SMF to configure the SNCS structure; it expands the multipoint sensing contrasted to other traditional sensor for pH level to the best of our knowledge. Firstly, the effect of the length of the NCF on the transmitted wave has been experimentally examined at the stationary of 125 μm diameter. Then, the NCF diameter is reduced via the chemical etching method, it is considered to be as an efficient method to improve the sensitivity of the sensing system.

Finally, the optimum parameters of NCF length and diameter were coated with different materials. The sensitive coating for the pH level has been syntheses via blending the pH-sensitive material with PVA as a precursor and dropping it on the sensing probe surface via dip coating method. Polymers-based matrix coating substrate has been extensively utilized to enhance the sensing performance in different sensing areas based on fiber sensor structures.

1.2 Optical Fiber:

Optical fibers are flexible, transparent mediums used to transfer optical signals, usually; these fibers are made from silica or plastic, which consists of three parts: the buffer coating, the cladding, and the core as shown in Figure (1.1). Optical fibers principle work based on total internal reflection which their structures contain core with higher RI while the cladding at the lower RI to maintain light confinement inside the core [40].

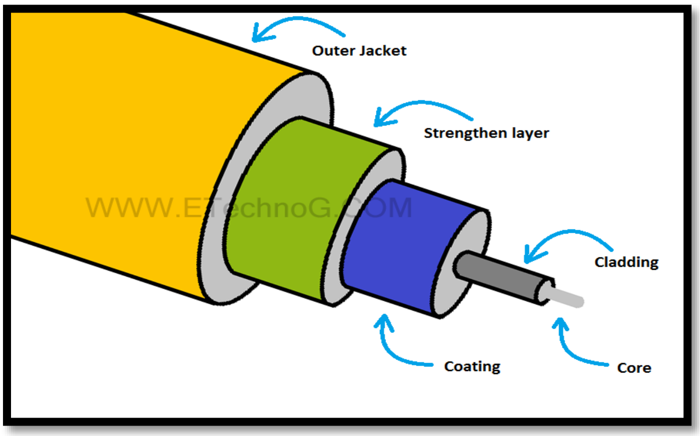

Figure (1.1): optical fiber structure [40].

1.3 Types of optical fiber

1.3.1 Single-Mode Fiber (SMF):

SMF is composed of a small diameter core (8-10 µm) that permits a single mode of lunched light to propagate through it considered as single-mode fiber as shown in Figure (1.2(a)). These fibers consist of highly doped silica as a core and with lower doping silica as cladding. The core refractive index can be denoted as n_1 , while the refractive index n_2 is the cladding where ($n_1 > n_2$) [41].

1.3.2 Multi-Mode Fiber:

Multimode fibers are optical fibers possess large core diameters of about (50-60 µm), which permits multi-modes of lunched light to propagate through it as shown in Figure (1.2(b)). There is a sub-division of multi-mode fibers based-on the how RI changed among core and cladding of fiber [41].

There are many types of MMF; the most important types of this fiber are listed as following:

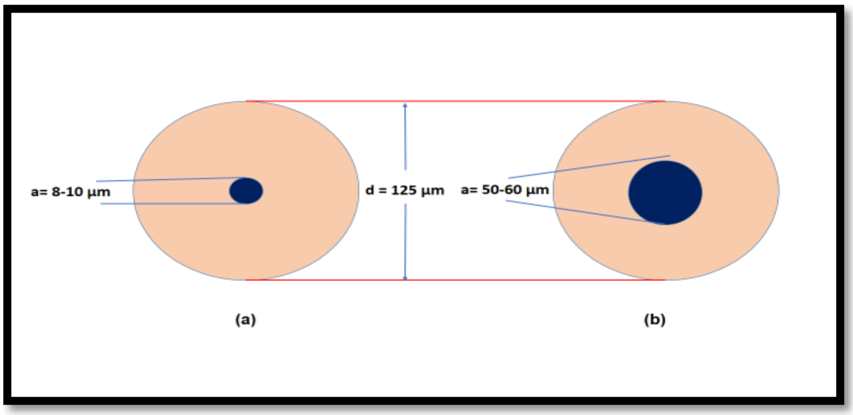

Figure (1.2): (a) Schematic of SMF, (b) Schematic of MMF [41].

i- Step index multimode fiber: is the type of MMF whose refractive index of core **(**n_1**)** is greater than cladding refractive index **(**n_2**)** by one step [41]. The light rays propagate in a zigzag manner inside the core as meridional rays.

ii- Graded-index multimode fiber: in this type of multimode fiber the RI of core **(**n_1**)** is highly RI at the center and decreased gradually changing up to **(**n_2**)** [41]. The light rays propagate in the helical or skew form. (Figure (1.3)).

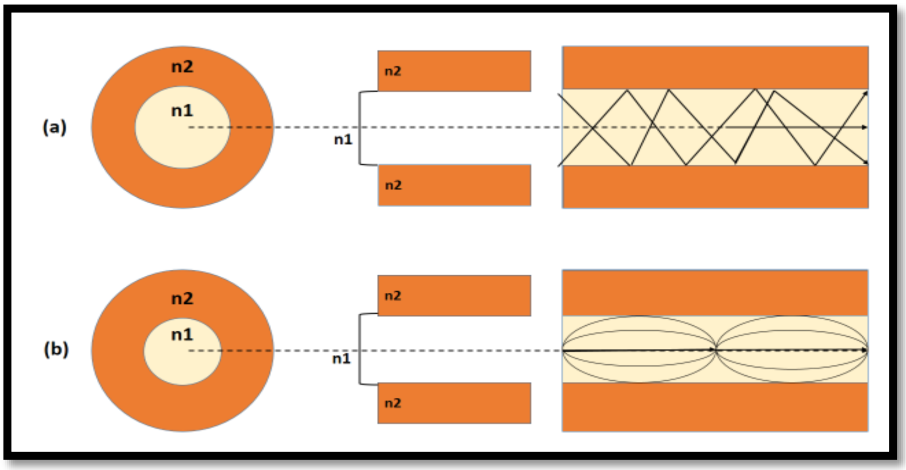

Figure (1.3): (a) Schematic of Step-index MM fiber, (b) Schematic of Graded-index Multimode fiber [41].

iii- No-Core Fiber (NCF): NCF is considered a special commercialized fiber with uniform RI. NCF has only a cladding with 125 µm diameter as shown in Figure (1.4 (b)) usually from fused silica which is the same as conventional fibers outer diameter [42]. NCF fabricated by different companies with various operation temperatures (-65±300 Cº), various diameters range (125-480 µm) and a wide range of operating wavelengths (400-2400 nm) for numerous applications. The ambient medium of NCF acts as cladding, when the surrounding medium has RI lower than the fused silica the total internal reflection is specified and the NCF behaves as a multi-mode waveguide [43].

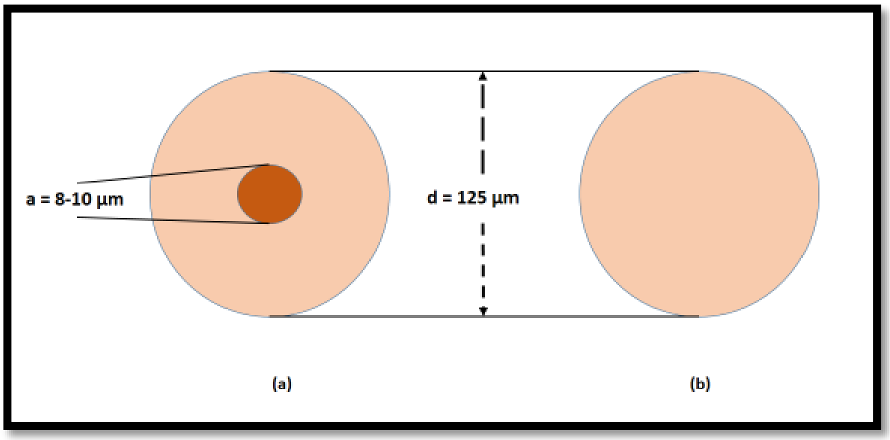

Figure (1.4): (a) Schematic of single-mode fiber, (b) Schematic of No-core fiber [43].

1.4 Waveguide Light in the Optical Fiber:

The coupling ray of the light into the optical fiber can be explained by the theoretical ray, it is substantial to observance the reason for the RI of the environmental matter. The RI of the medium is a value calculated from the relative amount of the velocity of light in a vacuum to the velocity of light in the medium of greater density.

The light ray is traveling faster through optically minimal dense medium than through optically which is denser, where the refractive index profile describes this influence [44]. When a ray of light incident on the boundary between two different isotropic like glass and air, the refraction phenomena happened. The total internal reflection (TIR) phenomenon happens when light ray travels from a matter of RI n_1 and is at an angleφ_1, approaches the other side of the smallest refractive index n_2 at an angle φ_2 greater than the incident angle φ_1, which is estimated concerning the normal. The refraction φ_2 and the incidence angles φ_1 are related to each other and to the refractive indices, where given by Snell's law refraction [45]:

$$\boldsymbol{n_1 sin\varphi_1 = n_2 sin\varphi_2} \quad \textbf{(1.1)}$$

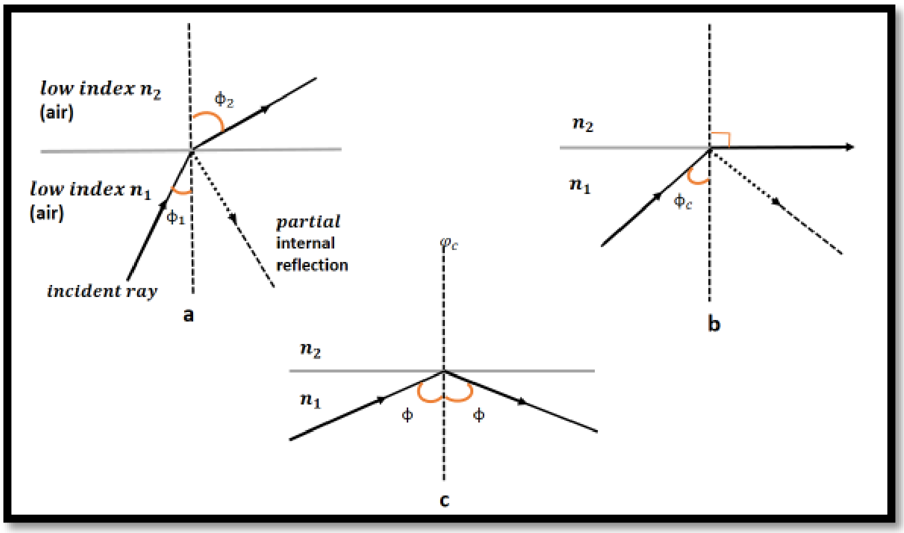

Figure (1.5): Light confinement in optical fiber. (a) The refraction (b) The refraction case explaining the critical angle φc, and (c) The TIR where φ greater than φc [44].

From Figure (1.5 (a)) when a light incident at the medium with refractive index n_1 to another medium with a lower refractive index n_2, the refraction depends on the angle of the refracted which is always greater than the incidence angle. The critical angle φ_c is the angle of the incidence ray when the angle of refraction ray is 90° as shown in Figure (1.5 (b)) and could be given by [44]:

$$\boldsymbol{\varphi_c = sin^{-1}\frac{n_2}{n_1}} \quad \textbf{(1.2)}$$

If the angle of light incident is larger than the critical angle φ_c, then all the light beams will be reflected into one medium as illustrated in Figure (1.5 (c)). TIR occurs where $n_2 < n_1$ [44]. Figure (1.6) illustrate the light ray enters the optical fiber and reflected at the first interface of the core-cladding at the angle **θ**. This signal beam enters core of the fiber at an angle of incidence **θ**in that is term the acceptance angle for which the ray undergoes TIR at the interface of the core-cladding and propagates through the fiber [45].

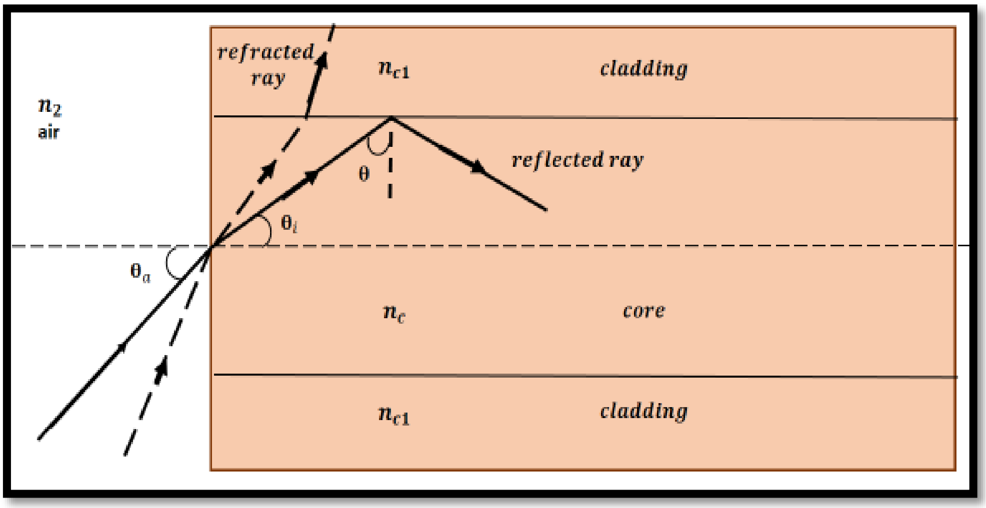

Figure (1.6): Transmission of light through an optical fiber [45].

The sine of the fiber of acceptance angle represented by the numerical aperture (NA) which for signal beam launched a fiber from the air (n_2=1) is given by[55-[47]:

$$\mathbf{NA} = \left(\mathbf{n_1^2} - \mathbf{n_2^2}\right)^{1/2} \qquad \textbf{(1.3)}$$

1.5. Types of optical fiber Interferometers

1.5.1 Sagnac Interferometer (SI)

SI contains an optical fiber loop. Two beams propagate in which fiber with different polarization. The 3 dB-coupler utilize to split the input signal and the two beams recombined in the same coupler. The optical path difference is determined by propagation speed dependent on the polarization.

Birefringent fibers are used in the sensing part to increase the polarization. A polarization controller (PC) is used to adjust the polarization [48]. Figure (1.7) shows the schematic design of the Sagnac interferometer.

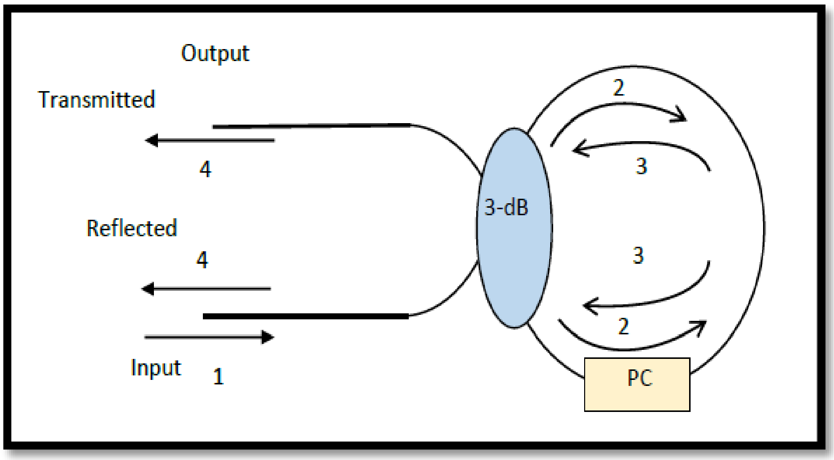

Figure (1.7): Schematic of Sagnac fiber interferometer [48].

1.5.2 Fabry-Perot Fiber Interferometer:

This type of optical interferometer consists of two optical parallel reflectors based on the Fabry-Perot effect, with a cavity of length L between those reflectors [44]. Reflectors can be the interface of two dielectrics mirrors, or two fiber Bragg gratings, or two internal mirrors achieved by splicing of polished fibers, or by coating the cleaved end side of the optical fiber [49]. Figure (1.8) displays the schematic of the Fabry-Perot interferometer.

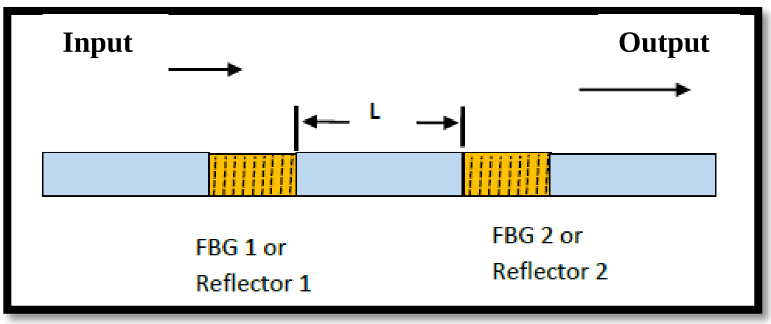

Figure (1.8): Schematic of Fabry-Perot fiber interferometer [49].

1.5.2 Moiré Fiber Interferometer:

This type of optical interferometer is based on the Moiré fringe pattern when two or more gratings lie in contact at a small angle θ to form the Moiré fringes. By suitable arrangement of two or three optical fibers, Moiré fringe pattern could be designed based on the generation of the interference grid pattern. Three polarization-maintaining fiber (PMF) connected to a 1×3 optical fiber coupler at the input side and the output side are inserted into a glass tube and glued with epoxy [50]. Figure (1.9) shows the schematic of the Moiré interferometer.

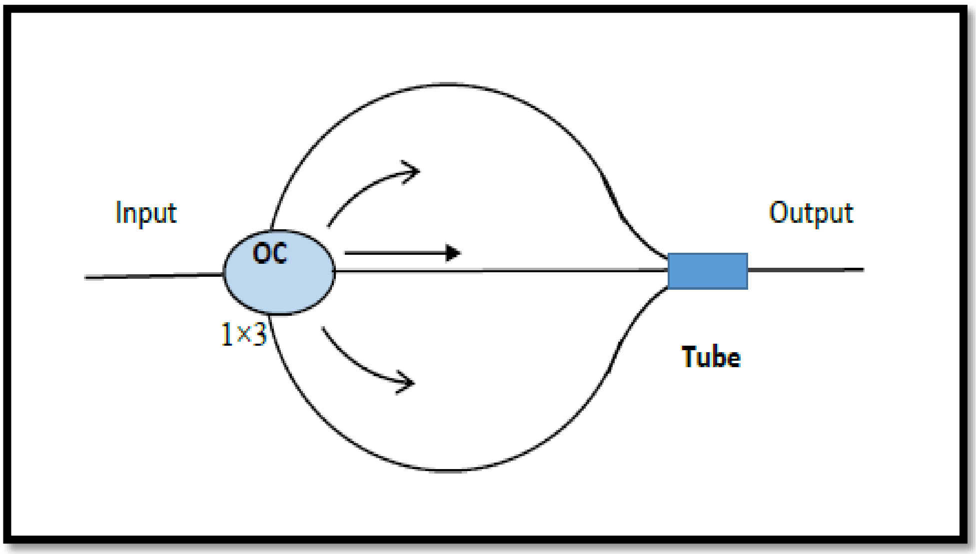

Figure (1.9): Schematic of Moiré fiber interferometer [50].

1.5.4 Mach-Zehnder Interferometry:

Mach-Zehnder interferometers (MZI) have attracted a lot of interest for various sensing applications due to their flexible structure, ease to fabricate, the capability of responding to a surrounding variety, and low cost [1]. All-optical MZI by constructed in two methods, first method by using two outer couplers connected in series with two fibers. The first coupler splits the input signal into two parts, the sensing arm, and reference arm, another fiber coupler is used to recombine the signal. The rejoined light has the interference into element regarded to the Optical Path Difference (OPD) among the two parts [51-52]. Figure (1.10) shows a schematic of MZI using outer couplers.

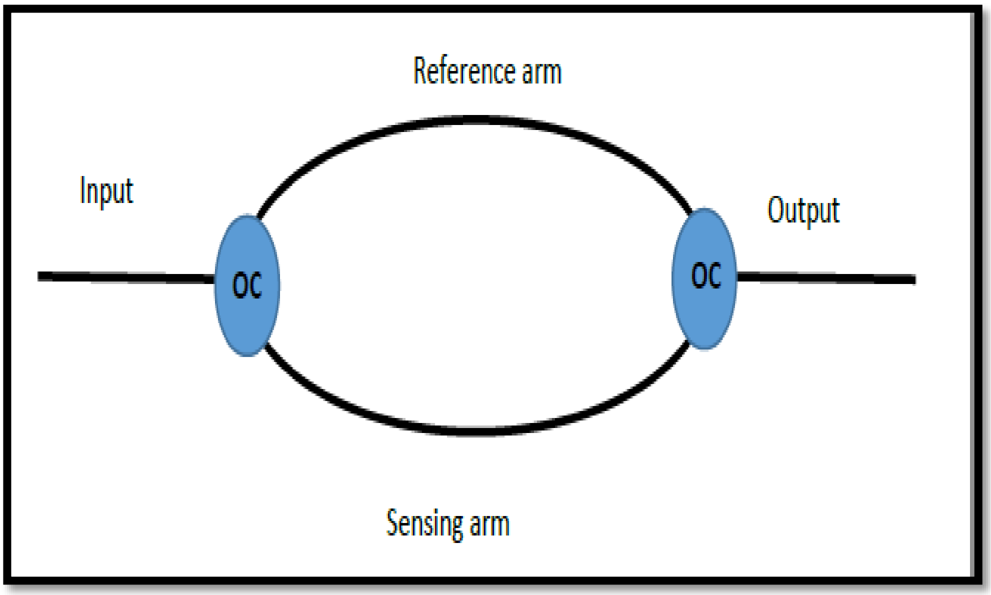

Figure (1.10): Schematic of MZI fiber interferometer with outer couplers [52].

The second method is achieved by one optical fiber using the splicing technique and it has the same principle. In such a method splicing region between two similar or different fibers acts as an inner coupler [53].

In the splicing region, the refractive indices of both core and cladding of identical or hybrid fibers fused resulting in a new area with attributed variation in refractive index. There are two splicing regions, first region act as a beam splitter coupler where the entry beam will split into two beams, the reference beam and the sensing beam.

The fundamental modes guided through the core acts as the reference beam and high exited order modes which are guided through cladding can act as sensing beams since they influence with surrounding environment variation. While the second splicing region acts as a combiner coupler and the two-beam will recombine. The two-beam has interference and can be given by[53]:

$$\boldsymbol{I_{Tot} = I_1 + I_2 + 2\sqrt{I_1 I_2}\ \cos(\theta_1 - \theta_2)} \qquad \textbf{(1.4)}$$

Here, I_1 and I_2 are intensities of the light core and cladding modes at the end of the MZI[53].

$\boldsymbol{\Delta\theta = (\theta_1 - \theta_2)}$ is the optical path difference(OPD) among the core and the cladding modes and can be expressed as:

$$\boldsymbol{\Delta\theta = k\Delta n_{eff} L_{MZI} = \frac{2\pi}{\lambda}\, \Delta n_{eff} L_{MZI}} \qquad \textbf{(1.5)}$$

where, L_{MZI} is the physical length of MZI is, $\Delta n_{eff} = n_{eff}^{core} - n_{eff}^{clad}$ is the difference between the effective RI of the core and RI of cladding. Equation (1.5) plays a very important role to determine whether the interference pattern is constructive or destructive. When $\Delta\theta$ satisfies $\Delta\theta=2m\pi$, where m= 0, ±1, ±2… is constrictive of the interference. While, if $\Delta\theta = (2m-1)\,\pi$, where m=0, ±1, ±2… is destructive of the interference.

If the optical path difference among the core and the cladding modes varies continuously, it will result in an interference pattern and the measured intensity will change from a maximum $\mathrm{I_{max}} = \mathrm{I_1} + \mathrm{I_2} + 2\sqrt{\mathrm{I_1 I_2}}$, (if $\Delta\theta$=0) to a smallest of ($\mathrm{I_{min}} = \mathrm{I_1} + \mathrm{I_2} + 2\sqrt{\mathrm{I_1 I_2}}$). Therefore, the fringe visibility constant or fringe modulation depth can be defined as:

$$\boldsymbol{\frac{I_{max}-I_{min}}{I_{max}+I_{min}} = \frac{2\sqrt{I_1 I_2}}{I_1+I_2}} \qquad \textbf{(1.6)}$$

The spacing $\Delta\lambda$ between adjacent constructive peaks (or the free spectral range FSR) can be described as[54][55]:

$$\boldsymbol{\Delta\lambda = \frac{\lambda^2}{\Delta n_{eff}\, L_{MZI}}} \qquad \textbf{(1.7)}$$

The various configuration of MZI in the second method such as single mode-multimode-single mode (SMS) MZI, mismatch core MZI, transition PCF MZI, reflection MZI, Tapered Fiber MZI, and NCF MZI as display in Figure (1.11).

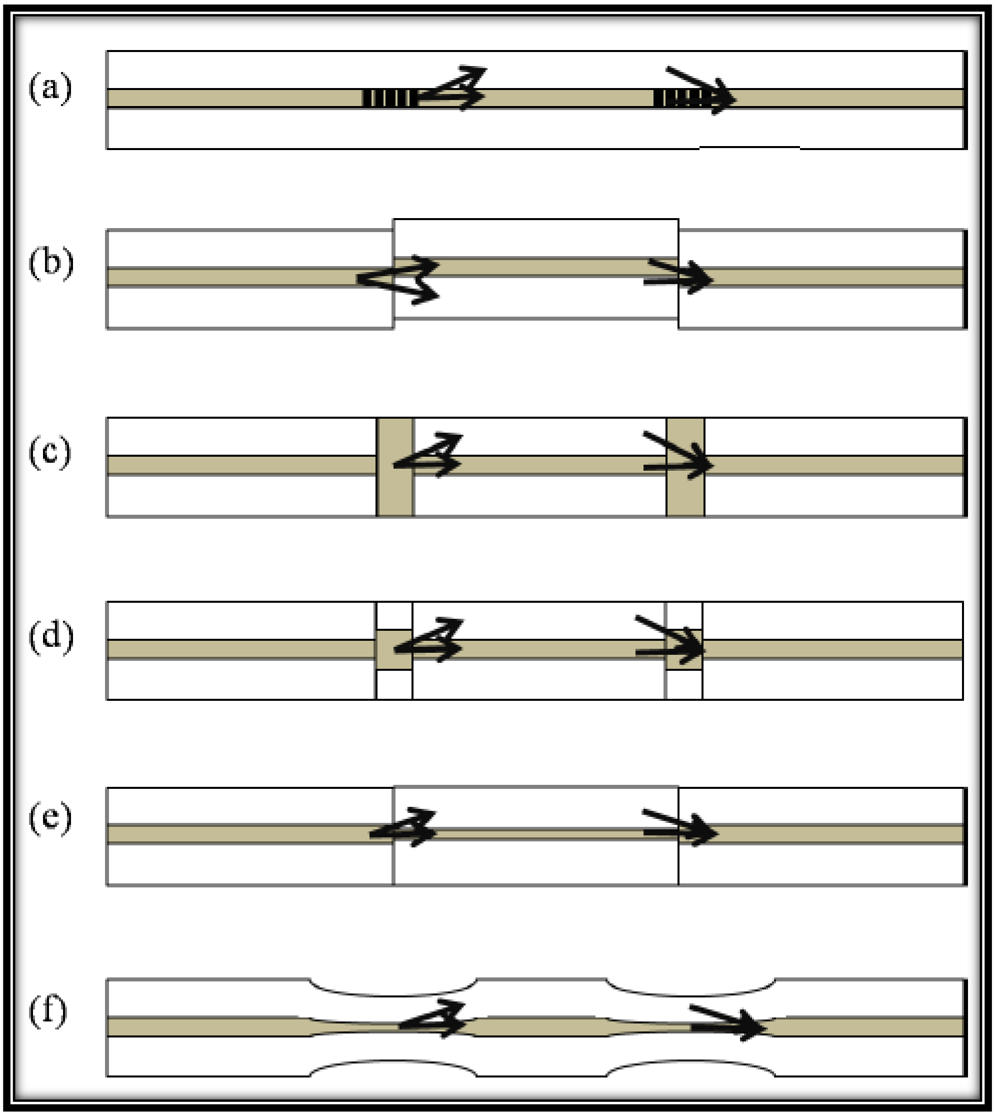

Figure (1.11): Schematic of different kinds of MZI (a) a pair of Long Period Grating (LPG), (b) core mismatch, (c) PCF air-holes collapse region, (d) Multi-Mode fiber, (e) SMF small core, and (f) fiber tapered [56].

All types above depending on the extremely interference principle and can be expressed by equation (1.6). The present work will be attended to fabricate NCF-MZI. This structure of the interferometer can be formed by fusion splicing two segments of standard SMF to the two ends of NCF (Figure 1.11 (f)). The discrimination of modes here based on the MMI effect in SNCS fiber structure.

It can be divided the modes into two categories, according to the modes involved in the interference. One is the interference among fundamental core and higher-order modes (core–core intermodal interference), another is the interference among fundamental core and cladding modes (core–clad intermodal interference). Depending on the self-imaging effect the MMI can occur between modes [57].

The self-imaging (also named lensless imaging) means that an input field distribution repeats itself in periodic repetition in a certain distance without any helped device between object and image [58]. The mismatch modes among SMF and NCF permit the essential mode in SMF to join into an NCF. Then, the fundamental mode begins to diffract within the NCF. Excited and propagated of the high order modes are independently through the NCF section.

These high order modes are interfered with each other and appeared as a superposition of their mode field. Generally these high-order modes construct a complex field distribution owing to MMI consequence. However, bright images or what is termed self-imaging of the input field can be created at special positions where the modes which that excited are in phase [59].

1.5.5 Michelson Interferometer:

Michelson interferometers optical fiber sensors are similar to MZIs sensors, both of them contain two arms and the sensing depends on interference between these arms. The difference between them is that Michelson interferometer sensors have a reflecting mirror at the end of each arm. The configuration of the Michelson interferometer like half of MZI [21,61,62]. Figure (1.12) shows the schematic of the Michelson interferometer.

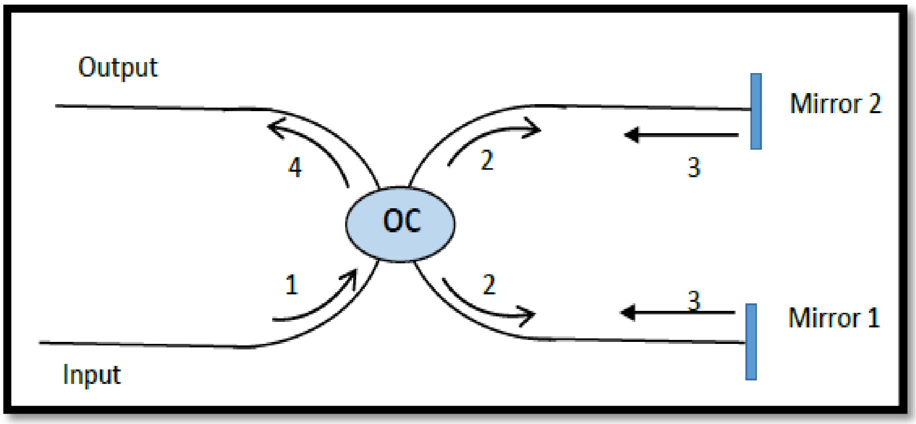

Figure (1.12): Schematic of Michelson fiber interferometer [62].

1.6 Optical Fiber Sensor (OFS):

In recent years OFS have played a significant role in scientific study because of their numerous benefits like slight size, electromagnetic immunity, compact, electrically isolated, and wide dynamic range. The optical fiber sensors are categorized depending on the operating principle, their application, and the sensing location. Many kinds of optical fiber pH sensors (OFpHS) are manufactured to detect the pH levels [64-65].

Essentially, OFS are depends on intensity or wavelength modulation. The intensity sensor senses the variation of the light intensity transmitted through the fiber by using a detector placed at the end of the fiber. The evanescent wave sensor can be considered one of the intensity-based sensors which use evanescent field created whenever light transmitted between two dielectric media and total internal reflection occurs[65-67]. This type of sensor is used in chemical sensors that useful in measuring chemical concentrations. The sensing process is achieved by shedding the cladding from a piece of the optical fiber and a signal ray has been exhibits a wavelength absorbed by the chemical that is to be detected.

Intensity-modulated methods suffer many fluctuations in the intensity of light which reasons errors in pH measurements [68]. While, wavelength modulated methods have been described for better and their response was stable sensing [69-70], so wavelength modulated fiber optic sensors use for detection of the variations in the wavelength of the source. Bragg grating sensors (FBG), Fluorescence sensors, and black body sensors are models of wavelength-modulated sensors.

1.7 pH Sensing:

The power of Hydrogen (pH) is a significant parameter because it is used in several significant areas like medicine, environmental, and biotechnology. So, the litmus paper considers the simplest technique to measure pH solution, but it doesn't know the exact pH value it can only distinguish either base or acid condition. The other paper which can be used for measuring pH value is a universal indicator paper which has better sensitivity to distinguish the pH value until 0.5 pH scale.

The next generation in pH measurement is pH electrode after the invention of glass membrane which sensitive to pH. It is known with the pH meter after equipped with a special electronic system whose sensitivity could reach 0.01 pH scale. The pH meter principle is dependent on (Nernst's law) which involves the balance of the concentration of H^+ from the central mixture and H^+ from the outward mixture, and in turn, it generates a specific potential among the anode and the cathode. The pH electrode has a measurement range that is from 0.0 to 14.0. The faintness of this type of pH sensor has a stiff shape, comparatively big (it requires reference electrodes), and brittle (the glass membrane part) [71-74]. Figure (1.13) shows the developed of pH sensors.

In recent days, various attempts have been made to the developed instrument to measure the pH of the solution. One of them being developed is a pH sensor dependent on optical fiber. Optical fiber was widely studying for many applications including sensors [75-79]. This kind of pH measurement method is still developed since the research started [80-82].

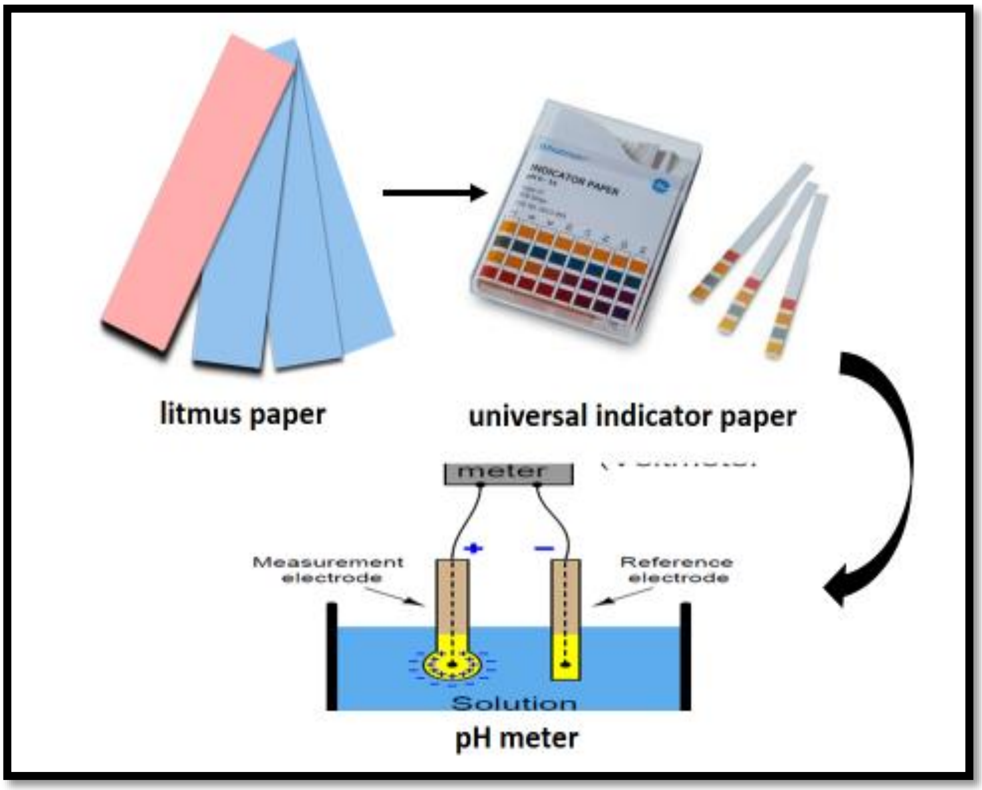

Figure (1.13): The developed of pH sensors.

The popular one is a pH sensor based on optical fiber that is coated with active materials which sensitive to H^+ activity in solution by using sol-gel or hydrogel technique. The active material is used to replace the cladding layer on the fiber optic. The hydrogel technique can immobilize active materials on fiber optic when the porous matrix layer is formed. Then this layer will trap the active materials [81].

1.8 Operating Principle of the pH Sensor:

The SNCS structure contains an NCF spliced by a fusion splicer between two SMFs. When the incident light propagates from the input SMF to NCF, the higher-order modes will be excited when incident light was propagation from the input SMF to the NCF. These modes will interface during spreading along the NCF part, that which leads to a multimode interference (MMI)[82]. The NCF length has to be exactly chosen to have a self-image right at the SMF output. The MMI effect has been studied and the length of the NCF can be given according to equation (1.8) [9,84].

$$\boldsymbol{L}_{\mathbf{NCF}} = \boldsymbol{m}\left(\frac{3\boldsymbol{L}_{\boldsymbol{\pi}}}{4}\right) \ \textbf{With m = 1, 2, 3} \qquad \textbf{(1.8)}$$

Where m refer to self-imaging number and L_{π} is the beat length,

$$\boldsymbol{L}_{\boldsymbol{\pi}} = 4\ \boldsymbol{n}_{\mathbf{NCF}}\ \boldsymbol{D}_{\mathbf{NCF}}/3\boldsymbol{\lambda}_{\mathbf{0}} \qquad \textbf{(1.9)}$$

According to MMI theory, the interference wavelength can be given from the following formula [83]:

$$\boldsymbol{\lambda}_{\mathbf{0}} = \boldsymbol{m}\left(\frac{\boldsymbol{n}_{\mathbf{NCF}}\ \boldsymbol{D}_{\mathbf{NCF}}^{2}}{\boldsymbol{L}_{\mathbf{NCF}}}\right) \qquad \textbf{(1.10)}$$

Where m, L_{NCF}, D_{NCF}, and n_{NCF} are interference number, length of NCF, the diameter of NCF, and the effective refractive index, respectively.

The planned sensor performance is essentially associated with the difference in the refractive index between NCF and surrounding medium. The change in pH levels, the change RI around the NCF region, thus would change in the output wavelength [84].

1.9 Multi-Mode Interference (MMI) Optical Fiber Sensors:-

Multi-mode interference (MMI) Optical Fiber sensor within a segment of multi-mode fiber (MMF) provides a useful basis for emerging a variety of optical fiber devices and sensors, filters, RI sensors, temperature sensors, pH sensors [85]. These sensors have properties of operating over moderate distance with good optical power, cost-effectiveness, and high sensitivity [86].

To use multi-mode interference devices in sensing systems, the physical variable capable of either modifies the multi-mode fiber parameters or interacts with the modes of propagating. MMI sensor is usually fabricated by a splicing piece of MMF between two single modes fibers [87]. The length and diameter of MMF play an important function in the formation of propagation modes.

Environmental changes affected the effective refractive index and resulted in variation in central wavelength which is the key parameter in MMI sensor detection. The incident field from SMF higher-order modes will be excited together with the fundamental mode of the NC fiber. These modes interfere along the NCF length and are subject to the multimode interference effect then these modes are recombined in the other end of SMF at the second splicing point [87]. Therefore, that the length and diameter of NCF plays important role in the formation of these multimode interference phenomena.

1.10 Coating Material:

In this work, several coating materials have been used such as polymer, nanoparticle, and dye, which are used to enhance pH sensor sensitivity.

Consider polyvinyl alcohol (PVA) is biocompatible, non-toxic, and can be straight handled with biological membranes. Also, it has promising features such as a water-soluble polymer, easy to form, cost-effective, and has good flexibility, with good thermal properties, excellent sensitivity, and exhibits fast dynamic response [38,95,96].

On the other side, Silicon Dioxide (SiO_2) has been a topic of intense research due to its stellar chemical and physical features. SiO_2 attracts significant interest in the optoelectronics proposed studies, which it is inexpensive to produce, easy to prepare, and are used as additives or modifier in the formulation of plastics, paints, and rubber [90]. Generally, PVA has a good capability for film-forming with SiO_2 which has a refractive index comparable to that of silica material. Also, SiO_2 based-polymer films have excellent thermal stability with promising strength features of the resulting composites [92-93].

While, PAA accepts a compact (but not fully collapsed) spherical conformation. the ionization occurs when pH increase and the polymer swells into a fully solvated open coil conformation [93]. PAA is a significant manufacturing polymer, with a mainly significant role in dispersants, larger molecules are less effective so, smaller molar mass polymers are regularly used [93].

Methyl red (MR) is an organic semiconductor material, specifically an azo dye indicator, which has acid dissociation constant (pK_a) of 5.1, and sampled as 2-(N, N-dimethyl-4-aminophenyl, and is a dark red crystalline powder. MR is is a dark red crystalline powder that exhibits insoluble in water, but it shows to be a high response to humidity and acts as a pH indicator dye. It is usually utilized as an indicator for acid-base solutions, in which its color is red in acidic solutions, and yellow in basic solutions; it has been explored as a promising enhancer of (sonochemical) damage of chlorinated hydrocarbon pollutants [94].

1.11 Literature Review:

All-fiber interferometers sensors have played an important role in both fundamental and applied research during the past ten years. Fiber interferometer has been proposed and constructed experimentally with different optical fiber types and configurations. The survey will be focused on this approach. The most significant published works are listed in the Table (1-1).

Table (1-1): List of the Published Works in OFHS

Year	***Author***	***Structure and illumination source and coating***	***pH range and the Sensitivity***	***Ref.***
2013	Shao, et al.	The SMF-small core of SMF-single-mode fiber structure (SMF-SCSMF-SMF), Broadband source (1500-	pH ranged from 4.66-6.02	[95]

		1600)nm coating with (PDDA) Poly diallyldi methyl ammonium chloride) and (PAA)	Sensitivity 117 arbitrary unit (a.u.)/pH unit	
Dece. 2013	Bastien Schyrr, et al.	PMMA optical fibers Broadband source (400-700) nm with coat Tetraethyl orthosilicate (TEOS),	PH ranged from 3-9. Sensitivity 0.2 pH unit	[96]
February 2015	Jakub Zajíc, et al.	Polymer clad silica (PCS) fibers coated with three types of absorption pH indicators, namely, methyl, light source (400-1000nm)	pH ranged from 3.1-7.6 Sensitivity 0.11/pH unit.	[97]
March 2015	Pengbing Hu, et al.	PCF coating PVA/PAA hydrogel by using 1500-1600 nm Super Luminescent Diode.	pH ranged from 2.5- 6.5 Sensitivity 0.9 nm/pH	[21]
APRIL 2016	Yangzi Zheng, et al.	(HCPCF) Hollow-core photonic crystal fiber coated (PVA)/(PAA)hydrogel, Broadband source (1500-1600nm),	pH ranged from 4.1- 6.9. Sensitivity 11 nm/pH	[6]
2016	Satyendra Kumar Mishra,	(LPFG) coated with hydrogel, Broadband source (1500-1600nm),	pH ranged from 2–12. Sensitivity 0.66 nm/pH	[22]
May 2017	Vanita Bhardwaj, et al.	SNC, broadband source (1400 to 2000) nm coated with tetraethyl orthosilicate (TEOS).	pH ranged from 2-13 Sensitivity 1.02 and −0.93 nm/pH	[7]

Sept. 2017	Akhilesh Kumar Pathak, et al.	NCF sensor using hydrogel coating for pH measurement white LED, light (1400-1600nm).	pH ranged from 3-10. Sensitivity 1.94 nm/pH	[23]
Aug. 2018	A. K. Pathak, et al.	MMF coating with hydrogel over Zinc Oxide (ZnO) micro flowers, white Light Sources with Wavelength range (500–600 nm)	pH ranged from 3-11. Sensitivity 2.59nm/pH and. 70nm/pH	[98]
Sept. 2018	Jianxin Zhang, et al.	SNCS fiber structure coating with tetraethyl orthosilicate (TEOS) and cellulose acetate, Broadband source (300-600 nm)	pH ranged from 2.5–11. Sensitivity 0.2 nm/ pH	[99]
Dec. 2019	Magnus Engholm, et al.	Mach-Zehnder based on thin core fiber spliced between two standard single mode fibers, coated with 1.3-BDDA and PIP	pH ranged from 1.95-11.89 Sensitivity 3.5 nm/pH	[1]
July 2020	M. Hussayeen, et al.	PCF sensor based on surface plasmon resonance using gold layer as plasmonic metal along with a TiO2 layer, Broadband source (1500-1950 nm)	pH ranged from 2.51-1.90 sensitivity 229.2 nm/pH	[100]

1.12 Aim of the Work:

1. Fabrication a simple, low cost, ecofriendly and compact optical fiber pH sensor based on tuned length and diameter of No-core fiber as a pH sensor.

2. Testing the sensitivity of the system by varying coating material like PVA/PAA, SiO_2@PVA/PAA, and MR@PVA.

Chapter Two

Experimental Setup and Procedures

2.1 Introduction

In this chapter, all parts of the system were explained. The experimental setup and work procedure for the fabrication of pH sensors based on SNCS fiber structure and Multimode Interferometer (MMI) were illustrated. Many types of interferometers have been established and investigated. MZI is one of the most promising interferometers used in the sensing field for monitoring and measuring a parameter of pH. SNCS fiber sensors were fabricated and constructed by cleaving and splicing different lengths of NCF (from Thorlabs) with conventional optical fiber (SMF-28).

Sensor sensitivity was enhancement by the etching process which applied to NCF to tune its diameter or coated the active segment of the sensor with a nanomaterial.

2.2 System Layout:-

The pH sensor based on the SNCS system layout is shown in figures (2.1).

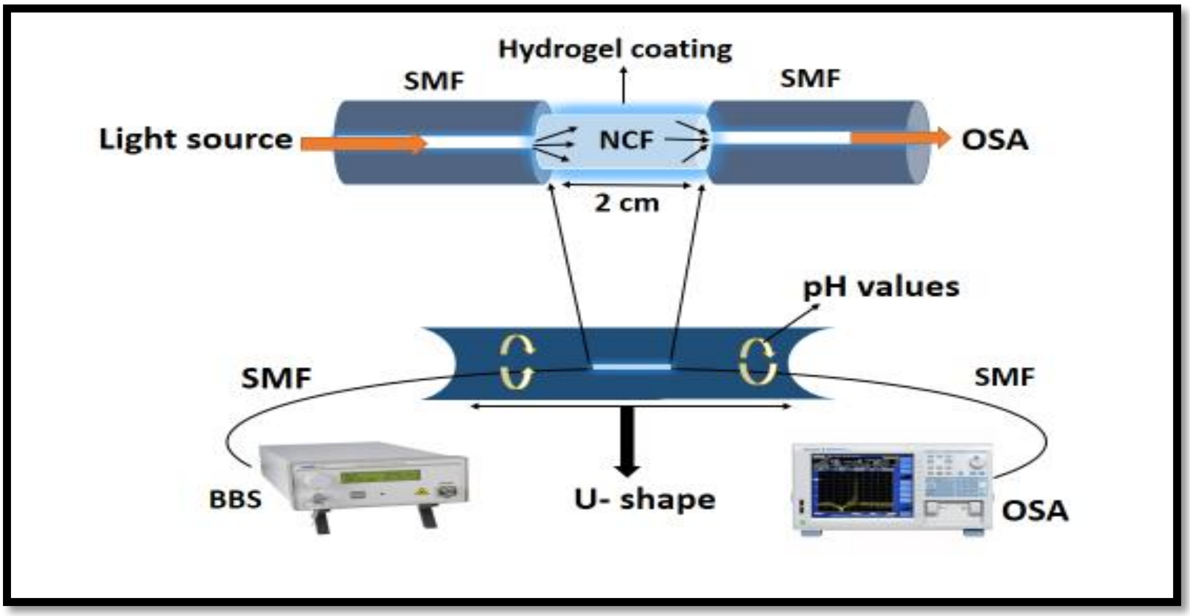

Figure (2.1): The experimental setup for measuring the pH based on SNCS fiber structure.

2.2.1 Broadband Source (B.B.S):-

In this experiment, a butterfly-packaged Super-Luminescent Diodes (Thorlabs SLD1550s-A1) with 1400-1600 nm emission range has been used as a broadband light source, as shown in figure (2.2). This source has excellent power, near-Gaussian as well as low-ripple.

This device is constructed into a 14-pin butterfly set with a joint thermistor and a thermoelectric cooler (TEC) to prove the stability of the output light. The output is coupled into an SMF that ended with a 2.0 mm fine knob FC/APC adapter. (Appendix A)

Figure (2.2): Photo-image of Broadband source (B.B.S).

2.2.2 Single-Mode Fiber (SMF-28):-

Single mode fiber (SMF-28) is considered the "standard" optical fiber for submarine, telephony, cable television, and private network applications in the transmission of data, voice and \ or video services. The SMF-28 was fabricated to operate in the 1310 nm and 1550 nm wavelength region with the lowest dispersion and the highest capacity of information-carrying. The SMF-28 has robust geometric characteristics such as low attenuation and high strength. Corning single-mode fiber can be used for excellent delivery performance and high precision [Appendix B]. The top view of SMF-28 under a microscope is shown in figure (2.3), which shows the quality of the cleaved end of SMF.

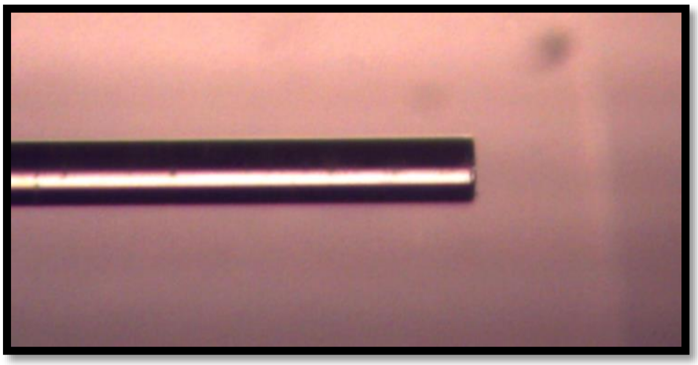

Figure (2.3): Top view for the SMF under an optical microscope with magnification power (4x) magnification.

2.2.3 No-Core Fiber (NCF):-

No-core fiber (FG125LA from Thorlabs Company) has been used in this experiment. It considers a special type of multimode fiber with an outer diameter of 125 µm could be spliced to the ends of SMF. Moreover, NCF considers a special type of multi-mode fiber when it's spliced to the ends of SMF, NCF operated with a wide wavelength range with return loss > 65 dB. NCF has a different operating wavelength at different refractive indexes, where NCF has RI about 1.444 at wavelength 1550 nm. The optical specifications of NCF are given in table (2.1).

Table (2.1): Optical specifications of NCF [from Appendix C]

Wavelength range (nm)	**400-2400**
The diameter of Glass (µm)	125±1
The diameter of Coating (µm)	250±5%
Operating Temperature C°	-40 to 85
Glass Refractive index and operating wavelength	1.444 @1550 nm, 1.450703 @1020 nm, 1.458965 @ 589.3 nm 1.467287 @ 436 nm

2.2.4 Optical Spectrum Analyzer (OSA):-

OSA (YOKOKAWA, Ando AQ6370) has been utilized to monitor the variation in the interference spectra of the OFpHS. It is a precision tool used to calculate and displays the power distribution of the optical source above a specific wavelength span. And it trace displays the wavelength on the horizontal scale, while on the vertical scale is power. The picture of OSA which using in the experimental set-up is shown in figure (2.4). Table (2.2) shows the main characteristic of OSA.

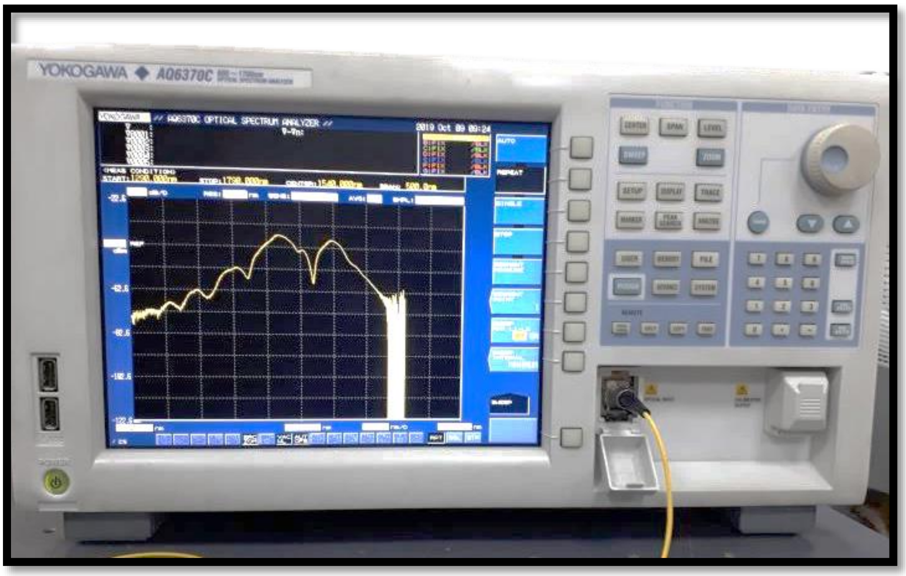

Figure (2.4): Photo-image of the optical spectrum analyzer (OSA).

Table (2.2): OSA Characteristics used to perform this work.

Wavelength range	**600 nm to 1700 nm**
High wavelength accuracy	± 0.01nm
Wide Dynamic range	78 dB type.
Fast measurement	0.2 sec. (100nm span)
Wide level range	+20 dBm to -90 dBm
High wavelength resolution	0.02 nm
applicable to	SMF, MMF Patch cable fibers

2.2.5 U-shaped or U-groove:

U-shape is a homemade container look like U-shaped from the side which made from plastic material and it used experimentally by filling it with different pH range and the dipping the fiber in it. It was noted that it was not affected by the chemicals used in pH range, as shown in figure (2.5).

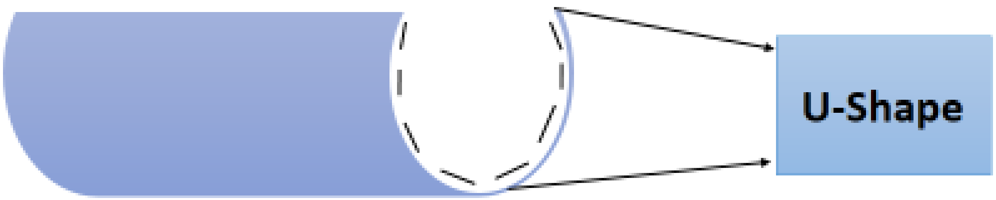

Figure (2.5): U-shape.

2.3 Experimental Procedures

Experimental procedure divided into two steps to fabricate an optical fiber pH sensor based on SNCS fiber structure. The schematic block diagram summarizes the experimental work as shown in figure (2.6).

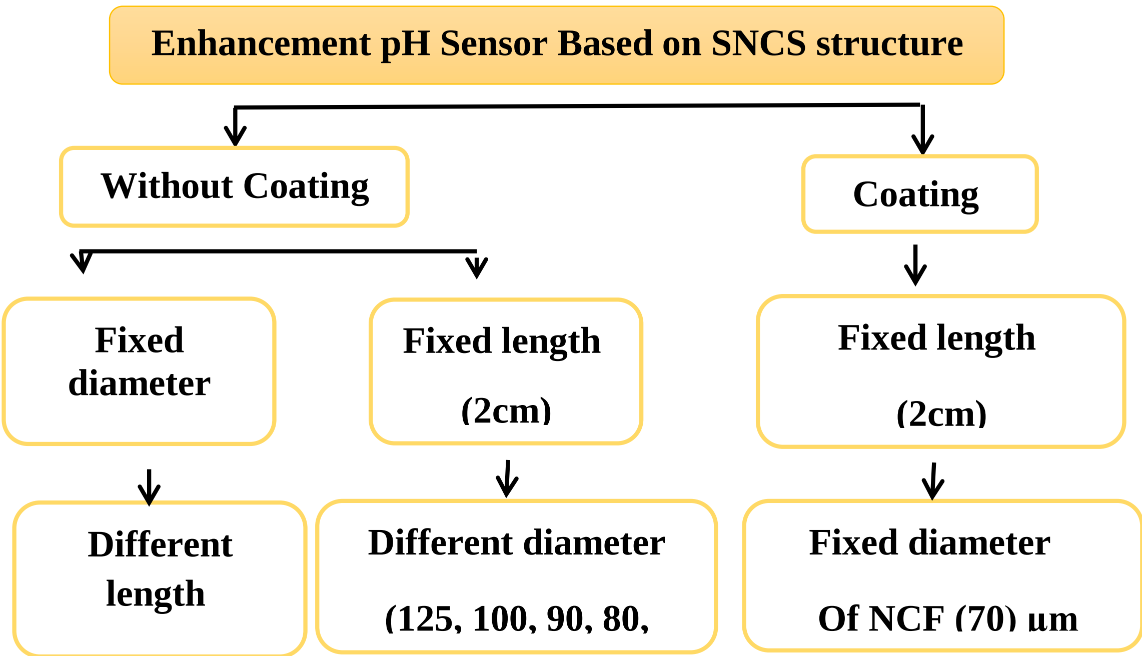

Figure (2.6): The schematic block diagram of experimental work.

2.3.1 Singlemode-No-Core fiber-Singlemode (SNCS) Structure:

SNCS sensors have been designed and constructed by cleaving and splicing NCF (FG125LA Thorlabs, 2 cm in length) between two conventional optical fibers (SMF-28), as shown in figure (2.7). The SMFs have core and clad diameters of 9 µm and 125 µm, respectively. The NCF has a cladding diameter of 125 µm, and then the optimum parameters of no-core fiber length was testing with different NCF diameters.

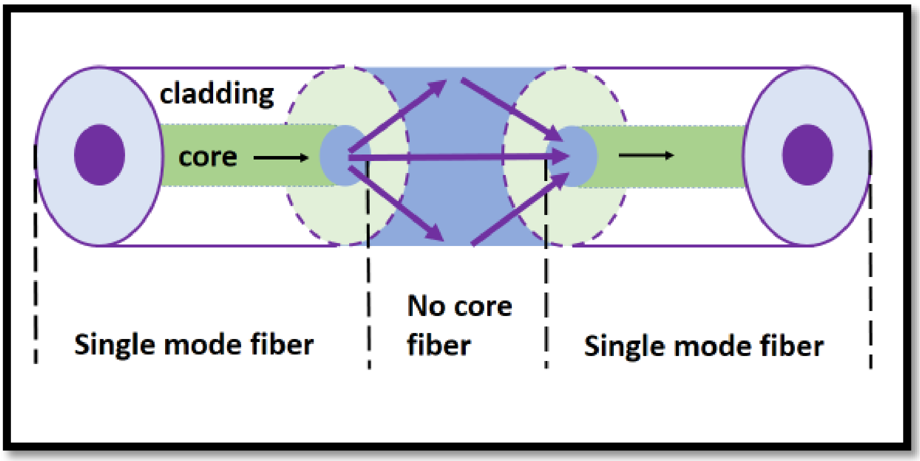

Figure (2.7): Schematic of the SNCS structure.

2.3.2 NCF and SMF Cleaving:

To prepare the NCF and SMF for fusion splicing, firstly cleaving fibers was done by removing the protective polymer coating before splicing to minimize splicing loss and obtain good splicing characteristics. Removing the protective polymer layer could be done by alcohol or mechanical stripping. In this experiment mechanical Fiber Stripper (JIC – 375 Tri – Hole) was used to remove the polymer layer. Secondly, the optical fiber cut with the right angle using the cleaver machine (CT-30) (Fujikura).

The optical fiber cleaving allows the clamping of the fiber into the specified position, also presented to make an optical fiber flat face and perfectly smooth. By putting the edge of the optical fiber above the cutting blade of the cleaving machine, a cleaved end surface of optical fiber with 90^0

angles and flat cleaved surfaces can be obtained. Finally, the fiber was cleaned with a wet wipe or alcohol or other any solvent. Figure (2.8) Top view of NCF under an optical microscope, which shows the edges of the fiber were well-cleaved.

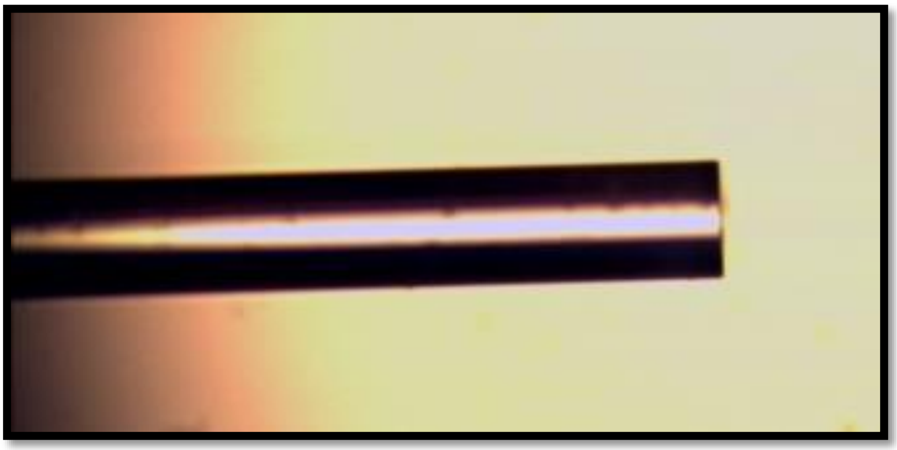

Figure (2.8): Optical microscope images of NCF end after cleaving under 4x.

2.3.3 NCF and SMF Splicing.

Splicing is the process of connecting two segments of optical fibers like NCF and SMF. In this experiment, a Fusion splicer from Fujikura (FSM-60S) splicing machine, is used in AUTO_MODE to fusion splice the SMF has core and cladding refractive index 1.451 and 1.444 respectively. The NCF has a diameter of 125 with a 1.444 refractive index, so the same refractive indices and diameter for the SMF and the NCF. This compatibility made the splicing easier and homogeneous.

The NCF ends with different diameters and lengths are cleaved according to a certain length range and both ends are spliced with two standard SMFs-28 using the electric arc technique. A fusion splicer with automatic mode was used to form SMF-NCF-SMF (SNCS) structure with a reiterated arc discharge technique to minimize the splicing loss as much as achievable as shown in Figure (2.9). In general, fusion splicing based on the electric arc technique has been most utilized and has been much best created than the other techniques.

SMF-28 of 125 µm diameter was spliced to the NCF at a diameter of 125 µm and length at 2 cm on from both sides. AUTO MODE function is using in the fusion splicer menu (Fujikura FSM-60S) with a low loss, and good mechanical strength. For each splicing region the loss of splicing about 0.01 dB, where prepared different lengths of NCF with a fixed diameter, after study the influence of the length, and then, the best length with different diameters were tested. The diameters of NCF recalculated to be (100, 90, 80, and 70) µm by using chemical etching.

Figure (2.9): Fusion splicer between NCF and SMF.

2.3.4 NCF Etching Procedures:

One of the mechanisms used to improve the sensitivity of SNCS structure is the chemical Etching process to decreasing the NCF diameter. The hydrofluoric acid (HF) was used to reduce the NCF diameter to obtained different diameters of 100, 90, 80, and 70 µm respectively. The purpose of optical fiber etching to allow more interaction of propagating light with pH.

Etching time is the important factor which adjusted carefully to control the diameters of the NCF. The diameter of NCF needed etching time of about 12 min to decreased the diameter from 125µm to 100 µm, and 17, 22, 27 min for each 90µm, 80µm, and 70µm diameter respectively. The rate of average-etching was ~2.14 µm/min at room temperature. From all these results, a calibration curve can be illustrated as in Figure (2.10).

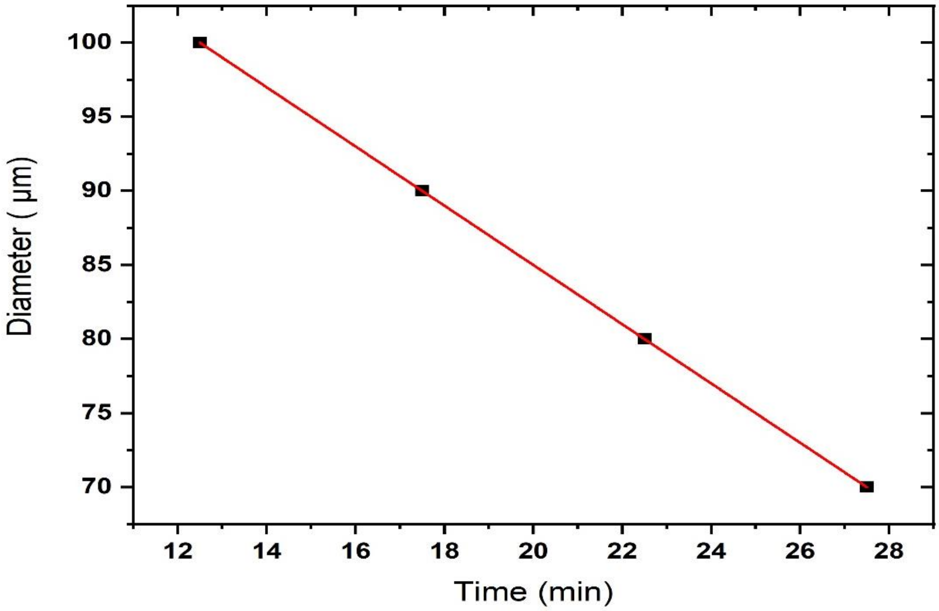

Figure(2.10): Calbration curve of diameter as a function of time.

In this work, The SNCS fiber structure fixed on both sides and the NCF segment emerged in the hydrofluoric solution HF (~ 40%) using a quartz U-shape groove. NCF diameter was reduced to 70µm by controlling the etching time. In this step, the NCF length was fixed on 2 cm.

To see top view NCF after the etching process, a transmission optical microscope from (Euromex Company, Holland) was used. This microscope has different magnification power (4 X, 10 X, 40 X, and 50 X). Figure (2.11) shows microscopic images of NCF etching with different diameters imaged under an optical microscope.

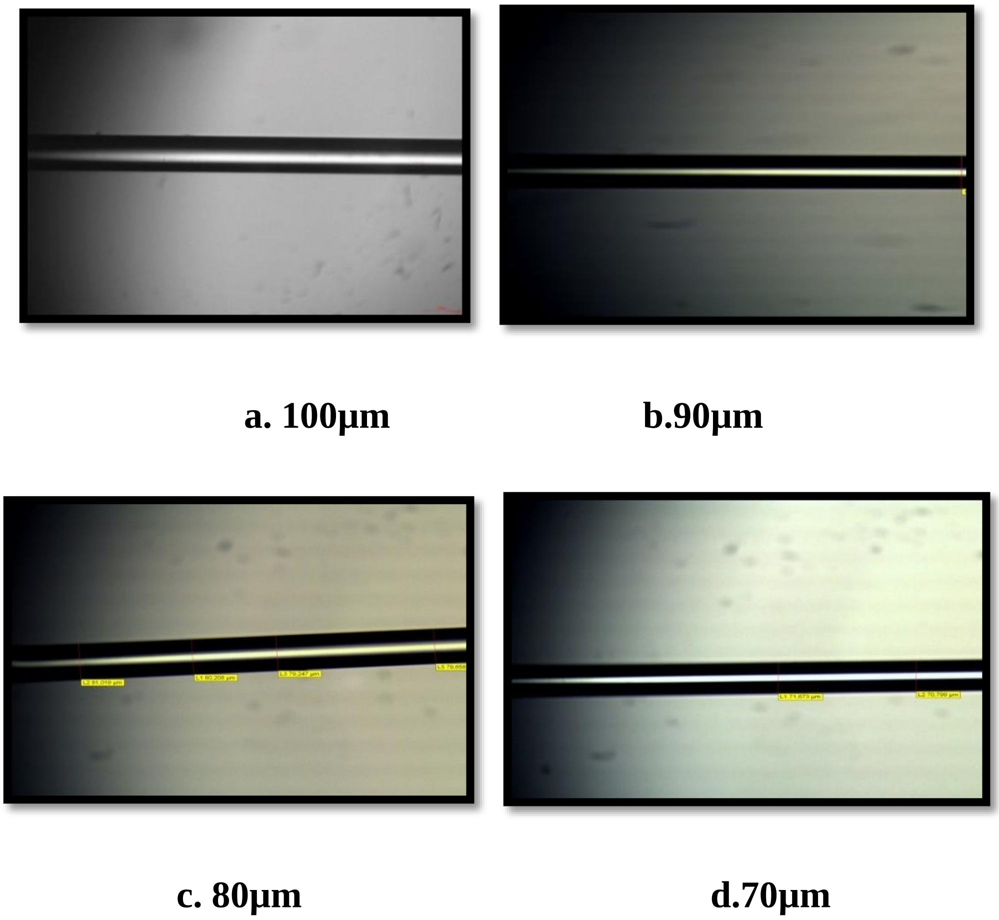

Figure (2.11): Optical microscopic image of NCF diameter etching (a) 100 µm (b) 90 µm (c) 80 µm (d) 70 µm with 4X.

2.3.5 Hydrochloric acid (HCl) and Hydroxide Sodium (NaOH) Solution Preparation:

The testing solution of pH levels from 1-7 was prepared by taking different concentration values from (Hydrochloric acid). 5 and 75 ml of HCl diluted in deionized water of 100 ml. By the magnetic stirrer, the concentration was exactly mixing at room temperature (25 C^{o}). Then 5% was dilute to obtain the rest of the ranges.

While, the testing solutions of pH levels from 8 to 14 are prepared by taking different concentration values from Hydroxide Sodium (NaOH). 0.5, 1, 5, 10, and 25 mg of NaOH dissolved in deionized water of 100 ml. By the magnetic stirrer, the concentration was exactly mixing at room temperature (25 C^{o}). Then these concentrations were diluted to get different values of pH.

The preparation of different concentrations of pH (1-14) and their refractive index was showing in the Table (2.3).

Table (2.3): Refractive index and Preparation of pH levels from (1 to 14).

pH	CON. Of acid	RI	pH	CON. Of base	RI
pH 1	75% Hcl	1.3426	pH 8	0.01ml from 0.5%	1.3435
pH 2	5% Hcl	1.3428	pH 9	0.03ml from 0.5%	1.3436
pH 3	8ml from 5%	1.3430	pH 10	0.06ml from 1%	1.3437
pH 4	0.8 from 5%	1.3431	pH 11	0.1 ml from 3%	1.3438
pH 5	0.1 from 5%	1.3432	pH 12	0.5ml from 5%	1.3439
pH 6	0.02from 5%	1.3433	pH 13	5ml from 10%	1.3440
pH 7	DI water	1.3434	pH 14	25% from NaOH	1.3442

The testing solutions with different concentrations are used as samples with different RIs. Abbe refract meter (Abbe refract meter is a bench-top device utilized for refractive index measurement with a high degree of accuracy. Analogue Abbe Refract meter (AR4) fabricated by Krüss is used for refractive index measurement. AR4 offers reading via an eyepiece.

2.4 Optical Fiber pH Sensors based on Multimode Interference Using SNCS Setup:

The SNCS fiber structure was designed and fabricated. The sensor was tested by studied the influence of two parameters, the length and the diameter of the NCF segment. The following procedures to study the effect of those parameters were illustrated in this section on the optical fiber pH sensor sensitivity. The sensor was fabricated using fusion splicing of four different lengths of NCF: 1, 2, 3, and 4 cm in-between two SMFs. The resultant SNCS were tested as optical fiber pH sensors when the pH changed from 1-7 and 8-14 for acid and base, respectively. SNCS structure with 2 cm of the NCF length was etched from 125 µm to 100, 90, 80, and 70 µm by chemical etching.

The influence of length and diameter on the pH sensor sensitivity of optical fiber was tested. After testing the sensor, the NCF was coating with a thin layer from PVA/PAA and SiO_2/PVA/PAA for acid and base, respectively. Then NCF coated with Methyl red@PVA for acid and base, which these different coating acts as a cladding for NCF instead of air with optimum parameters of NCF length and diameter for further more enhancement of the sensitivity.

2.5 Preparation of PVA/PAA and SiO_2/PVA/PAA Composite:

After the etching process, two NCF sections were coated with hydrogel coatings using the PAA/PVA and SiO_2@PVA/PAA, respectively. Both coating composite preparation and structure coating processes are shown in Figure (2.12).

After fabrication of the SNCS fiber structure with the optimum NCF length and diameter, the coating process was prepared using the drop-casting method in three main stages. Firstly, a mixture of PVA and PAA with a volume ratio of 8:1 [21] was used to prepare a polymeric aqueous solution with 11 wt. % by dissolving and diluting this mixture in distilled water under magnetic stirring for 1 h at 90°C. The solution was thereafter left to cool at room temperature. Then, NCF segments were decorated with PVA/PAA composite and left to dry at room temperature for 24 h and after that left to cross-link at 50 °C for 15 min. Finally, the NCF section with the uniform coating with 6 μm thickness was obtained which measured in optical microscope.

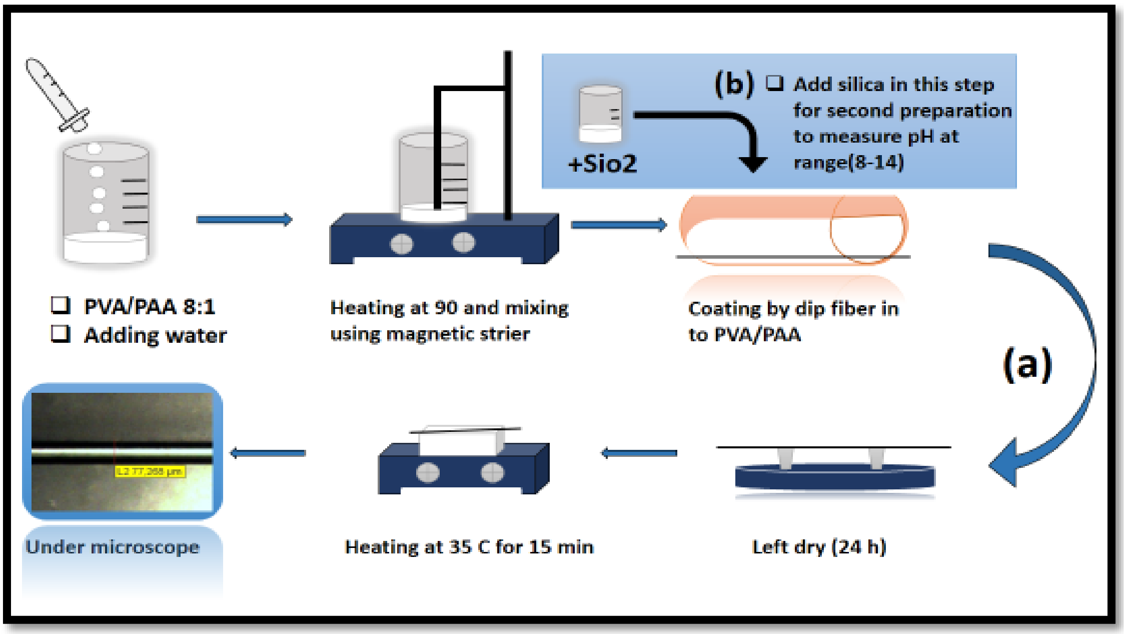

Figure (2.12): The preparation coating process (a) PVA/PAA coating (b) SiO_2@PVA/PAA coating.

While in second coating we add silica (SiO_2) which particle size 20-40 nm as shown in Figure (2.13). Silica based hybrid materials have demonstrated attractive electronic, optical and chemical properties. The properties of silica nanoparticles have been carefully investigated to understand their behavior under different conditions, including the surface charge density and the aggregation of these particles as a response to pH changes. Silica has also been utilized as a substrate material for pH sensing[101].

The process of the preparation of the fiber sensor based on SiO_2@PVA/PAA is as follows. At the first, the SiO_2@PVA/PAA solution was prepared by mixing 5 mg of SiO_2 nanoparticles with 10 ml of PVA/PAA solution was prepared above. Then, the mixture was stirred at a moderate rate with a magnetic stirrer for 1h to obtain a homogenous solution. To remove the effect of bubbles, the solution was let to them settle for two hours.

Then, NCF segments were decorated with SiO_2@PVA/PAA composite and left to dry at room temperature for 24 h and after that left to link at 35 °C for 15 min, Finally, NCF section with uniform coating ~8 μm thickness were obtained which measured in optical microscope.

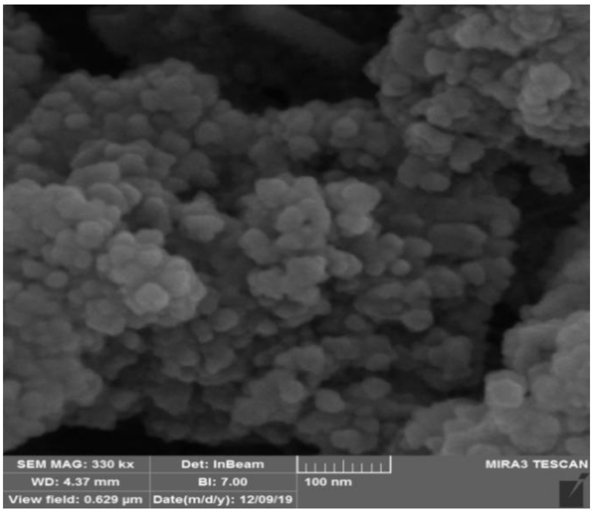

Figure (2.13): SEM images of SiO_2-NPs at 100 nm scales.

2.6 Preparation of Methyl red@PVA Composite:

NCF section of 70 μm diameter was coated with hydrogel coatings using Methyl red@PVA. The coating composite preparation and structure coating processes are shown in Figure (2.14).

After fabrication of the SNCS fiber structure with the optimum parameter of NCF length and diameter, the coating process was prepared using the drop-casting method in three main stages. Firstly, a mixture of SDS and with 1:1 was used to dissolve methyl red because it's insoluble in water.

Secondly, a mixture of PVA and methyl red with a volume ratio of 10:10 was used to prepare a polymeric aqueous solution by dissolving and diluting this mixture in distilled water under magnetic stirring for 1 h at 90. Then, NCF segments were decorated with methyl red@ PVA composite and left to dry at room temperature until drying. Finally, the NCF section with the uniform coating with 8 μm thickness was obtained.

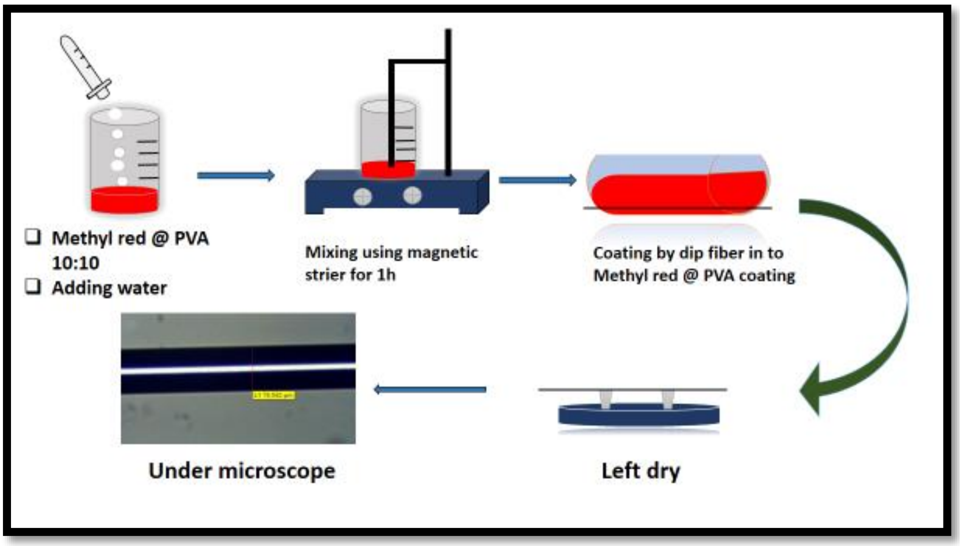

Figure (2.14): The preparation methyl red@ PVA coating process.

2.7 The Influence of the Coating on the pH Sensitivity:-

The SNCS structure with optimum length (2 cm) and diameter of the NCF was dipped in the different coating (silica@ PVA/PAA, PVA/PAA, and Methyl red@ PVA) which acts as a cladding for NCF instead of air then the SNCS fiber structures were tested as optical fiber pH sensor when the pH levels changed from 1-7 and 8-14 for acid and base, respectively. The influence of each coating on the sensor sensitivity was tested for furthermore enhancement of the sensitivity.

Chapter Three

Results and Discussion

3.1 Introduction

This chapter includes characteristics of the fabricated pH sensor probes which are investigated experimentally and presents the results, discussions, conclusions, and future works of the pH sensor based on multimode interference. A pH sensor has been designed and demonstrated. The influence of different lengths, diameters of NCF, and coated with different pH values were studied.

3.2 Transmission Spectrum and the Stability of SNCS Structure:

The broadband source (B.B.S) transmission stability was tested to ensure the reliability of sensor measurements. As shown in Figure (3.1), the black bold curve represents the SMF test while the SNCS is represented by the red bold curve to tests the function of the structure. This structure consist of NCF spliced between two pieces of SMFs. The one side of SMF was connected to OSA and the other side to the B.B.S as shown in Figure (3.2 bold red curves).

The next step was carried out with SNCS fiber structure at NCF diameter of 125 μm and 2 cm length. The SNCS filtered some of the wavelengths so it acts as a band pass filter due to a multimode interference where the fundamental mode from the SMF at the first splicing region will split into multimode and coupled at the second splicing region. The SNCS structure can be shown in Figure (3.2). These modes propagate along the direction of NCF and interfere with another, causing the rise in multimode interference (MMI) and re-emerged into SMF.

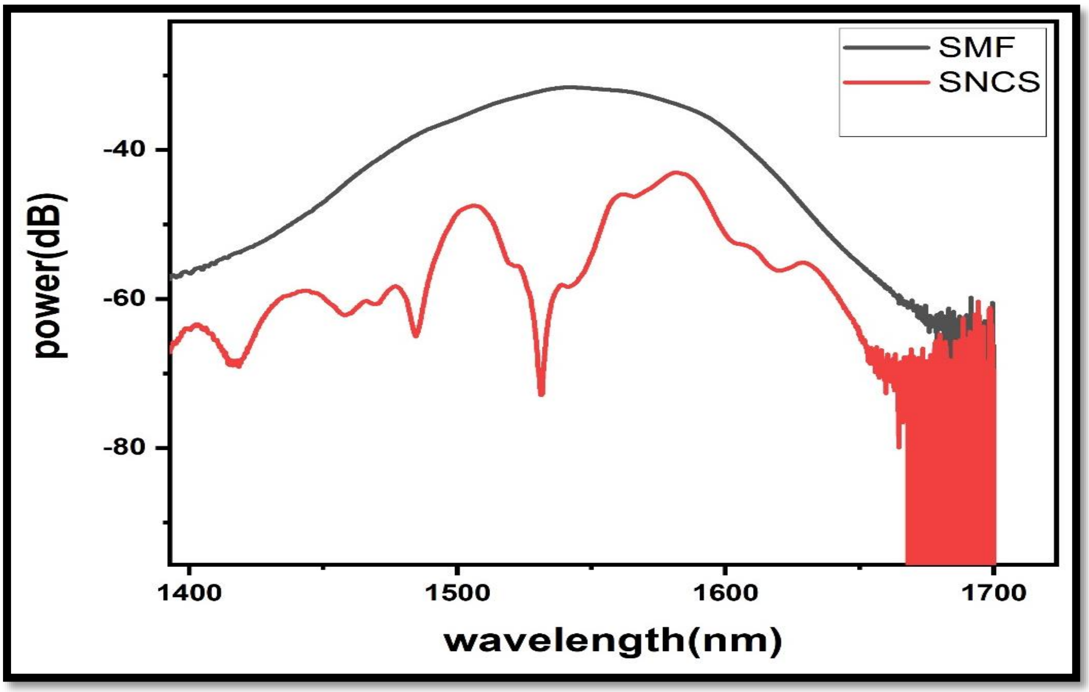

Figure (3.1): Output Spectra of B.B.S of SMF and SNCS.

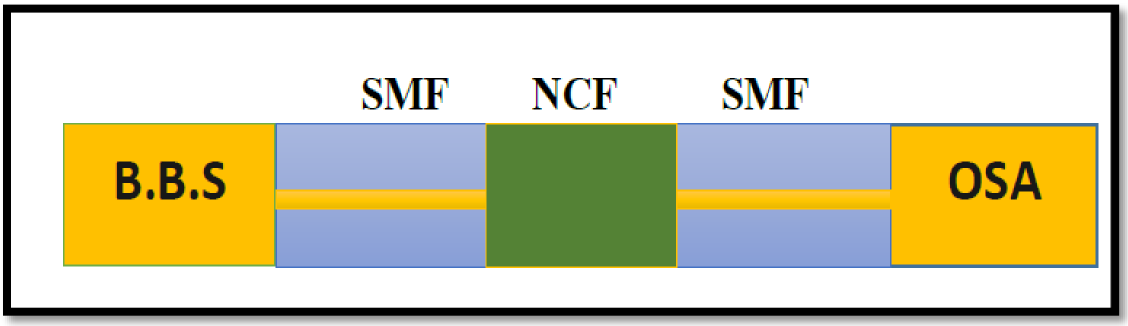

Figure (3.2): Schematic of experimental setup of SNCS.

3.3 The Influence of NCF Length on the pH Sensor Sensitivity:

In this work, the influence of the NCF length on the pH sensor sensitivity was studied by using an NCF fixed diameter of 125 µm with different NCF lengths (1, 2, 3, and 4 cm). Herein, the wavelength shift as a function of the refractive index of pH solution was clarified by the experimental result.

Table (3.1) shows the sensitivity and the polynomial fitting coefficient for different lengths of bare NCF at fixed diameter of 125 µm for both acid and base which the pH changed from (1-14).

Table (3.1): The sensitivity and the polynomial fitting coefficient for different lengths of bare NCF at fixed diameter of 125 μm for both acid and base which the pH changed from (1-14).

NCF length (cm)	Sensitivity (nm/pH) of acid	Adj. R^2 of acid	Sensitivity (nm/pH) for base	Adj. R^2 of base
1 cm	0.4	0.93	1.1	0.96
2 cm	1.19	0.93	1.02	0.93
3 cm	1.62	0.85	1.1	0.98
4 cm	0.66	0.96	0.73	0.89

From these results, it can be noted that increases in length lead to increases in sensitivity of pH sensor until reach to 4 cm length its decreases. It can be concluding that increasing in length must be limited. While R^2 for lengths from (1-3) for acid it can be noted that R^2 its highest possible at length at 2 cm, so the optimum length of our proposed structure placed at 2 cm length of NCF.

Figure (3.3) and (3.4) show the transmission spectra response of the proposed pH sensor for the acid (1-7) and base (8-14) range, respectively for the different NCF lengths. The evanescent waves that are excited will react with the environmental pH and introduce the output spectrum changing

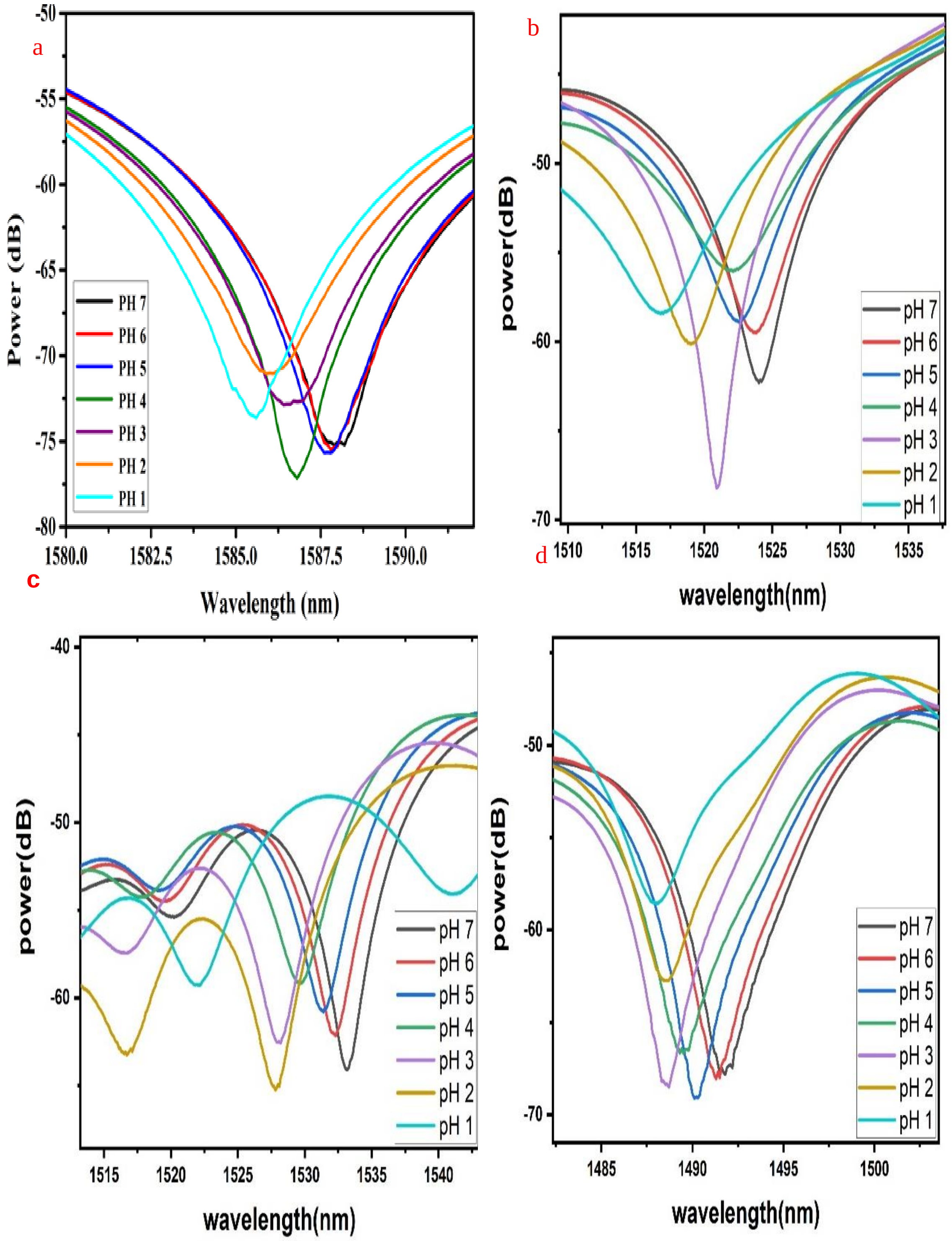

Figure (3.3): Transmission spectra response of the OFpHS as a function of pH for (a) 1cm, (b) 2cm, (c) 3cm, and (d) 4cm NCF length for acid.

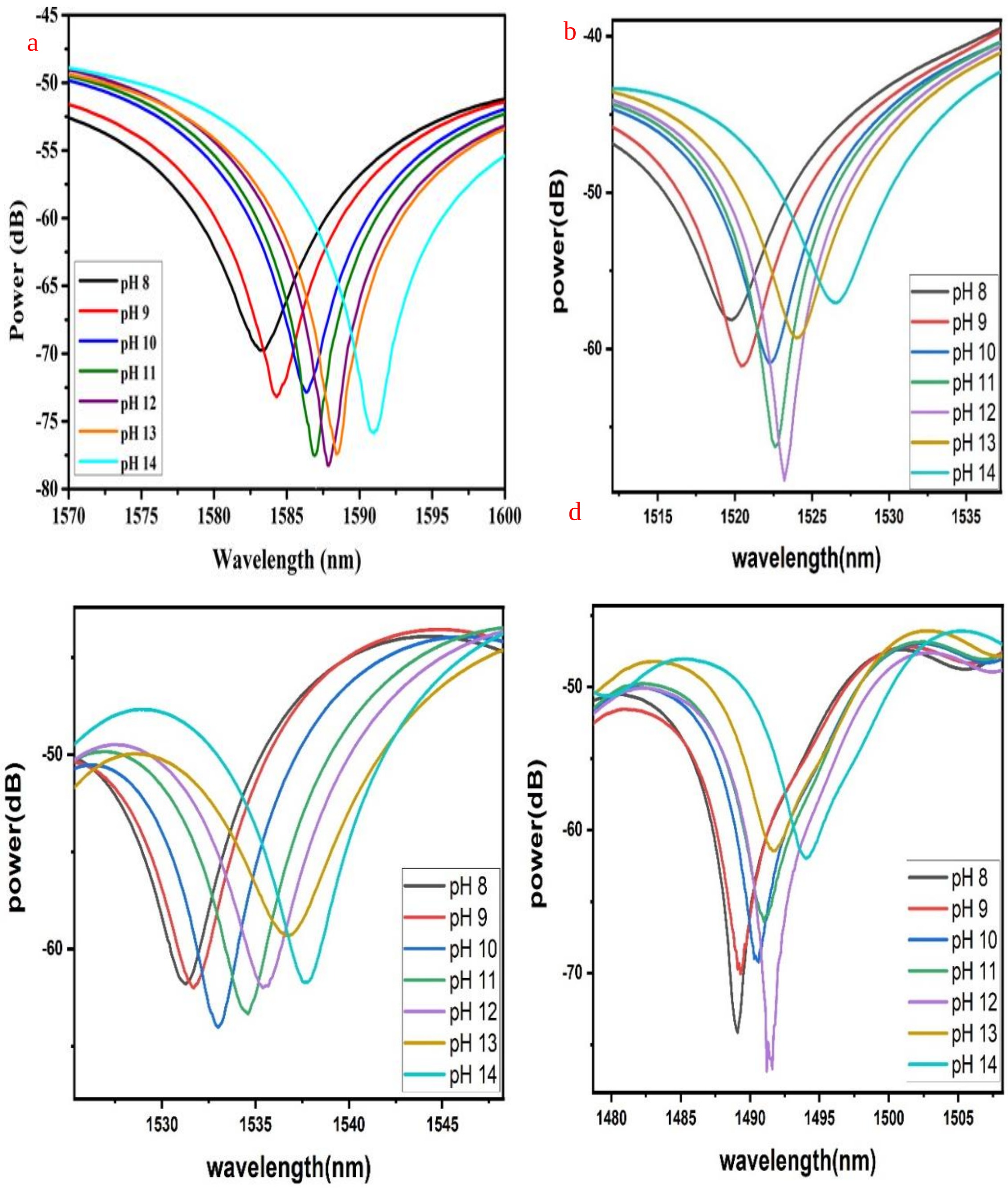

Figure (3.4): Transmission spectra response of the OFpHS as a function of pH for (a) 1cm, (b) 2cm, (c) 3cm, and (d) 4cm NCF length for base.

From these figures, it can be noticed that the transmission spectra shifted towards longer wavelengths (red shift) at each increase in pH. Because increasing in concentration of HCL for acid range from 1-7 lead to increase in RI of acid so, it's shifted toward longer wavelengths. On the other side, Figures (3.5) and (3.6) show the linear response for both pH levels 1–7 and 8-14 for acid and base, respectively. The sensitivities of the proposed sensor are calculated by linear fitting.

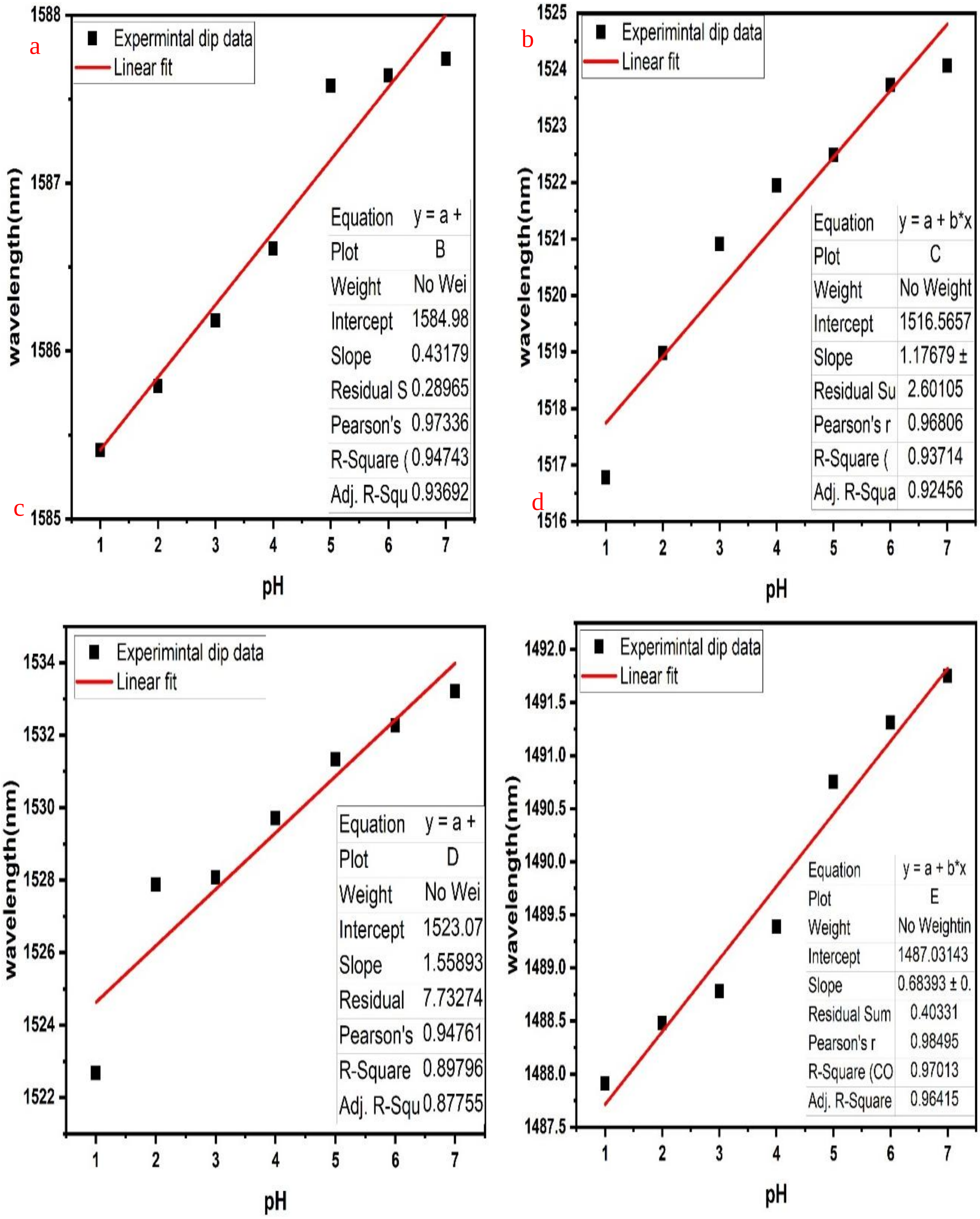

Figure (3.5): Linear fitting plots of the shifted dips against pH change in the function of wavelengths shift for (a) 1cm, (b) 2cm, (c) 3cm, and (d) 4cm length of NCF for acid.

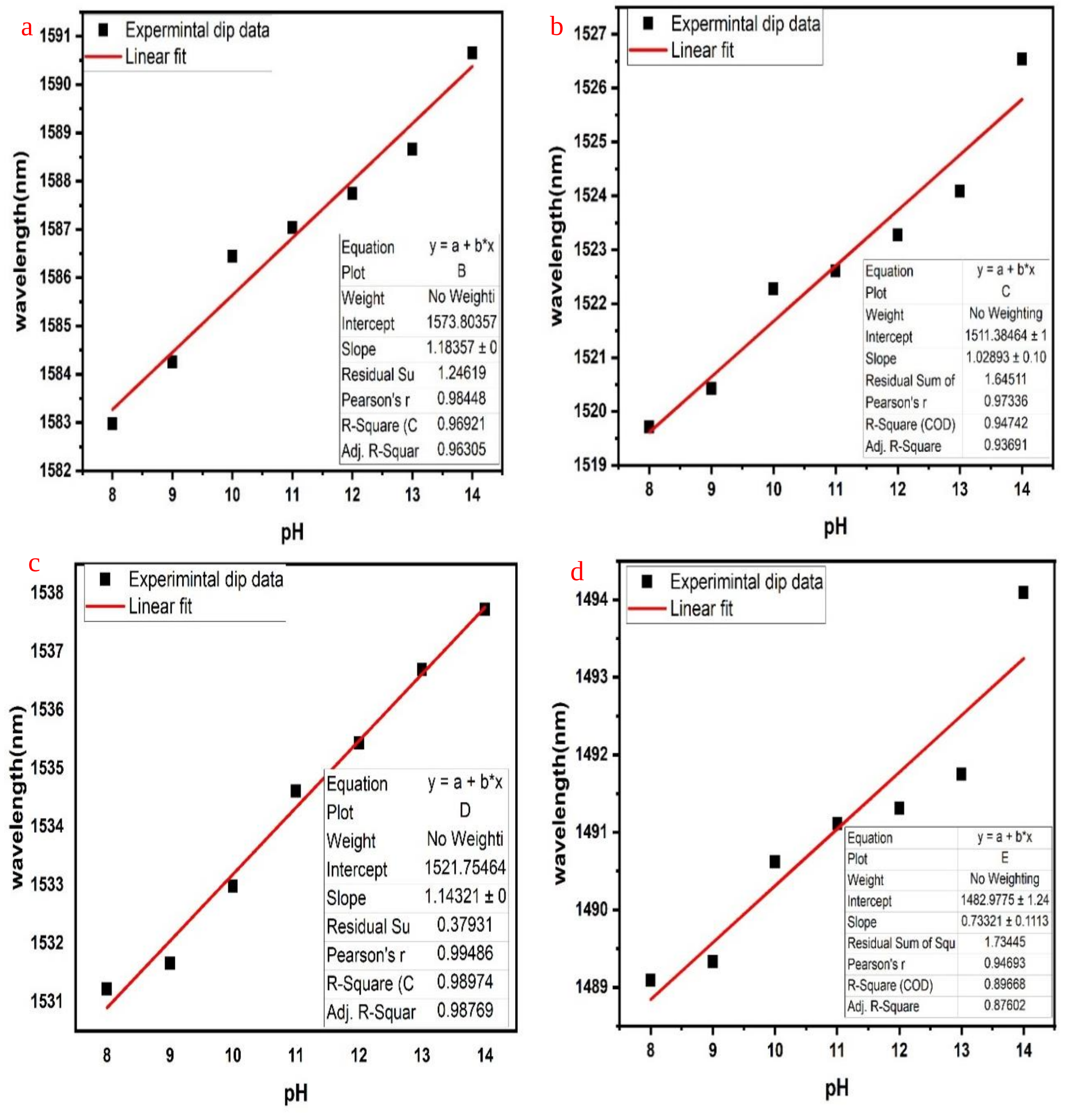

Figure (3.6): Linear fitting plots of the shifted dips against pH change in the function of wavelengths shift for (a) 1cm, (b) 2cm, (c) 3cm, and (d) 4cm length of NCF for base.

Figures (3.5) and (3.6) indicate that the better performance of the pH sensor based on NCF structure detected at a length of 2 cm, which possesses sensitivity of 1.19 and 1.02 nm/pH, and R^2 of 0.93, for acid and base respectively. Additionally, the relationship between the pH and the wavelength shift can be seen in Figure (3.7). There was a slight variation in the wavelength shift and sensitivity for different NCF lengths and fixed diameter 125 μm, because of the self-imaging on the MMI principle.

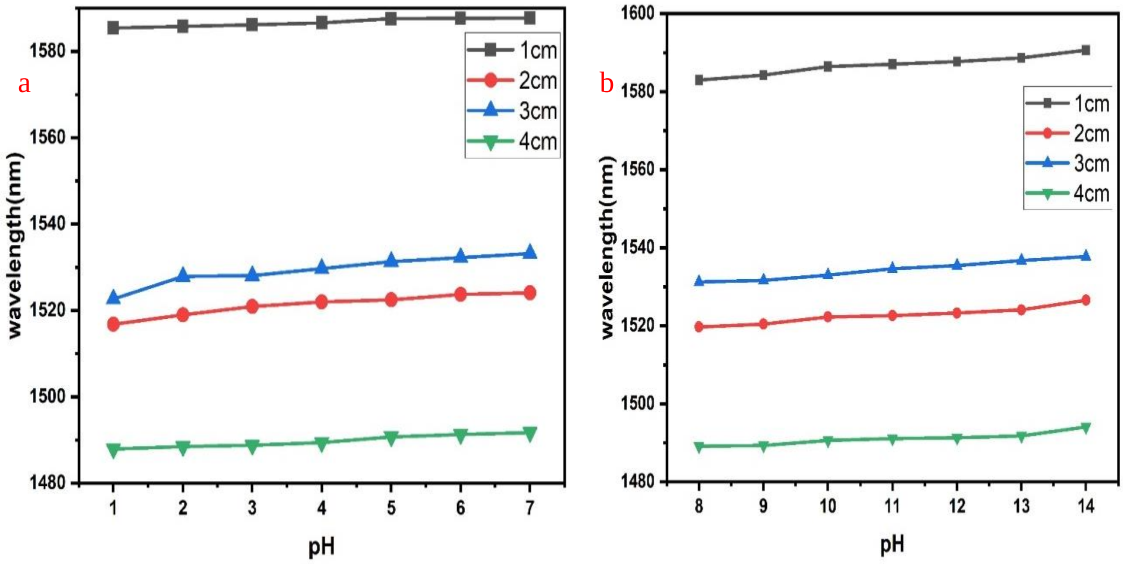

Figure (3.7): The response sensors to variations in pH from (1-14) with different NCF lengths for (a) acid and (b) base.

3.4 The Influence of NCF Diameter on the pH Sensor:

The influence of the NCF diameter on the pH sensor sensitivity was investigated by using different diameters of NCF with fixed length of 2 cm. The etching process executed by emerging the NCF in HF acid to decrease the outer diameter of NCFs from 125 μm to 100, 90, 80 and 70 μm, respectively. The response of transmission spectra of the etched NCF with the change of surrounding pH was recorded.

Firstly, the response without etching of the SNCS fiber structure at 125 μm of NCF diameter to the variations of the pH was investigated as mentioned in the previous section. After that, the fabricated sensor was placed in a U-shape equipped with different pH levels for observing the pH changes from 1-7 and 8-14 for acid and base, respectively.

Figures (3.8) and (3.9) show the transmission spectra for SNCS fiber sensors for different diameters (100, 90, 80, and 70 μm), which are depicted when changing in pH levels from 1-7 and 8-14 for acid and base respectively. It shows that the NCF diameter will directly affect the sensor sensitivity.

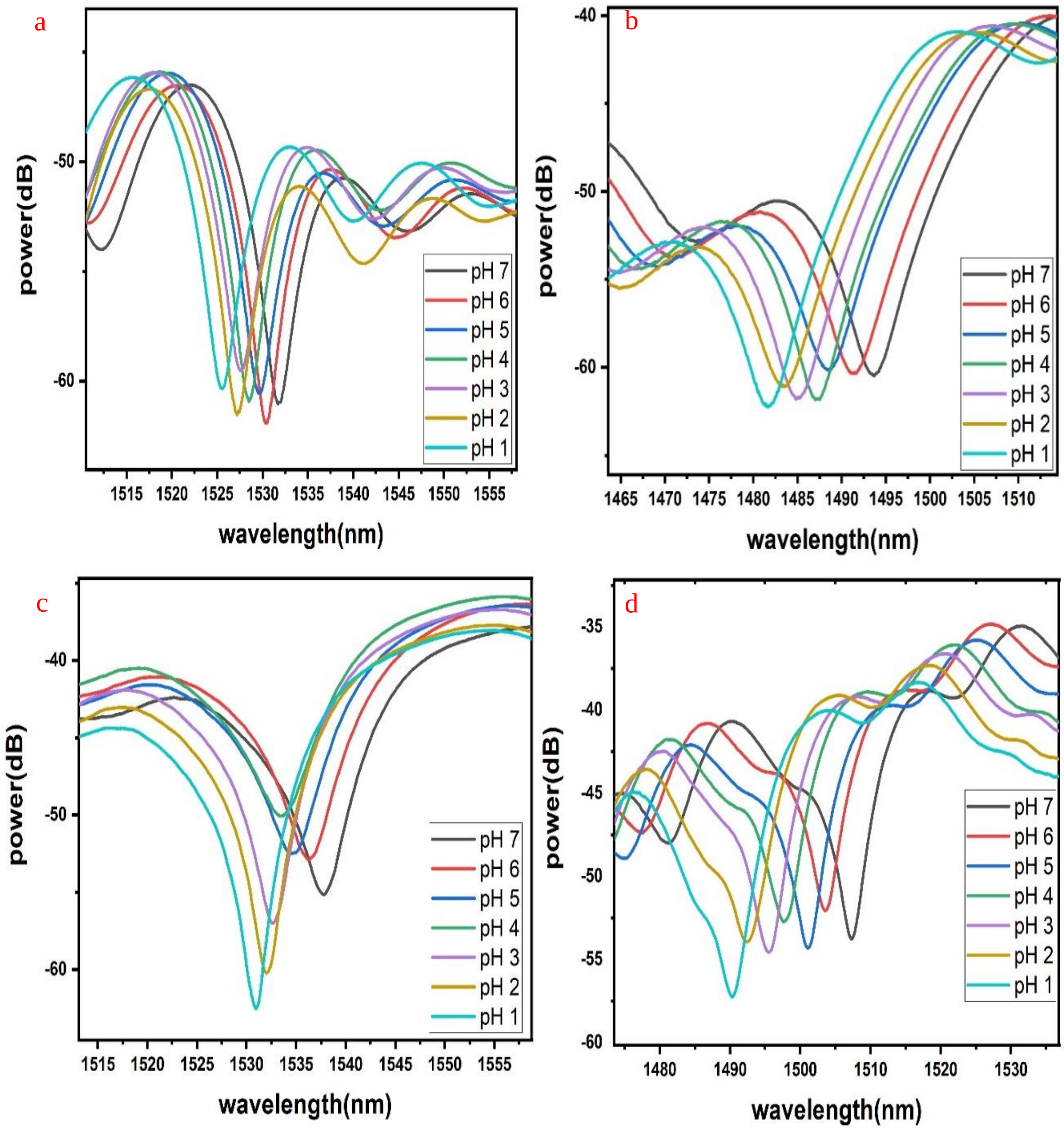

Figure (3.8): Transmission spectra response of the OFpHS as a function of pH for (a) 100 µm, (b) 90 µm, (c) 80 µm, and (d) 70 µm NCF diameter for acid.

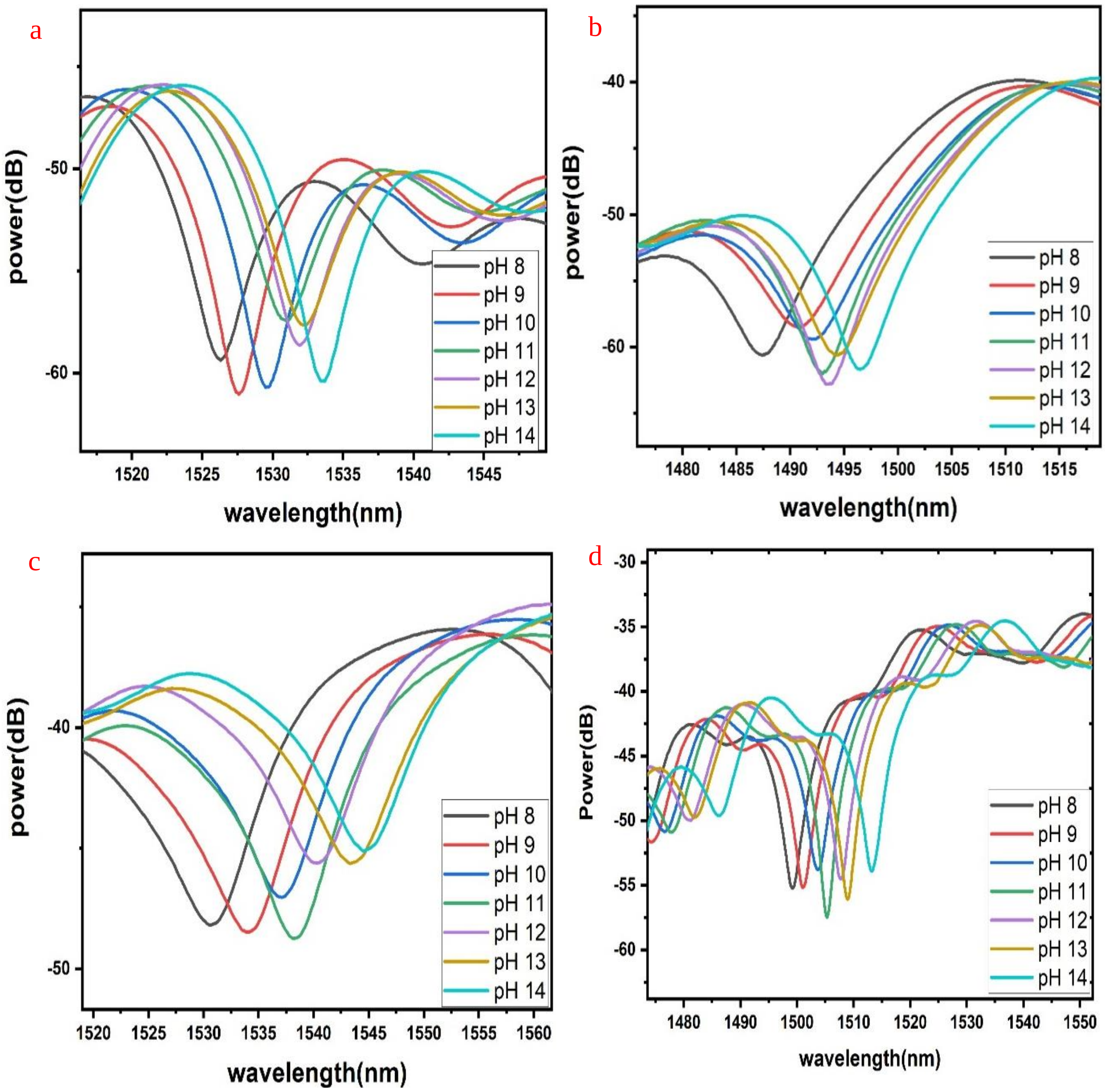

Figure (3.9): Transmission spectra response of the OFpHS as a function of pH for (a) 100 µm, (b) 90 µm, (c) 80 µm, and (d) 70 µm NCF diameter for base.

In the case of 100 µm, when the pH increased from 1-7 (acid range) the dip in the spectrum shifted from 1525 to 1531 nm. While the spectrum shifted from 1526 to 1533 nm in the base range from 8-14. But in the case of 90 and 80 µm, as the pH varied from 1-7 the dip in the spectrum shifted from 1481 to 1493 nm and from 1530 to 1537 nm, respectively. And the transmission spectra shifted from 1488 to 1496 nm; and from 1530 to 1545 nm, respectively in the base range from 8-14. But in the case of 70 µm, the wavelength shift was from 1490 to 1507 nm for acid and from 1499 to 1513 nm for the base. From these results, the transmission spectra shifted towards red when the pH increased from 1-7 and 8-14 for acid and base, respectively. The wavelength shift was continued in a red shift when the pH was increased. For more examinations, linear response for both pH levels 1–7 and 8-14 for acid and base have been graphed as shown in Figure (3.10) and (3.11), respectively.

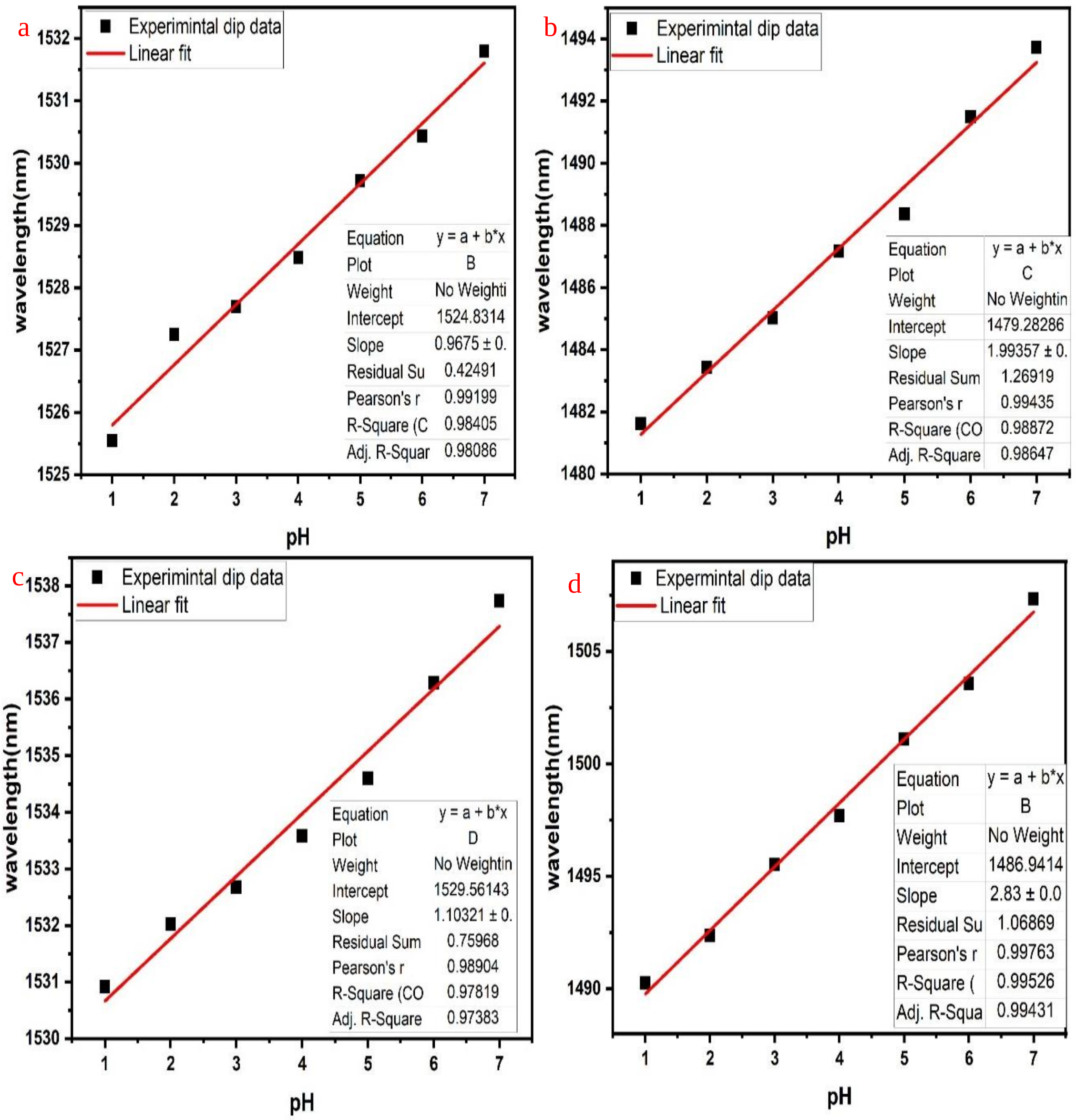

Figure (3.10): Linear fitting plots of the shifted dips against pH change in the function of wavelengths shift for (a) 100 µm, (b) 90 µm, (c) 80 µm, and (d) 70 µm NCF diameter for acid.

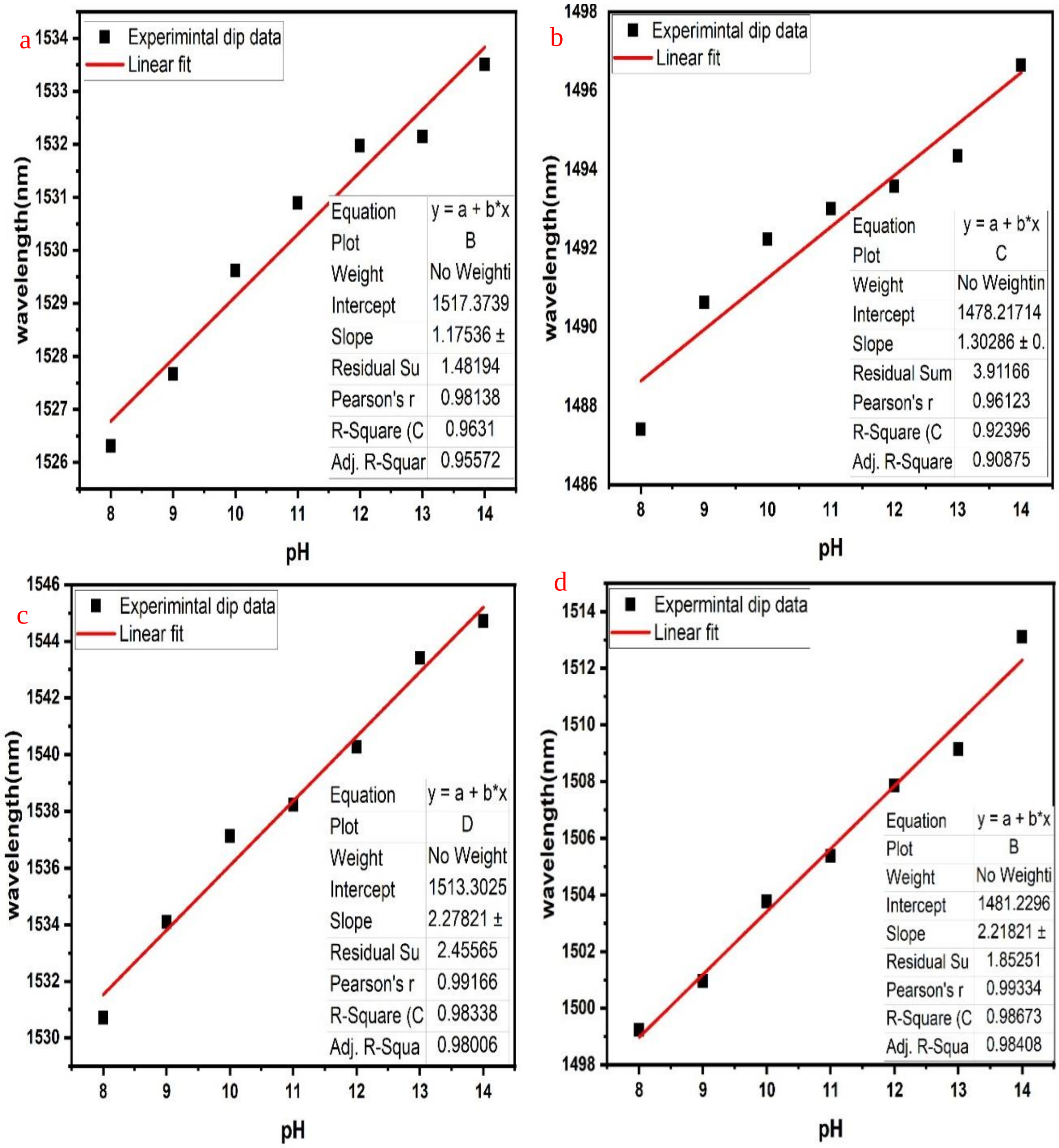

Figure (3.11): Linear fitting plots of the shifted dips against pH change in the function of wavelengths shift for (a) 100 µm, (b) 90 µm, (c) 80 µm, and (d) 70 µm NCF diameter for base.

The sensitivities of SNCS fiber structure for different NCF diameters are illustrated in Table (3.2). The reduction in NCF diameter from 125 to 70 µm contributes to an enhancement of the sensor sensitivity that due to the enhanced evanescent field. The best sensitivity of the proposed sensor is calculated to about 2.8 nm/pH and 2.2 nm/pH for acid and base, respectively at NCF diameter of 70 µm.

Table (3.2): The sensitivity and the polynomial fitting coefficient for different diameters of bare NCF at fixed length (2 cm) for both acid and base which the pH changed from 1-14.

NCF diameter (µm)	Sensitivity (nm/pH) of acid	Adj. R^2 of acid	Sensitivity (nm/pH) for base	Adj. R^2 of base
100 µm	0.96	0.98	1.17	0.95
90 µm	1.99	0.98	1.30	0.90
80 µm	1.1	0.97	2.2	0.98
70 µm	2.8	0.99	2.2	0.98

Hence, the obtained result shows that the fabricated sensor can be used effectively in both high and low pH ranges. On the other hand, SNCS fiber configuration with 70 µm diameter and 2 cm length reveals excellent pH-sensing characteristics of the SNCS-based sensor. It possesses a good polynomial fitting coefficient (R^2) of more than 0.99 and 0.98 for both acid and base, respectively.

The average error bar in the figure shows the maximum fluctuations during the examination. Error bar (standard deviation) for both acid and base have been evaluated also, as shown in Figure (3.12). The results show that the acid and base have a standard deviation of 6.1% and 4.8%, respectively.

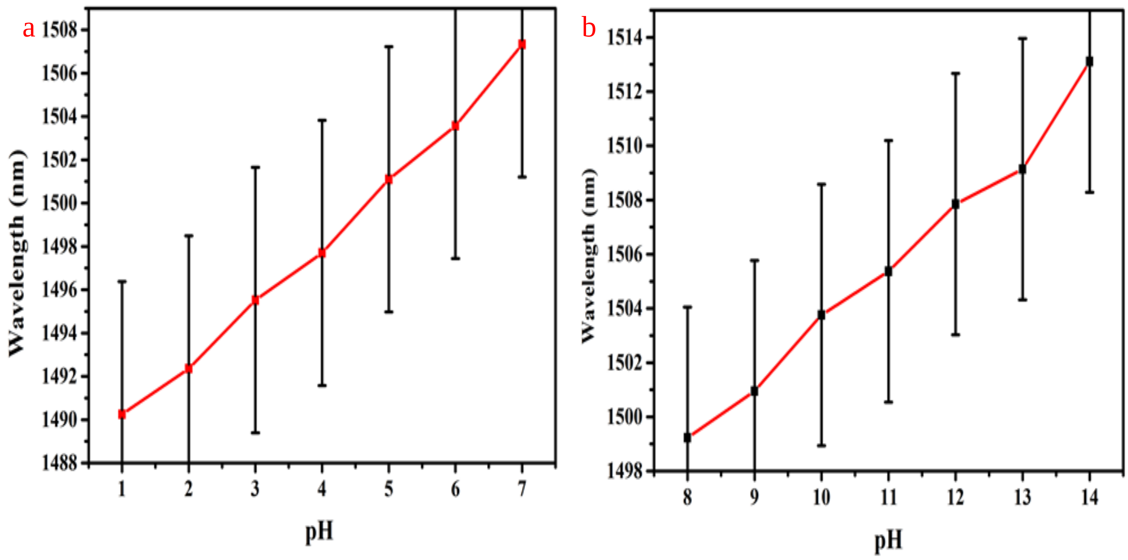

Figure (3.12): wavelength with an error bar, of the proposed sensor for (a) acid and (b) base.

From these results, the wavelength as a function of refractive index possesses wavelength dips shifted toward a longer wavelength (redshift) when the pH increases from 1-7 and 8-14 due to the increases of the refractive index of pH solutions. The relationship between the pH and the wavelength shift can be seen in Figure (3.13). There was a slight variation in the sensitivity and wavelength shift of different diameters of NCF at a fixed length, because of self-imaging on the MMI principle.

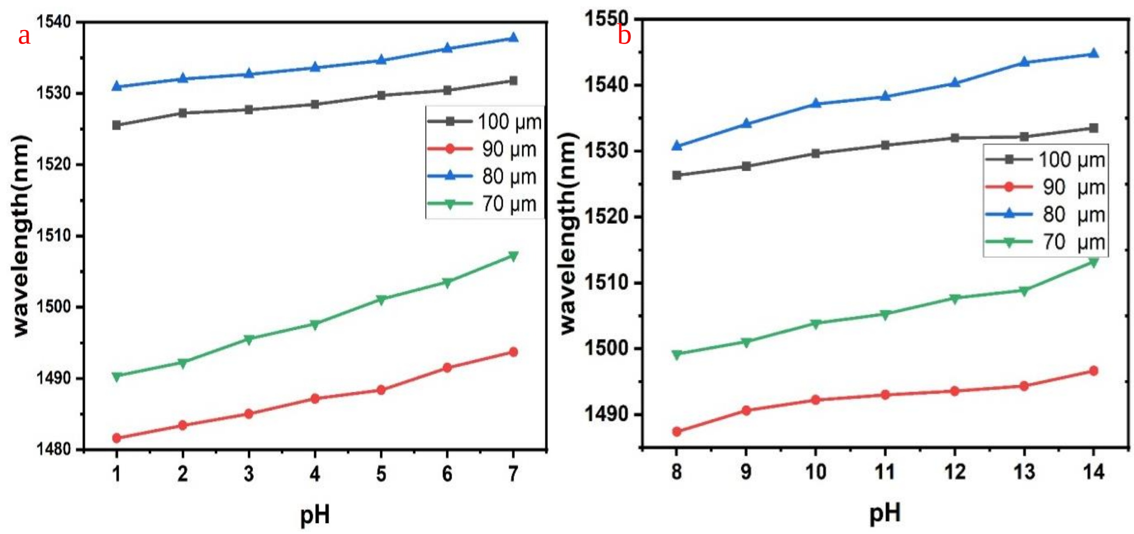

Figure (3.13): The response sensors to variations in pH from (1-14) with different NCF diameters for (a) acid and (b) base.

3.5 The Influence of the Coating on OFpHS Sensitivity:

3.5.1 The Influence of both PAA/PVA and SiO_2@PVA/PAA Coating on OFpHS Sensitivity:

To enhance the sensitivity of the fabricated sensor further, Both PVA/PAA and SiO_2@PVA/PAA were selected as the sensitive film coating for 70 µm diameter of the NCF. The interaction of strong light with coated was enhanced remarkably at reduced diameter waist, thus, the pH sensor becomes more sensitive to pH variations.

In addition, considerable effort has been made to further enhance the performance of fiber sensors such as by utilizing a combination of interferometric structure (e.g. MZI) with resonance-assisting material supports. Pure polymer, conductive polymer and polymer composited coatings are widely utilized as hydrogel to enhance the pH-sensing performance in optical-fiber-based sensors. So, we firstly use PVA/PAA hydrogel composite coating which these polymer materials have excellent goo permeability and a high swelling ratio also adopts a compact (but not fully collapsed) globular conformation, which these make it as a good acid sensor and consequently it assists to enhanced the sensitivity of pH range from 1-7.

On the other side, SiO_2 has attracted significant interest in optoelectronics-proposed studies, as it is inexpensive to produce, easy to prepare, and used in many industries and application including the pH sensing. Also, these nanomaterials add more surfaces to volume ratio to coating to enhance the sensitivity. Additionally silica it's more interaction with range 8-14 of pH sensor. Generally, PVA has good capability for film-forming with SiO_2, which has a refractive index comparable with that of silica material. Also, SiO_2-based-polymer films have excellent thermal stability with promising strength features of the resulting composites. So, the silica in PVA/PAA coating represents a candidate coating material for enhancing the pH sensing performance.

Figure (3.14) shows the images under the optical microscope of the PVA/PAA and SiO_2@PVA/PAA. From this figure it can be observed that the coating layer exhibited a smooth behavior.

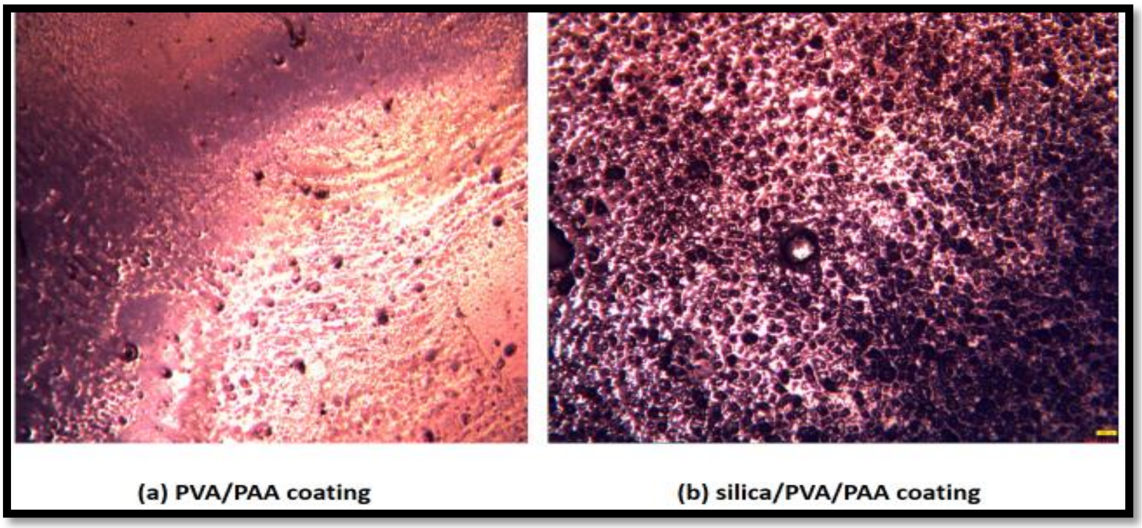

Figure (3.14): Optical microscope image (a) PVA/PAA coating (b) silica/PVA/PAA coating under 4x.

Additionally, Figure (3.15) (a, b) field scan electron microscopy (FESEM) images of the etched NCF was coated with Both PAA/PVA and SiO_2@PVA/PAA at a diameter of 70 µm, the coated layer is homogeneous with little aggregations in some points.

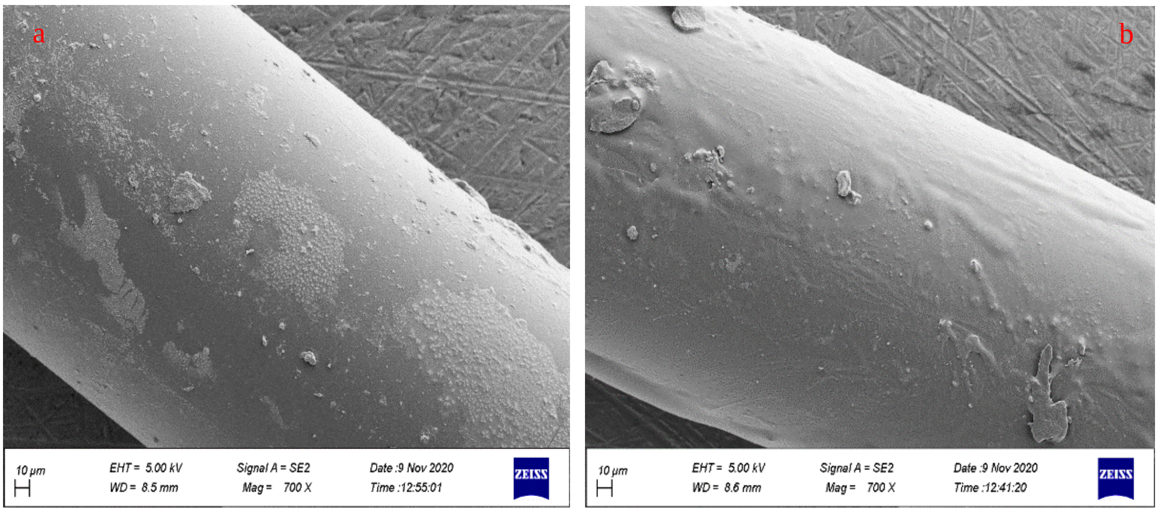

Figure (3.15): The FSEM images for NCF coated with (a) PVA/PAA, and (b) SiO_2@PVA/PAA.

The performance of 70 μm diameter of NCF sensor head coated with PAA/PVA and SiO_2@PVA/PAA have been examined for both the acid and base. Figure (3.16) shows the wavelength shift dependence on the pH based on the PVA/PAA coating of 70 μm diameter of NCF segments for both acid and base. The position of the transmission dip was blue-shifted as the surrounding pH increases from (1-7) pH level. While in the base range the position of the transmission dip was red-shifted as the surrounding pH increases from 8-14 pH level. This phenomenon can be explained as when the sensor head was exposed to an increase in the surrounding pH, the effective refractive index of PVA/PAA and SiO_2@PVA/PAA coating was modulated and increased in the same way as the pH increased. This results in an increase in the leakage evanescent light from the etched core and an increase. Output spectra of the proposed sensor when the pH changes from 1-7 and 8-14 for acid and base with an etched NCF.

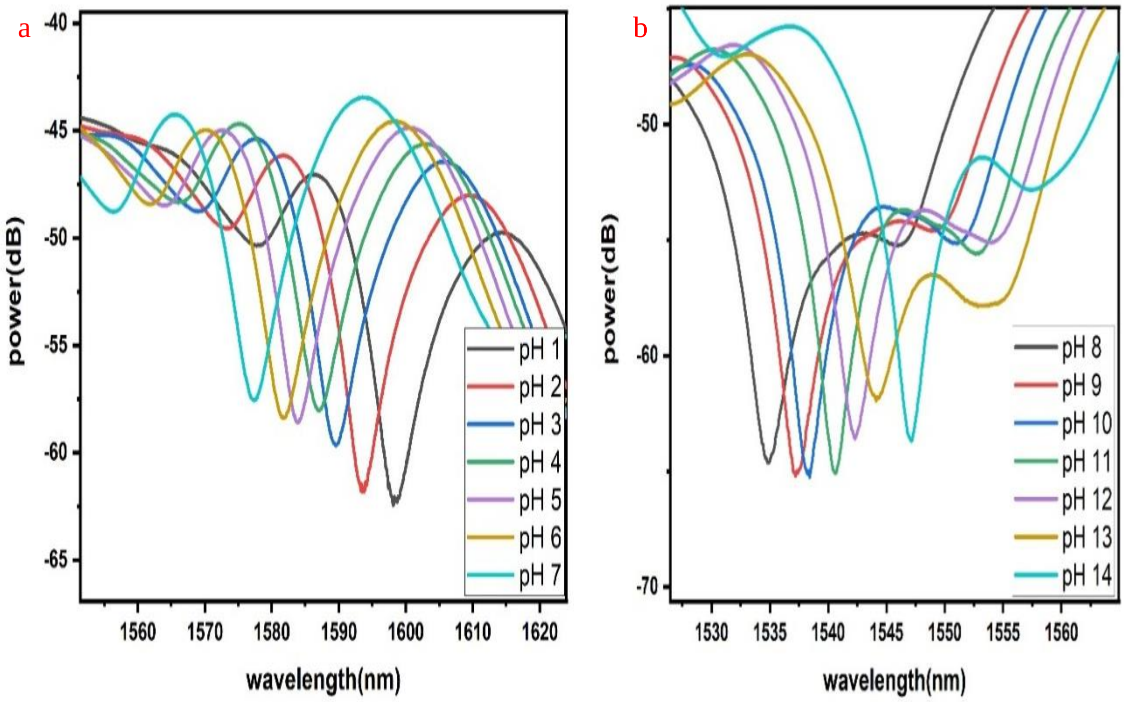

Figure (3.16): Transmission spectra of 70 μm NCF coated with PVA/PAA for sensing different pH values for (a) acid and (b) base.

The blue shift of the dips in transmitted spectra suggests that the refractive index (n_2) of the cladding material PVA/PAA decreases with an increase in pH. While the red shift of the dips in transmitted spectra suggests that the refractive index (n_2) of the cladding material SiO_2@PVA/PAA increases with an increase in pH. While Figure (3.17) shows the wavelength shift dependence on the pH based on SiO_2@PVA/PAA coating of 70 μm diameter of NCF segments for both acid and base.

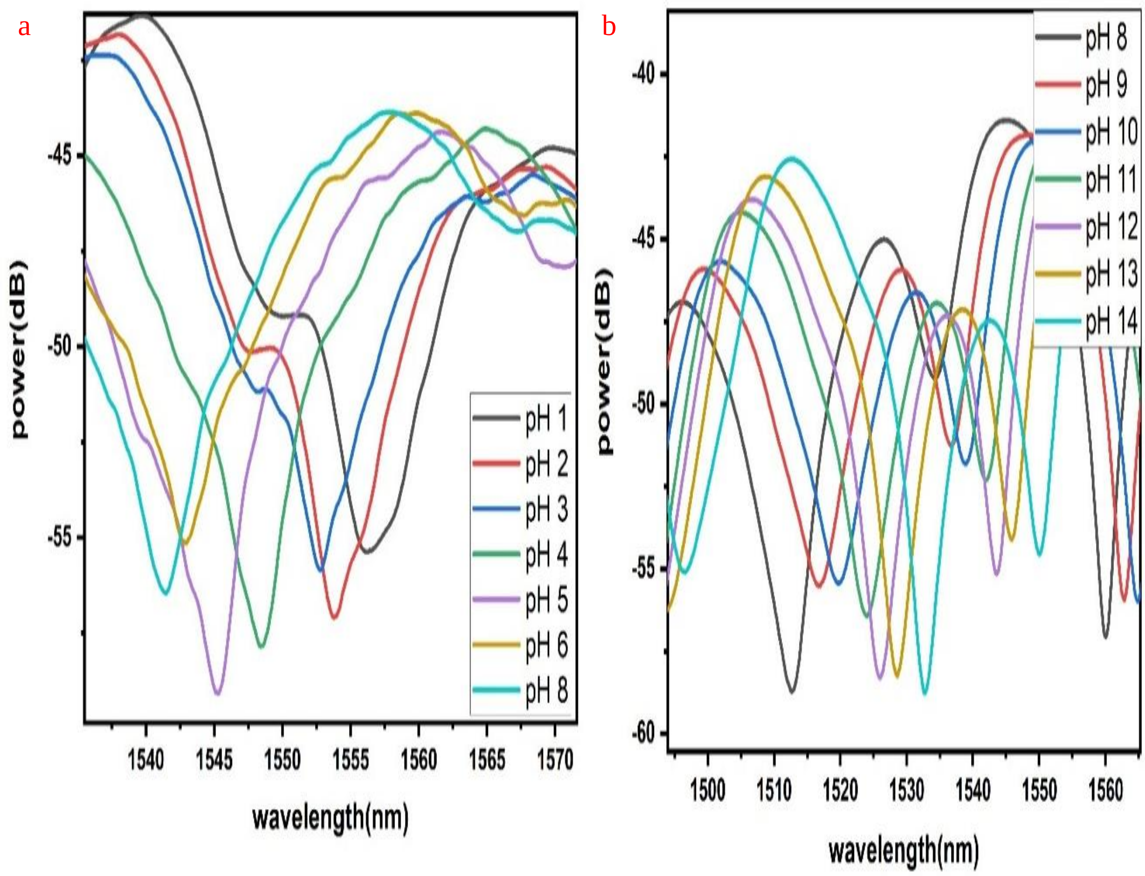

Figure (3.17): Transmission spectra of 70 μm NCF coat with Silica/PVA/PAA for sensing different pH values for (a) acid and (b) base.

From this figure, it can be found that the position of the transmission dip has been red-shifted as the surrounding pH increases from 8-14 pH level. Also, these results indicate that PAA/PVA coating encapsulated the fiber head possesses a good enhancement of sensitivity which has been raised to ~3.42 nm/pH for acidic range, and 2.1 nm/pH for base range[21]. While, as coated the fiber head with the other coating (SiO_2@PVA/PAA), the response of the sensor shows the sensitivity of about 2.5 nm/pH acidic range and about 3.2 nm/pH base range[101]. So, the PAA/PVA coating is a candidate coating material acidic sensing [21] while, SiO_2@PVA/PAA is more appropriate for the base sensing, which these coating materials show an enhancement in the sensitivity above the NCF structure before uncoated sensor due to more enhancement of the evanescent field affected by the coating layer. The strength of the light interaction with both coated has been remarkably enhanced at reduced waist diameter, and consequently, the sensor became more sensitive to pH changes. Herein, the obtained spectra at different wavelength dips are observed corresponding to each pH which takes place due to the swelling property of uses hydrogel. The fitted curve and the error bar of the proposed sensor based on PVA/PAA coating for 1-7 pH are shown in Figure (3.18). While Figure (3.19) shows the fitted curve and the error bar of the proposed sensor based on SiO_2@PVA/PAA for a range from 8-14 pH level.

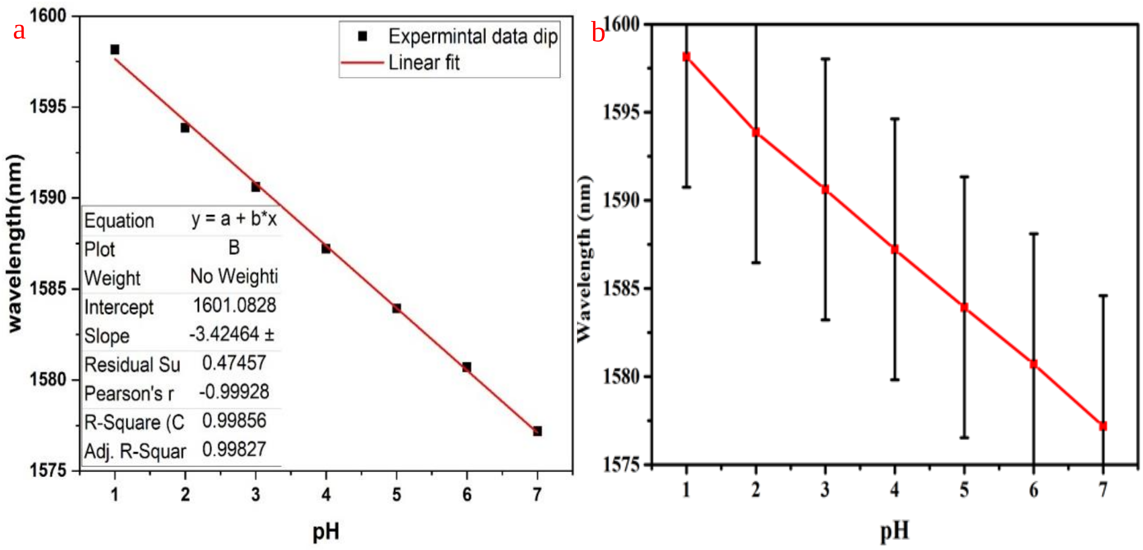

Figure (3.18): (a) Linear fitting plots of the shifted dips (b) wavelength with an error bar, of the proposed sensor based on PVA/PAA for acidic pH range.

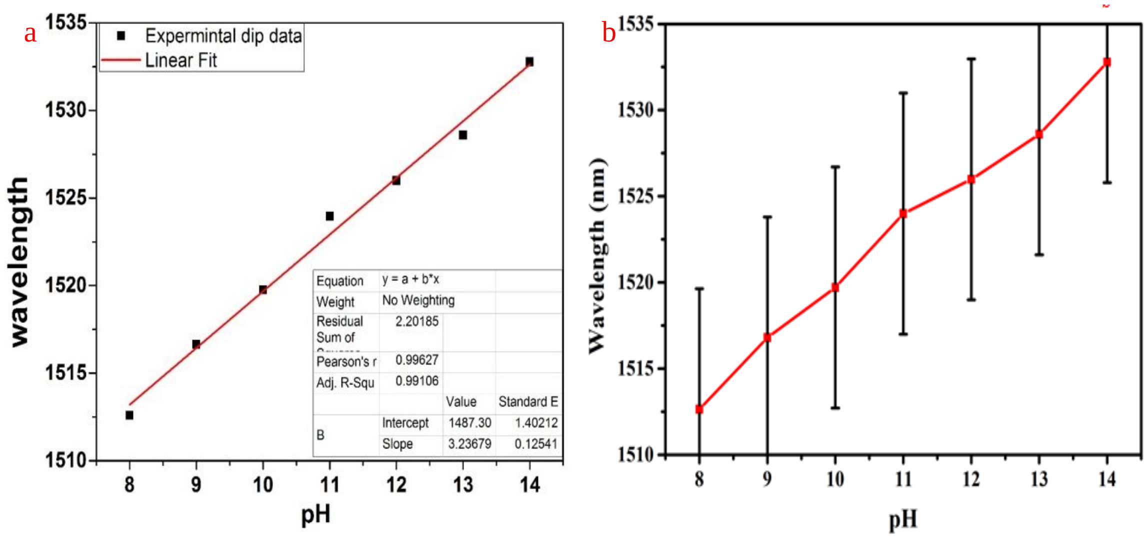

Figure (3.19): (a) Linear fitting plots of the shifted dips (b) wavelength with an error bar, of the proposed sensor based on SiO_2@PVA/PAA for base pH range.

From these results, R^2 is calculated for both of the fabricated coating sensor structures, which is more than 0.998 and 0.991, for acid and base, respectively. Also, it can be noted that the acid and base have a standard deviation of 7.4% and 6.99%, respectively.

Reproducibility is an essential property required to measure for practical usages. To check the reproducibility, the same experiment was performed in reverse order at room temperature. Initially, to check the reproducibility, the fabricated sensor was immersed in aqueous solutions of varying pH in ascending order from 1-14 and the transmission spectra were recorded by the spectrum analyzer. In the second step, we repeat the same experiment with aqueous solutions of varying pH in reverse order starting from 7-1 and then 14-8. Figure (3.20) represents the wavelength dip of the sensor with varying pH solutions in both ascending and descending ways which show the very small fluctuation in output spectra with maximum hysteresis of about 0.06 nm and 0.26 nm, for acid and base range, respectively. Also, the standard deviation for both ascending and descending pH has been evaluated, which the results indicate that both ascending and descending pH are almost similar with a standard deviation of 7.4% and 6.99% acid and base, respectively.

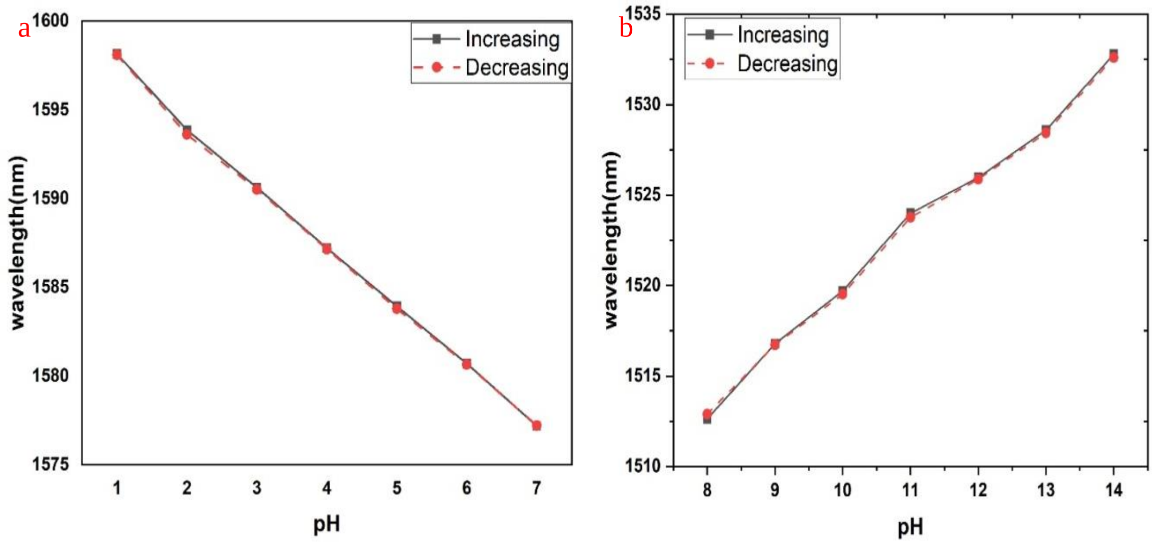

Figure (3.20): Wavelength reproducibility of the proposed sensor for (a) acid and (b) base.

3.5.2 The Influence of Methyl red@PVA Coating on OFpHS Sensitivity:

The SNCS structure was coated with another material namely Methyl red@PVA for more enhancement of the sensitivity of the fabricated pH sensor at 70 µm diameter NCF. Also, the interaction of strong light with coated was enhanced remarkably at reduced diameter waist, thus, the pH sensor becomes more sensitive to pH variations. Figure (3.21) shows the images under the optical microscope of the methyl red@PVA. From this figure it can be observed that the coating layer exhibited a smooth behavior and it's appear in red color that return to color of methyl material.

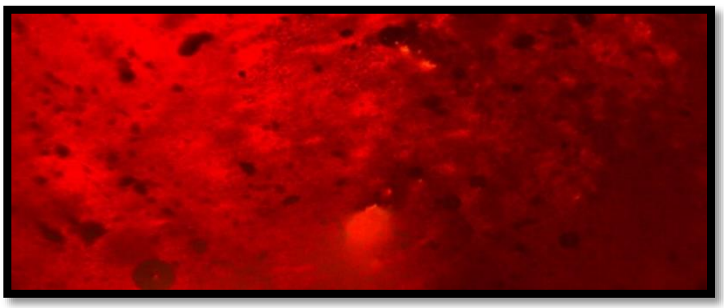

Figure (3.21): Images under the optical microscope of the methyl red@PVA under 4X.

The performance of 70 µm diameter of NCF sensor head coated with Methyl red has been examined for both the acid and base. Figure (3.22) shows the wavelength shift dependence on the pH based on the Methyl red@PVA coating of 70 µm diameter of NCF segments for both acid and base. The position of the transmission dip was blue-shifted as the surrounding pH increases from 1-7 pH level. While the position of the transmission dip was red-shifted as the surrounding pH increases from 8-14 pH level.

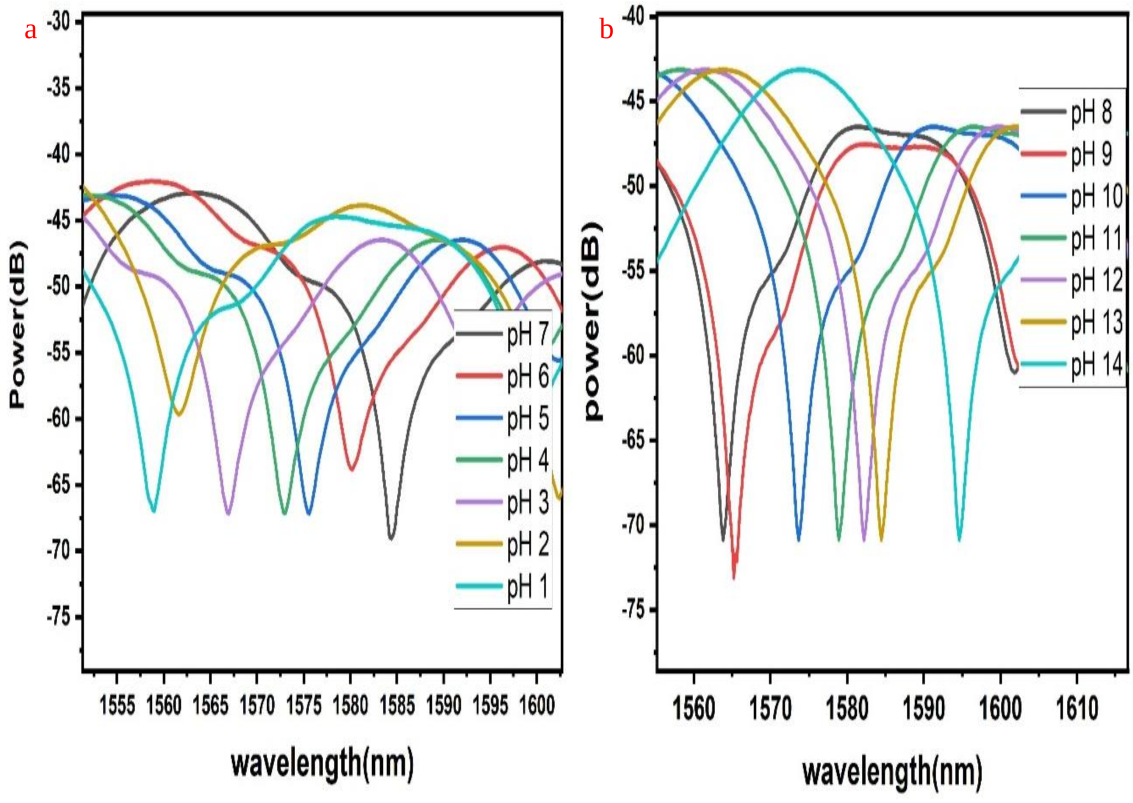

Figure (3.22): Transmission spectra of 70 µm NCF coat with Methyl red@PVA for sensing different pH values for (a) acid and (b) base.

From these results, Methyl red@PVA coating encapsulated the fiber head, a good enhancement of sensitivity has been obtained which is raised to about 4.3 nm/pH for acidic range, and about 4.1 nm/pH for base range. So, the Methyl red coating is a candidate coating material acidic and base sensing, which these coating materials show an enhancement in the sensitivity above the NCF structure before uncoated sensor due to more enhancement of the evanescent field affected by the coating layer. The strength of the light interaction with coated was remarkably enhanced at reduced waist diameter, and consequently, the sensor became more sensitive to pH changes. Herein, the obtained spectra at different wavelength dips are observed corresponding to each pH which takes place due to the swelling property of uses hydrogel. It is known that with an increase in pH the deposited hydrogel will swell under electrostatic repulsion available due to the ionization of hydrogel. The ionization leads to more absorption of aqueous solutions by coated hydrogel causes a decrease in the RI of the hydrogel [].

The fitted curve of the proposed sensor based on Methyl red coating is shown in Figure (3.23). From these results, R^2 is calculated for both of the fabricated coating sensor structures, which is more than 0.991 and 0.96, for acid and base, respectively.

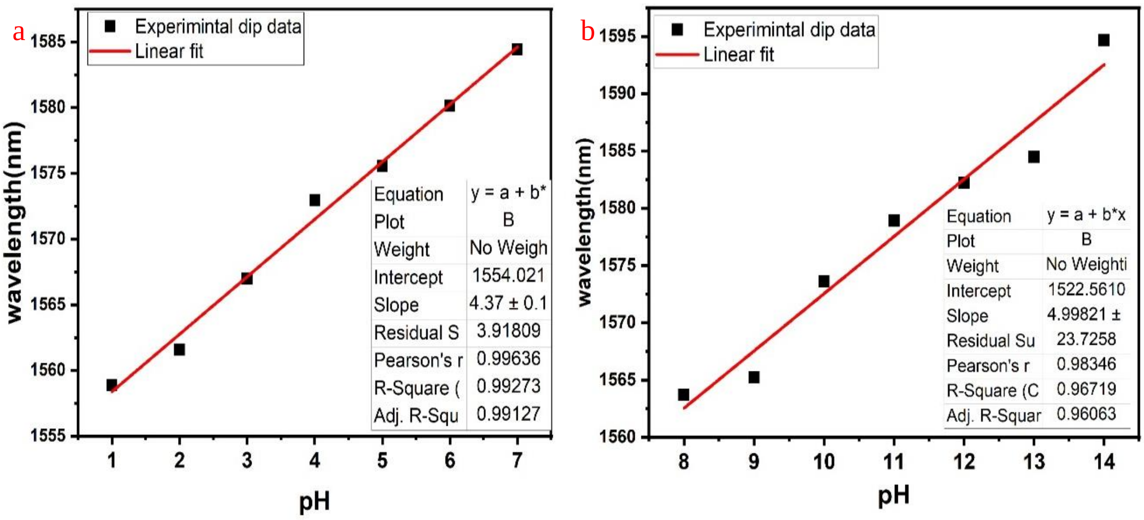

Figure (3.23): Linear fitting plots of the shifted dips against pH change in the function of wavelengths shift for (a) acid, and (b) base of the proposed sensor based on methyl red@PVA coating.

Finally, Table (3.2) summarizes the performance of 70 μm before and after coated sensors. The response time of the seeded sensor was estimated by real-time observation from the OSA spectra when the pH was increased from 1-14.

Table (3.3): The performance of the proposed sensor before and after coating the NCF.

Parameters	Acid	Base
Sensitivity (nm/pH) without coat	2.8	2.2
Sensitivity (nm/pH) with coat PVA/PAA	3.42	2.1
Sensitivity (nm/pH) with coat SiO_2@PVA/PAA	2.5	3.2
Sensitivity (nm/pH) with coat Methyl red @PVA	4.3	4.1

Table (3.3) shows a comparison of the performance of the present proposed sensor in various cases including: bare 70 µm etched NCF, and the same etched NCF based different coating materials (PVA/PAA, SiO_2@PVA/PAA and Methyl red @PVA). From these results, it can be noted that the best structure is that coated with the Methyl red @PVA shows enhancement in the sensitivity above the NCF structure before an uncoated sensor of more than 1.5 times due to greater enhancement of the evanescent field affected by the coating layer.

Also, the performance of the proposed fiber pH sensor based on the different hydrogel coating has been compared with a recently reported pH sensor based on different MZI configurations. The coating materials, sensitivity, and the pH range are listed in Table (3.3).

Table (3.4): Comparison of Sensitivity for different optical fiber pH sensors**.**

Coating material	Sensitivity (nm/pH)	Measurement range (pH)	Ref.
PVA/PAA	0.9 nm/pH	2.5-6.5	[21]
Smart hydrogel	0.66 nm/pH	2-12	[22]
tetraethyl orthosilicate	1.02 nm/pH for acid and 0.9nm/pH for base	2-13	[7]
Polyacrylamide	1.9 nm/pH	3-10	[23]
PVA/PAA	3.42 nm/pH	1-7	Present work
silica/PVA/PAA	3.2 nm/pH	8-14	
Methylred@PVA	4.3 nm/pH and 4.1 for acid and base	1-14	

From Table (3.3), our proposed sensor is superior in terms of sensitivity compared to the previously published work. We expect that the sensitivity could be enhanced further by reducing the waist diameter of NCF and using another hydrogel coating.

3.6 Conclusions:

In summary, an SNCS pH sensor based on wavelength interrogation technique is fabricated and successfully demonstrated. Fabrication of SNCS structure involves only splicing short pieces of NCF (FG125LA from Thorlabs) between two standards SMF (Corning-28).The conclusions obtained from this work are:

1. The sensor sensitivity of the pH depends on the NCF length, and the sensor with (2cm) NCF length is more sensitive to pH variations, in the pH ranges of 1 to 14 are 1.17 and 1.02 nm/pH for acid and base respectively, however for more or less than of NCF length the sensitivity decrease.
2. The obtained sensitivity has been improved when the diameter of the NCF etched from 125 µm to 70µm and obtained wavelength shift will increase toward the redshift.
3. A maximum obtained sensitivity at 2.8 nm/pH and 2.2 nm/pH for acid and base respectively when the diameter of the NCF decreased to 70 µm with 2 cm length when the PH changes 1 to 14.
4. The optimum NCF length and diameter of sensor structure was coating firstly PAA/PVA and SiO_2@PVA/PAA.
5. The maximum wavelength sensitivity of 3.4 nm/pH and 3.2 nm/pH for acid and base respectively, was attained for the PH range altering from (1-14).
6. pH sensor was improving by coating NCF with a Methyl red@PVA coat which enhances the sensitivity of 4.3 nm/pH and 4.1 nm/pH for acid and base respectively.

3.7 Future Works:

1. Decreasing the NCF diameter by chemical etching below 70 µm.
2. Recalculating the NCF length with the reduced diameter according to MMI theory to decrease the losses.
3. Can try different concentrations of coating PAA/PVA, SiO_2@PVA/PAA, and Methyl red@PVA.
4. Adding more layers of coating PAA/PVA, SiO_2@PVA/PAA, and Methyl red@PVA.
5. Sensing enhancement of PH sensor based on bending NCF.

References

[1] M. Engholm, K. Hammarling, H. Andersson, M. Sandberg, and H. E. Nilsson, “A bio-compatible fiber optic pH sensor based on a thin core interferometric technique,” *Photonics*, vol. 6, no. 1, 2019, doi: 10.3390/photonics6010011.

[2] B. Gu, M. Yin, A. P. Zhang, J. Qian, and S. He, “Biocompatible fiber-optic pH sensor based on optical fiber modal interferometer self-assembled with sodium alginate/polyethylenimine coating,” *IEEE Sens. J.*, vol. 12, no. 5, pp. 1477–1482, 2011.

[3] V. Semwal and B. D. Gupta, “Highly sensitive surface plasmon resonance based fiber optic pH sensor utilizing rGO-Pani nanocomposite prepared by in situ method,” *Sensors Actuators B Chem.*, vol. 283, pp. 632–642, 2019.

[4] B. Gu, M.-J. Yin, A. P. Zhang, J.-W. Qian, and S. He, “Low-cost high-performance fiber-optic pH sensor based on thin-core fiber modal interferometer,” *Opt. Express*, vol. 17, no. 25, pp. 22296–22302, 2009.

[5] M. Lei, Y. N. Zhang, B. Han, Q. Zhao, A. Zhang, and D. Fu, “In-Line Mach-Zehnder Interferometer and FBG with Smart Hydrogel for Simultaneous pH and Temperature Detection,” *IEEE Sens. J.*, vol. 18, no. 18, pp. 7499–7504, 2018, doi: 10.1109/JSEN.2018.2862426.

[6] Y. Zheng, “Miniature pH Optical Fiber Sensor Based on Fabry-Perot Interferometer,” *IEEE J. Sel. Top. Quantum Electron.*, vol. 22, no. 2, pp. 331–335, 2016, doi: 10.1109/JSTQE.2015.2497438.

[7] V. Bhardwaj, A. K. Pathak, and V. K. Singh, “No-core fiber-based highly sensitive optical fiber pH sensor,” *J. Biomed. Opt.*, vol. 22, no. 5, p. 057001, 2017, doi: 10.1117/1.jbo.22.5.057001.

[8] J. A. Bebbington, “Rare earth doped silica waveguides on Si fabricated by flame hydrolysis deposition and aerosol doping Rare earth doped silica waveguides deposition and aerosol doping on Si fabricated by

flame hydrolysis," vol. 337, no. 1993, 2013, doi: 10.1063/1.109645.

[9] A. P. Polonica, "OPTICAL NONRECIPROCAL DEVICES AND THEIR APPLICATIONS," vol. 86, no. 1, pp. 245–255, 1994.

[10] C. Han, H. Ding, and F. Lv, "Demonstration of a refractometric sensor based on an optical micro-fiber three-beam interferometer," vol. 1, pp. 1–7, 2014, doi: 10.1038/srep07504.

[11] S. Tai, K. Kyuma, and M. Nunoshita, "Fiber-optic acceleration sensor based on the photoelastic effect," vol. 22, no. 11, pp. 1771–1774, 1983.

[12] D. Yuan, Y. Dong, Y. Liu, and T. Li, "Mach-Zehnder Interferometer Biochemical Sensor Based on Silicon-on-Insulator Rib Waveguide with Large Cross Section," pp. 21500–21517, 2015, doi: 10.3390/s150921500.

[13] Z. Wu, X. Yu, E. Gu, Z. Kong, W. Li, and Z. X. W. U. E. T. Al, "Characteristics Analysis of Chemical Concentration Sensor Based on Three-layer FBG," vol. 2013, no. June, pp. 268–271, 2013, doi: 10.4236/opj.2013.32B063.

[14] P. Likamwa, "Tunable multimode-interference bandpass fiber filter," vol. 35, no. 3, pp. 324–326, 2010.

[15] D. I. Al-Janabi, A. M. Salman, and A. H. M. Al-Janabi, "All fiber, highly sensitive sensor based on gold nanoparticle-coated macrobent single mode fiber for human temperature monitoring," *J. Nanophotonics*, vol. 14, no. 4, p. 46013, 2020.

[16] D. I. A.-J. and A. S. and A. H. Al-Janabi, "High sensitivity balloon-like thermometric sensor based on bent single mode fiber," *Meas. Sci. Technol.*, 2020.

[17] A. A.-J. Huda Alsweefe, Sarah Kadhim Al-Hayali, "Enhanced Relative Humidity Sensor via Diameter of No-Core Fiber Structure," *Iraqi J. Laser*, vol. 18, no. 1, pp. 19–23, 2019.

[18] H. Alsweefe, S. K. Al-Hayali, and A. Al-Janabi, "Efficient humidity sensor based on an etched no-core fiber coated with copper oxide

nanoparticles," *J. Nanophotonics*, vol. 12, no. 04, p. 1, 2018, doi: 10.1117/1.jnp.12.046018.

[19] S. K. Al-Hayali, A. M. Salman, and A. H. Al-Janabi, "Effect of hygroscopic polymer-coatings on the performance of relative humidity sensor based on macro-bend single-mode fiber," *Opt. Fiber Technol.*, vol. 62, p. 102460, 2021.

[20] T. A. Abdzaid and H. J. Taher, "No-core fiber interferometry pH sensor based on a polyvinyl alcohol/polyacrylic acid and silica/polyvinyl alcohol/polyacrylic acid hydrogel coating," *Appl. Opt.*, vol. 60, no. 6, pp. 1587–1594, 2021.

[21] P. Hu, X. Dong, W. C. Wong, L. H. Chen, K. Ni, and C. C. Chan, "Photonic crystal fiber interferometric pH sensor based on polyvinyl alcohol/polyacrylic acid hydrogel coating," *Appl. Opt.*, vol. 54, no. 10, p. 2647, 2015, doi: 10.1364/ao.54.002647.

[22] S. K. Mishra, B. Zou, and K. S. Chiang, "Wide-Range pH Sensor Based on a Smart-Hydrogel-Coated Long-Period Fiber Grating," *IEEE J. Sel. Top. Quantum Electron.*, vol. 23, no. 2, pp. 284–288, 2017, doi: 10.1109/JSTQE.2016.2629662.

[23] A. K. Pathak and V. K. Singh, "A wide range and highly sensitive optical fiber pH sensor using polyacrylamide hydrogel," *Opt. Fiber Technol.*, vol. 39, no. September, pp. 43–48, 2017, doi: 10.1016/j.yofte.2017.09.022.

[24] J. Rayss, G. Sudolski, A. Gorgol, W. Janusz, and A. M. Gałgan, "Optical aspects of Na+ ions adsorption on sol-gel porous films used in optical fiber sensors," *J. Colloid Interface Sci.*, vol. 250, no. 1, pp. 168–174, 2002.

[25] S. Khodadoust, N. C. Kouri, M. S. Talebiyanpoor, J. Deris, and A. A. Pebdani, "Design of an optically stable pH sensor based on immobilization of Giemsa on triacetylcellulose membrane," *Mater. Sci. Eng. C*, vol. 57, pp. 304–308, 2015.

[26] G. Beltrán-Pérez, "Fabrication and characterization of an optical fiber pH sensor using sol–gel deposited TiO2 film doped with organic dyes," *Sensors Actuators B Chem.*, vol. 120, no. 1, pp. 74–78, 2006.

[27] L. F. Rickelt, L. D. M. Ottosen, and M. Kühl, "Etching of multimode optical glass fibers: A new method for shaping the measuring tip and immobilization of indicator dyes in recessed fiber-optic microprobes," *Sensors Actuators B Chem.*, vol. 211, pp. 462–468, 2015.

[28] R. Zhao, T. Lang, J. Chen, and J. Hu, "Polarization-maintaining fiber sensor for simultaneous measurement of the temperature and refractive index". Optical Engineering, 56, 5, ID 057113, pp. 1-5, 2017.

[29] D. Niu, "High-resolution and fast-response optical waveguide temperature sensor using asymmetric Mach-Zehnder interferometer structure," *Sensors Actuators, A Phys.*, vol. 299, 2019, doi: 10.1016/j.sna.2019.111615.

[30] A. Richter, G. Paschew, S. Klatt, J. Lienig, K.-F. Arndt, and H.-J. P. Adler, "Review on hydrogel-based pH sensors and microsensors," *Sensors*, vol. 8, no. 1, pp. 561–581, 2008.

[31] X. Cheng, J. Bonefacino, B. O. Guan, and H. Y. Tam, "All-polymer fiber-optic pH sensor," *Opt. Express*, vol. 26, no. 11, p. 14610, 2018, doi: 10.1364/oe.26.014610.

[32] J. Gong, M. G. Tanner, S. Venkateswaran, J. M. Stone, Y. Zhang, and M. Bradley, "A hydrogel-based optical fibre fluorescent pH sensor for observing lung tumor tissue acidity," *Anal. Chim. Acta*, vol. 1134, pp. 136–143, 2020.

[33] V. N. K. Pabbisetti and S. S. Madhuvarasu, "Hydrogel-coated fiber Bragg grating sensor for pH monitoring," *Opt. Eng.*, vol. 55, no. 6, p. 66112, 2016.

[34] S. A. Moiz, K. S. Karimov, and N. D. Gohar, "Orange dye thin film resistive hygrometers," *Eurasian Chem. J.*, vol. 6, no. 3, pp. 179–183,

2004.

[35] C.-W. Lee, H.-S. Park, J.-G. Kim, B.-K. Choi, S.-W. Joo, and M.-S. Gong, “Polymeric humidity sensor using organic/inorganic hybrid polyelectrolytes,” *Sensors Actuators B Chem.*, vol. 109, no. 2, pp. 315–322, 2005.

[36] Z. Ahmad, M. H. Sayyad, M. Saleem, K. S. Karimov, and M. Shah, “Humidity-dependent characteristics of methyl-red thin film-based Ag/methyl-red/Ag surface-type cell,” *Phys. E Low-dimensional Syst. Nanostructures*, vol. 41, no. 1, pp. 18–22, 2008.

[37] Y. Li and M. J. Yang, “Bilayer thin film humidity sensors based on sodium polystyrenesulfonate and substituted polyacetylenes,” *Sensors Actuators B Chem.*, vol. 87, no. 1, pp. 184–189, 2002.

[38] K. S. Karimov, I. Qazi, T. A. Khan, P. H. Draper, F. A. Khalid, and M. Mahroof-Tahir, “Humidity and illumination organic semiconductor copper phthalocyanine sensor for environmental monitoring,” *Environ. Monit. Assess.*, vol. 141, no. 1, pp. 323–328, 2008.

[39] Y. Sakai, Y. Sadaoka, and M. Matsuguchi, “Humidity sensors based on polymer thin films,” *Sensors Actuators B Chem.*, vol. 35, no. 1–3, pp. 85–90, 1996.

[40] B. E. A. Saleh, M. C. Teich, and C. J. Wiley, *Fiber optics 8.1*, vol. 5. 1991.

[41] J. M. Senior, "Optical Fiber Communications principles and practice", 3rd edition, Prentice Hall, ch2, pp. 26-28, (2009).

[42] A. M. R. Pinto and M. Lopez-amo, “Photonic Crystal Fibers for Sensing Applications,” vol. 2012, 2012, doi: 10.1155/2012/598178.

[43] W. A. Khaleel and A. H. M. Al-Janabi, “High-sensitivity sucrose erbium-doped fiber ring laser sensor,” *Opt. Eng.*, vol. 56, no. 2, p. 026116, 2017, doi: 10.1117/1.oe.56.2.026116.

[44] P. Taylor and J. I. Vukusic, “Optica Acta : International Journal of Optics Optical Fiber Communications : Principles and Practice,” no.

November 2014, 2010, doi: 10.1080/716099703.

[45] C. Kim, “Simultaneous measurement of strain , temperature and vibration frequency using a fibre optic sensor Simultaneous Measurement of Strain , Temperature , and Vibration Frequency Using a Fiber Optic Sensor Chang-Sun Hong § and Chun-Gon Kim Division of Aerospa,” no. December, 2013, doi: 10.1088/0957-0233/13/8/305.

[46] Z. Bielecki, T. Stacewicz, and J. Smulko, “applied sciences Ammonia Gas Sensors : Comparison of Solid-State and Optical Methods,” 2020.

[47] B. H. Timmer, K. M. Van Delft, R. P. Otjes, W. Olthuis, and A. Van Den Berg, “Miniaturized measurement system for ammonia in air,” vol. 507, pp. 137–143, 2004, doi: 10.1016/j.aca.2003.09.038.

[48] L. Alwis, T. Sun, and K. T. V. Grattan, “Optical fibre-based sensor technology for humidity and moisture measurement: Review of recent progress,” *Meas. J. Int. Meas. Confed.*, vol. 46, no. 10, pp. 4052–4074, 2013, doi: 10.1016/j.measurement.2013.07.030.

[49] M. Sensor, “High-Visibility Photonic Crystal Fiber Interferometer as Multifunctional Sensor,” pp. 2349–2358, 2013, doi: 10.3390/s130202349.

[50] M. Corres, J. Goicoechea, and Y. Rodr, “Vibration Detection Using Optical Fiber Sensors,” vol. 2010, pp. 10–17, 2010, doi: 10.1155/2010/936487.

[51] R. Mehra, “Mach Zehnder Interferometer and its Applications,” pp. 31–36, 2014.

[52] J. Du, Y. Dai, G. K. P. Lei, W. Tong, and C. Shu, “Photonic crystal fiber based Mach-Zehnder interferometer for DPSK signal demodulation,” vol. 18, no. 8, pp. 7917–7922, 2010.

[53] A. Aslian, “Design and Analysis of an Optical Coupler for Concentrated Solar Light Using Optical Fibers in Residential Buildings,” vol. 2016, 2016.

[54] H. Search, C. Journals, A. Contact, M. Iopscience, L. Phys, and I. P.

Address, “A tunable multi-wavelength laser based on a Mach – Zehnder interferometer with photonic crystal fiber,” vol. 055105, 2013, doi: 10.1088/1054-660X/23/5/055105.

[55] S. Qiu, Y. Chen, J. Kou, F. Xu, and Y. Lu, “Miniature tapered photonic crystal fiber interferometer with enhanced sensitivity by acid microdroplets etching,” 2011.

[56] K. Fidanboylu, “Fiber Optic Sensors and Their Applications,” no. May 2009, 2017.

[57] Y. Li, Z. Liu, and S. Jian, “Multimode Interference Refractive Index Sensor Based on Coreless Fiber,” vol. 4, no. 1, pp. 21–27, 2014, doi: 10.1007/s13320-013-0137-0.

[58] A. W. Lohmann, H. Knuppertz, and J. Jahns, “Fractional Montgomery effect : a self-imaging phenomenon,” vol. 22, no. 8, pp. 1500–1508, 2005.

[59] X. Zhu, “Detailed investigation of self-imaging in large- core multimode optical fibers for application in fiber lasers and amplifiers,” vol. 16, no. 21, pp. 16632–16645, 2008.

[60] P. C. Beard, “Optical fiber photoacoustic-photothermal probe,” no. September 1998, pp. 21–24, 2014, doi: 10.1364/OL.23.001235.

[61] S. Chopra, P. International, U. S. River, and A. Chopra, “Journal of Purchasing & Supply Management,” vol. 14, pp. 273–274, 2008, doi: 10.1016/j.pursup.2008.08.001.

[62] Z. Djinovi, M. Tomi, L. Manojlovi, Ž. Lazi, and M. Smiljani, “Non-contact Measurement of Thickness Uniformity of Chemically Etched Si Membranes by Fiber-Optic Low- Coherence Interferometry,” no. Miel, pp. 11–14, 2008.

[63] F. J. Arregui, M. Otano, C. Fernandez-valdivielso, and I. R. Matias, “An experimental study about the utilization of Liquicoat 1 solutions for the fabrication of pH optical fiber sensors,” vol. 87, pp. 289–295, 2002.

[64] T. Gotou, M. Noda, T. Tomiyama, H. Sembokuya, M. Kubouchi, and K. Tsuda, “In situ health monitoring of corrosion resistant polymers exposed to alkaline solutions using pH indicators,” vol. 119, pp. 27–32, 2006, doi: 10.1016/j.snb.2005.11.035.

[65] W. Kong, Y. Wan, Z. Zheng, X. Zhao, Y. Liu, and Y. Bian, “High-sensitivity sensing based on intensity- interrogated Bloch surface wave sensors,” vol. 1, pp. 204–205, 2012.

[66] A. Norouzi, A. H. Zaim, and B. B. Ustundag, "An integrated survey in Optical Networks: Concepts, Components and Problems", 11, 1, pp. 10-26, (2011).

[67] S. Dong, M. Luo, G. Peng, and W. Cheng, “Broad range pH sensor based on sol – gel entrapped indicators on fibre optic,” vol. 129, pp. 94–98, 2008, doi: 10.1016/j.snb.2007.07.078.

[68] I. Yulianti, “Sensitivity improvement of a fibre Bragg grating pH sensor with elastomeric coating My IOPscience Sensitivity improvement of a fibre Bragg grating pH sensor with elastomeric coating This content has been downloaded from IOPscience . Please scroll down to ,” no. May 2016, 2011, doi: 10.1088/0957-0233/23/1/015104.

[69] J. M. Corres, I. R. Matias, S. Member, I. Villar, and F. J. Arregui, “Design of pH Sensors in Long-Period Fiber Gratings Using Polymeric Nanocoatings,” vol. 7, no. 3, pp. 455–463, 2007.

[70] S. Karastogianni, S. Girousi, and S. Sotiropoulos, *pH : Principles and Measurement*, 1st ed., no. December. Elsevier Ltd., 2016.

[71] P. J. Brewer, “International comparison on Ag | AgCl electrodes for pH measurement,” vol. 66, pp. 131–138, 2015, doi: 10.1016/j.measurement.2015.01.029.

[72] J. J. Patil, “Measurement of pulse oximetry , capnography and pH,” *Anaesth. Intensive Care Med.*, vol. 15, no. 11, pp. 522–525, 2014, doi: 10.1016/j.mpaic.2014.08.006.

[73] I. Bouhadda, O. De Sagazan, and F. Le Bihan, "Electronic sensor for pH measurements in nanoliters," *Procedia Eng.*, vol. 87, pp. 915–918, 2014, doi: 10.1016/j.proeng.2014.11.304.

[74] B. Culshaw and A. Kersey, "Fiber-Optic Sensing : A Historical Perspective," no. June 2008 doi: 10.1109/JLT.0082.921915.

[75] B. Mhdi, "Study Pulse Parameters versus Cavity Length for Both Dispersion Regimes in Study Pulse Parameters versus Cavity Length for Both Dispersion Regimes in FM Mode Locked," no. December, 2015, doi: 10.11591/ijeei.v3i1.130.

[76] H. Mohamed, N. Irawati, F. Ahmad, and M. H. Ibrahim, "Optical Humidity Sensor Based on Tapered Fiber with Multi-walled Carbon Nanotubes Slurry," vol. 6, no. 1, pp. 97–103, 2017, doi: 10.11591/ijeecs.v6.i1.pp97-103.

[77] D. Sasmita, A. Pambudi, M. Rivai, and A. Arifin, "Detection of Organic Solvent Compounds Using Optical Fiber Interferometer Array and Neural Network Pattern Recognition," pp. 477–482, 2018.

[78] U. Stanley, V. M. Olu, C. Ochonogor, A. Peter, and A. Francis, "Experimental Analysis of Cable Distance Effect on Signal Attenuation in Single and Multimode Fiber Optics," vol. 8, no. 3, pp. 1577–1582, 2018, doi: 10.11591/ijece.v8i3.pp1577-1582.

[79] B. Gu, M. Yin, A. P. Zhang, and J. Qian, "Sensor Based on Thin-Core Fiber Modal Interferometer," *Opt. Express*, vol. 17, no. 25, pp. 613–618, 2009, doi: 10.1039/b911386j.20.

[80] T. H. Nguyen, T. Venugopalan, T. Sun, and K. T. V Grattan, "Development of intrinsic optical fiber pH sensors for industrial applications," pp. 89–94, 2009.

[81] J. Li, X. Huang, W. Xu, D. Xiao, and Z. Zhong, "Optical Fiber Technology A fiber-optic pH sensor based on relative Fresnel reflection technique and biocompatible coating," *Opt. Fiber Technol.*, vol. 20, no. 1, pp. 28–31, 2014, doi: 10.1016/j.yofte.2013.11.002.

[82] S. Choi, S. Member, T. J. Eom, J. W. Yu, B. H. Lee, and K. Oh, “Novel All-Fiber Bandpass Filter Based on Hollow Optical Fiber,” no. October, pp. 10–13, 2002, doi: 10.1109/LPT.2002.804658.

[83] N. Fibers, E. Engineering, and W. Rd, “A Refractive-index Fiber Sensor by Using,” no. 100, pp. 100–102, 2013.

[84] K. Hammarling, J. Hilborn, H.-E. Nilsson, and A. Manuilskiy, “Blood pH optrode based on evanescent waves and refractive index change,” *Opt. Fibers Sensors Med. Diagnostics Treat. Appl. XIV*, vol. 8938, p. 89381F, 2014, doi: 10.1117/12.2040077.

[85] S. Novais, M. S. Ferreira, and J. L. Pinto, “Relative humidity fiber sensor based on multimode interferometer coated with agarose-gel,” *Coatings*, vol. 8, no. 12, 2018, doi: 10.3390/COATINGS8120453.

[86] D. Lopez-torres, “Sensors and Actuators B : Chemical Enhancing sensitivity of photonic crystal fiber interferometric humidity sensor by the thickness of SnO 2 thin films,” *Sensors Actuators B. Chem.*, vol. 251, pp. 1059–1067, 2017, doi: 10.1016/j.snb.2017.05.125.

[87] A. B. Socorro, M. Hernaez, I. Del Villar, J. M. Corres, F. J. Arregui, and I. R. Matias, “Single-mode—multimode—single-mode and lossy mode resonance-based devices: a comparative study for sensing applications,” *Microsyst. Technol.*, vol. 22, no. 7, pp. 1633–1638, 2016, doi: 10.1007/s00542-015-2793-z.

[88] W. Yao, X. Chen, and J. Zhang, “A capacitive humidity sensor based on gold-PVA core-shell nanocomposites,” *Sensors Actuators, B Chem.*, vol. 145, no. 1, pp. 327–333, 2010.

[89] C. W. Li, “Silver nanoparticle/chitosan oligosaccharide/poly(vinyl alcohol) nanofibers as wound dressings: A preclinical study,” *Int. J. Nanomedicine*, vol. 8, pp. 4131–4145, 2013, doi: 10.2147/IJN.S51679.

[90] S. Nicoleta., “Silica Nanoparticles Induce Oxidative Stress and Autophagy but Not Apoptosis in the MRC-5 Cell Line,” pp. 29398–29416, 2015, doi: 10.3390/ijms161226171.

[91] Y. D. Glinka, S. H. Lin, and Y. T. Chen, "Time-resolved photoluminescence study of silica nanoparticles as compared to bulk type-III fused silica," *Phys. Rev. B - Condens. Matter Mater. Phys.*, vol. 66, no. 3, pp. 354041–3540410, 2002, doi: 10.1103/PhysRevB.66.035404.

[92] X. Wang, Z. Luo, M. Liu, R. Tang, A. Luo, and W. Xu, "Wavelength-switchable femtosecond pulse fiber laser mode-locked by silica-encased gold nanorods," *Laser Phys. Lett.*, vol. 13, no. 4, p. 45101, 2016.

[93] P. Re-, "Molecular Weight of Polyaerylic and Polymethacrylie Acid," vol. VI, no. 2, pp. 145–154.

[94] "of Methyl Red 1-3 Purpose: The pK," pp. 1–12.

[95] L. Shao, M. Yin, H. Tam, and J. Albert, "Fiber Optic pH Sensor with Self-Assembled Polymer Multilayer Nanocoatings," pp. 1425–1434, 2013, doi: 10.3390/s130201425.

[96] B. Schyrr, "Sensors and Actuators B : Chemical Development of a polymer optical fiber pH sensor for on-body monitoring application," *Sensors Actuators B. Chem.*, vol. 194, pp. 238–248, 2014, doi: 10.1016/j.snb.2013.12.032.

[97] J. Zajíc, L. Traplová, V. Mat, M. Pospíšilová, and I. Barto, "Optical pH Detection with U-Shaped Fiber-Optic Probes and Absorption Transducers," vol. 2015, 2015.

[98] A. K. Pathak, D. K. Chaudhary, and V. K. Singh, "Broad range and highly sensitive optical pH sensor based on Hierarchical ZnO microflowers over tapered silica fiber," *Sensors Actuators A. Phys.*, 2018, doi: 10.1016/j.sna.2018.08.013.

[99] B. Sol-gel, J. Zhang, and L. Zhou, "Preparation and Optimization of Optical pH Sensor," 2018, doi: 10.3390/s18103195.

[100] M. H. K. Anik, S. Mahmud, M. I. A. Isti, S. Nuzhat, S. K. Biswas, and H. Talukder, "A Novel Highly Sensitive Photonic Crystal Fiber Sensor

for Detecting PH Levels of Acetic Acid Aqueous Solution Based on Surface Plasmon Resonance," *2020 11th Int. Conf. Comput. Commun. Netw. Technol. ICCCNT 2020*, 2020, doi: 10.1109/ICCCNT49239.2020.9225269.

[101] C. Wang, P. R. Ohodnicki, X. Su, M. Keller, T. D. Brown, and J. P. Baltrus, "Novel silica surface charge density mediated control of the optical properties of embedded optically active materials and its application for fiber optic pH sensing at elevated temperatures," *Nanoscale*, vol. 7, no. 6, pp. 2527–2535, 2015, doi: 10.1039/c4nr06232a.

Appendix

(A)

THORLABS

Superluminescent Diode 1550 nm, Butterfly Package

SLD1550S-A1

Description

The SLD1550S-A1 is a 1550 nm, low-power, broadband Superluminescent Diode (SLD) with a near-Gaussian spectral profile and low ripple. This SLD is housed in a standard 14-pin butterfly package with FC/APC-connectorized, nonpolarization-maintaining fiber. An integrated thermistor allows for temperature control, thus stabilizing the power and spectrum.

Specifications

CW; T_{CHIP} = 25° C, T_{CASE} = 0 to 65° C

SLD1550S-A1				
	Symbol	Min	Typical	Max
Center Wavelength	λ_C	1520 nm	1550 nm	1580 nm
Operating Current	I_{OP}	-	450 mA	500 mA
ASE Power*	P_{ASE}	0.75 mW	1.0 mW	-
Optical 3 dB Bandwidth*	BW	100 nm	110 nm	-
RMS Gain Ripple *	ΔG	-	-	0.1 dB
Forward Voltage*	V_F	-	1.6 V	2.0 V
TEC Operation (Typical / Max @ T_{CASE} = 25 °C / 65 °C)				
- TEC Current	I_{TEC}	-	0.35 A	1.5 A
- TEC Voltage	V_{TEC}	-	0.5 V	3.5 V
- Thermistor Resistance	R_{TH}	-	10 kΩ	-

*@I_{OP}

Performance Plots

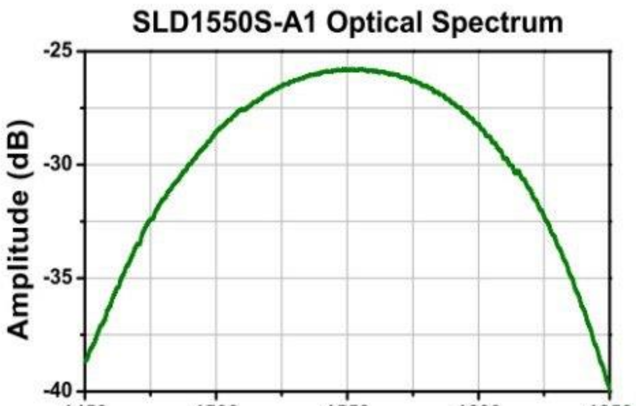

Drawings

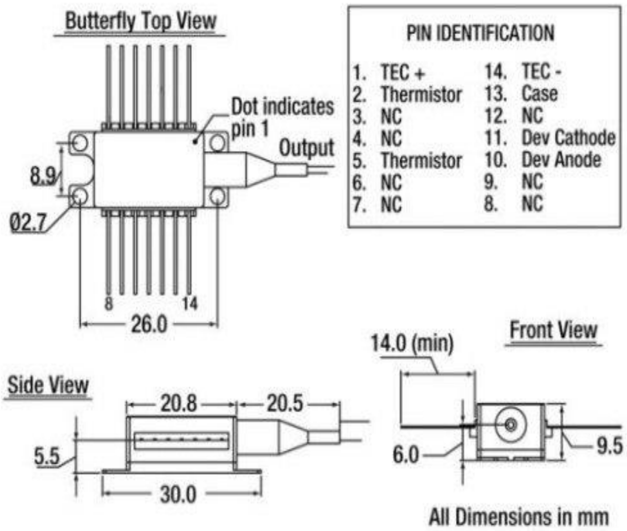

Note: Output isolator and monitor photodiode are available options for butterfly-packaged diodes. Please contact Technical Support for more information.

Appendix
(B)

Corning® SMF-28® Ultra Optical Fiber

Product Information

CORNING

Corning® SMF-28® Ultra optical fiber is an ITU-T Recommendation G.652.D compliant optical fiber with Corning's enhanced low-loss and bend fiber technologies. This full-spectrum fiber has bend performance that exceeds the ITU-T Recommendation G.657.A1 standard and still splices the same as the installed base of standard single-mode fibers such as SMF-28e+ fiber. SMF-28 Ultra fiber offers industry-leading specifications for attenuation, macrobend loss, and polarization mode dispersion values, which provide a solid foundation for new network deployments as well as upgrades to existing networks. Since Corning brought the first fiber to market more than 40 years ago, Corning's leadership in single-mode fiber innovation has been unparalleled.

Optical Specifications

Maximum Attenuation

Wavelength (nm)	Maximum Value* (dB/km)
1310	≤0.32
1383**	≤0.32
1490	≤0.21
1550	≤0.18
1625	≤0.20

* Alternate attenuation offerings available upon request.
** Attenuation values at this wavelength represent post-hydrogen aging performance.

Attenuation vs. Wavelength

Range (nm)	Ref. λ (nm)	Max. α Difference (dB/km)
1285-1330	1310	0.03
1525-1575	1550	0.02

The attenuation in a given wavelength range does not exceed the attenuation of the reference wavelength (λ) by more than the value α.

Macrobend Loss

Mandrel Radius (mm)	Number of Turns	Wavelength (nm)	Induced Attenuation* (dB)
10	1	1550	≤0.50
10	1	1625	≤1.5
15	10	1550	≤0.05
15	10	1625	≤0.30
25	100	1310, 1550, 1625	≤0.01

*The induced attenuation due to fiber wrapped around a mandrel of a specified radius.

Point Discontinuity

Wavelength (nm)	Point Discontinuity (dB)
1310	≤0.05
1550	≤0.05

Cable Cutoff Wavelength (λ_{cc})

$\lambda_{cc} \leq 1260$ nm

Mode-Field Diameter

Wavelength (nm)	MFD (µm)
1310	9.2 ± 0.4
1550	10.4 ± 0.5

Dispersion

Wavelength (nm)	Dispersion Value [ps/(nm.km)]
1550	≤18.0
1625	≤22.0

Zero Dispersion Wavelength (λ_0): $1304 \text{ nm} \leq \lambda_0 \leq 1324 \text{ nm}$
Zero Dispersion Slope (S_0): $S_0 \leq 0.092 \text{ ps}/(\text{nm}^2 \cdot \text{km})$

Polarization Mode Dispersion (PMD)

	Value (ps/√km)
PMD Link Design Value	≤0.04*
Maximum Individual Fiber PMD	≤0.1

*Complies with IEC 60794-3: 2001, Section 5.5, Method 1, (m = 20, Q = 0.01%), September 2001.

The PMD link design value is a term used to describe the PMD of concatenated lengths of fiber (also known as PMD_Q). This value represents a statistical upper limit for total link PMD. Individual PMD values may change when fiber is cabled.

How to Order

Contact your sales representative, or call the Optical Fiber Customer Service Department:
Ph: 1-607-248-2000 (U.S. and Canada)
+44-1244-525-320 (Europe)
Email: cofic@corning.com
Please specify the fiber type, attenuation, and quantity when ordering.

Dimensional Specifications

Glass Geometry	
Fiber Curl	≥ 4.0 m radius of curvature
Cladding Diameter	125.0 ± 0.7 μm
Core-Clad Concentricity	≤ 0.5 μm
Cladding Non-Circularity	≤ 0.7%

Coating Geometry	
Coating Diameter	242 ± 5 μm
Coating-Cladding Concentricity	< 12 μm

Environmental Specifications

Environmental Test	Test Condition	Induced Attenuation 1310 nm, 1550 nm, and 1625 nm (dB/km)
Temperature Dependence	-60°C to +85°C*	≤ 0.05
Temperature Humidity Cycling	-10°C to +85°C up to 98% RH	≤ 0.05
Water Immersion	23°C ± 2°C	≤ 0.05
Heat Aging	85°C ± 2°C	≤ 0.05
Damp Heat	85°C at 85% RH	≤ 0.05

*Reference temperature = +23ºC

Operating Temperature Range: -60ºC to +85ºC

Mechanical Specifications

Proof Test

The entire fiber length is subjected to a tensile stress ≥ 100 kpsi (0.69 GPa).*

*Higher proof test levels available.

Length

Fiber lengths available up to 63.0 km/spool.

Performance Characterizations

Characterized parameters are typical values.

Core Diameter	8.2 μm
Numerical Aperture	0.14 NA is measured at the one percent power level of a one-dimensional far-field scan at 1310 nm.
Effective Group Index of Refraction (N_{eff})	1310 nm: 1.4676 1550 nm: 1.4682
Fatigue Resistance Parameter (N_d)	20
Coating Strip Force	Dry: 0.6 lbs. (3N) Wet, 14-day room temperature: 0.6 lbs. (3N)
Rayleigh Backscatter Coefficient (for 1 ns Pulse Width)	1310 nm: -77 dB 1550 nm: -82 dB

CORNING

Corning Incorporated
One Riverfront Plaza
Corning, NY 14831 U.S.A.
Ph: 607-248-2000 (U.S. and Canada)
+44-1244-525-320 (Europe)
Email: cofic@corning.com
www.corning.com/opticalfiber

Appendix
(C)

THORLABS

Coreless Termination Fiber

FG125LA
FG250LA
FG400LA

Description

These coreless silica termination fibers can be spliced to the ends of standard fiber to reduce back reflections or prevent damage to the fiber end face. A return loss of greater than 65 dB is achieved by splicing 0.25 m of coreless fiber to the desired component.

Specifications

Specifications			
Item #	FG125LA	FG250LA	FG400LA
Wavelength Range	400 - 2400 nm		
Return Loss	>65 dB with 0.25 m		
Glass Diameter	125 ± 1 µm	250 ± 10 µm	400 ± 15 µm
Coating Diameter	250 µm ± 5%	400 ± 20 µm	550 ± 20 µm
Coating	Acrylate		
Glass Refractive Index	1.467287 @ 436 nm 1.458965 @ 589.3 nm 1.450703 @1020 nm 1.444 @1550 nm		
Operating Temperature	-40 to 85 °C		
Proof Test Level	>100 kpsi		
Recommended Stripping Tool	T06S13 or FTS4	T12S16	T18S25

الخلاصة

في هذه الرسالة تم تصميم مستشعر بسيط وصغير ومنخفض التكلفة وصديق للبيئة للأس الهيدروجيني باستخدام ألياف البصري حيث يعتمد على مبدئ التداخل متعدد الأنماط باستخدام بنية الماخ زندر وأيضا موظفين الليف البصري الخالي القلب كمسبار استشعار لتطبيقات مراقبة مستوى الأس الهيدروجيني.

في طريقنا لتصنيع بنية استشعار فعالة ، تم تغليف رأس الاستشعار بمواد طلاء مختلفة كالاتي: كحول بولي فينيل / حمض بولي أكريليك هيدروجيل (PVA / PAA) ، جزيئات نانوية سيليكا نقية مضمنة في كحول بولي فينيل / حمض بولي أكريليك (SiO_2 @ PVA / PAA) هيدروجيل ، وصبغ ميثيل أحمر مختلط مع كحول بولي فينيل (ميثيل أحمر @ PVA) ، على التوالي.

على الجانب الآخر ، تم تجريبً أحد عشر مسبارًا مختلفًا لاستشعار الألياف بناءً على بنية الليف البصري أحادي النمط- ليف بصري خالي القلب (SNCS). تم فحص أداء المستشعر بأطوال متفاوتة من الألياف الخالية القلب (NCF) 2(1، 2، 3 و4سم) وأقطار مختلفة (100 ، 90 ، 80 ، 70 ميكرومتر) للوصول إلى الابعاد المناسبة للحصول على تحسين للموجات الزائلة. كان الأداء الأمثل لجهاز الاستشعار المقترح في استشعار التباين في الأس الهيدروجيني بطول 2 سم وقطر 70 ميكرومتر. في وقت لاحق لمزيد من تحسين الاستشعار ، تم طلاء ثلاثة أقسام مختلفة من الليف البصري الخالي القلب ذو قطر 70 ميكرون باستخدام كحول بولي فينيل / حمض بولي أكريليك هيدروجيل ، و جزيئات نانوية سيليكا نقية مضمنة في كحول بولي فينيل / حمض بولي أكريليك ، و صبغ ميثيل أحمر مختلط مع كحول بولي فينيل ، على التوالي.

تُظهر النتائج التي تم الحصول عليها أنه قد تم تحقيق زيادة ثلاثة أضعاف تقريبًا في القطر الأمثل المخطط له (70 ميكرومتر) من الليف البصري الخالي القلب المطلي بمركب بوليمري ملفق بواسطة باستخدام كحول بولي فينيل / حمض بولي أكريليك هيدروجيل ، و جزيئات نانوية سيليكا نقية مضمنة في كحول بولي فينيل / حمض بولي أكريليك ، على التوالي. بغض النظر، يمكن ملاحظة أن طلاء كحول بولي فينيل / حمض بولي أكريليك هيدروجيل هو مادة طلاء حساسة للحمضية ؛ بينما يعد جزيئات نانوية سيليكا نقية مضمنة في كحول بولي فينيل / حمض بولي أكريليك أكثر ملاءمة لاستشعار الحالة الأساسية. أظهرت النتائج التجريبية حساسية متوسطة عالية تبلغ 3.42 نانومتر / وحدة أس هيدروجيني في نطاق الأس الهيدروجيني من 1 إلى 7 ، و 3.2 نانومتر / وحدة الأس الهيدروجيني في نطاق الأس الهيدروجيني من 8 إلى 14.

علاوة على ذلك ، يُظهر طلاء صبغ ميثيل أحمر مختلط مع كحول بولي فينيل مزيدًا من التحسين فوق الطلاء المذكور أعلاه ، والذي يمكن أن يستشعر كل من الحمضية والقاعدة معًا. أيضًا ، مستشعر ألياف الأس الهيدروجيني المعتمد على طلاء الميثيل الأحمر مع كحول بولي فينيل والذي يُظهر هذا الطلاء حساسية عالية تبلغ 4.3 نانومتر / وحدة الأس الهيدروجيني لنطاق الأس الهيدروجيني من 1 إلى 7 ، و 4.1 نانومتر / وحدة الأس الهيدروجيني في نطاق الأس الهيدروجيني من 8 إلى 14.

أخيرًا ، تُظهر مواد الطلاء هذه تحسينًا في الحساسية فوق هيكل الليف البصري الخالي القلب قبل المستشعر غير المطلي بسبب زيادة تعزيز المجال الزائل المتأثر بطبقة الطلاء. على حد علم المؤلفين ، كان الهيكل قادرًا على اكتشاف نطاق واسع من مستوى الأس الهيدروجيني بحساسية جيدة باستخدام بنية SNCS المطلية بطبقة رقيقة من بجزيئات السلكا النانوية و الميثيل الاحمر.

وزارة التعليم العالي والبحث العلمي
جامعة بغداد
معهد الليزر للدراسات العليا

حساسية عالية (ليف بصري احادي النمط-ليف بصري عديم القلب-ليف بصري احادي النمط) لمستشعر الأس الهيدروجيني للألياف الضوئية

رسالة مقدمة الى

معهد الليزر للدراسات العليا /جامعة بغداد /لاستكمال متطلبات نيل شهادة ماجستير علوم في الليزر/ الفيزياء

من قبل

ثمار أحمد عبدزيد

بكالوريوس علوم الفيزياء – ٢٠١٧

باشراف

أ. م. د. حنان جعفر طاهر

١٤٤٢ هـ **٢٠٢١ م**